UNIVERSIDAD DE CHILE
FACULTAD DE CIENCIAS
ESCUELA DE POSTGRADO

EFFECTS OF ERP57 OVEREXPRESSION IN A MUTANT SOD1 MOUSE MODEL OF AMYOTROPHIC LATERAL SCLEROSIS

PABLO SEBASTIÁN ROZAS ROJAS

TESIS ENTREGADA A LA UNIVERSIDAD DE CHILE EN CUMPLIMIENTO PARCIAL DE LOS REQUISITOS PARA OPTAR AL GRADO DE MAGISTER EN CIENCIAS BIOLÓGICAS

Director de tesis: Dr. Claudio Hetz Flores

Co-director de tesis: Dr. Danilo Bilches Medinas

Septiembre, 2017

UNIVERSIDAD DE CHILE
FACULTAD DE CIENCIAS
ESCUELA DE POSTGRADO

INFORME DE APROBACION

TESIS DE MAGÍSTER

Se informa a la Escuela de Postgrado de la Facultad de Ciencias que la Tesis de Magister en Ciencias Biológicas presentada por el candidato:

PABLO SEBASTIÁN ROZAS ROJAS

Ha sido aprobada por la comisión de Evaluación de la tesis como requisito para optar al grado de Magíster en Ciencias Biológicas, en el examen de Defensa Privada de Tesis rendido el día 21 de septiembre de 2017.

Director de Tesis:

Dr. Claudio Hetz Flores

Co-Director de Tesis

Dr. Danilo Bilches Medinas

Comisión de Evaluación de la Tesis

Dr. Lorena Norambuena Morales

Dr. Álvaro Glavic Maurer

A Rosario, reflejo del amor desinteresado.

BIOGRAFÍA

Nací el 2 de febrero de 1990. De ahí en adelante, todo ha sido descubrimiento. Estudié mi enseñanza básica y media en el Colegio San Ignacio en Santiago, Chile. Me entrené en el quehacer científico en la carrera de Ingeniería en Biotecnología Molecular en la Facultad de Ciencias de la Universidad de Chile desde 2008 a 2014. Con porfía, continué haciendo un Magíster en Ciencias Biológicas en la misma linda casa de estudios. Este trabajo es fruto de ese caminar por el sendero de la ciencia, que empezó hace varios años y que sigo recorriendo.

AGRADECIMIENTOS

Agradezco a los que acompañaron este proceso en sus distintos niveles: técnicos, teóricos, morales, presenciales, lejanos físicamente, formales, casuales y sinceros. Este producto científico es una amalgama de aquellas pequeñas y grandes contribuciones.

Gracias a mi familia por el apoyo constante y desinteresado. Gracias por darle sentido a la frase que reza que nuestro trabajo no solo es realización personal sino también deber social.

Gracias a mis compañeros de laboratorio (¡son muchos a los que agradecer!) por sus aportes técnicos, discusiones nutritivas y por, sobre todo, el cariño demostrado en la difícil rutina experimental. Gracias a Claudio por su críticas constructivas y por la oportunidad brindada. Agradezco afectuosamente al equipo ALS. A Vicente, Leslie, Martín, Nata, Pepe, Rod, Dani, Fran, Sole y Danilo, cuyo aporte a mi desarrollo científico y personal es invaluable.

A Danilo Medinas, mi mentor y amigo. Por compartir periódicamente el por qué hacemos ciencia. Por discutir frecuentemente el cómo hacemos ciencia; y por hacer ciencia día a día, codo a codo.

A Ute Whoelbier y Catherine Andreu, por encender la luz que guía el viaje de las proteínas disúlfuro isomerasas.

A Cristina Pinto, Jorge Ojeda, Jessica Mella y Juan Pablo Henríquez, por su increíble trabajo profesional en histología de músculo y maravillosa hospitalidad en el gran TropiConce.

A Francisca Martínez, por su extraordinario aporte técnico en la histología de médula espinal de ratón; y a Rodrigo Díaz y Daniela Becerra por continuar ese legado.

A Leslie Bargsted y Valentina Castillo, por ser unas invaluables compañeras de camino.

A Silvia Cantellano, por tanto.

TABLE OF CONTENTS

TABLES INDEX

FIGURES INDEX

ACRONYM INDEX

AAV – Adeno-associated virus
ALS – Amyotrophic lateral sclerosis
ANOVA – Analysis of variance
ATF4 – Activating transcription factor 4
ATF6 – Activating transcription factor 6
BiP – Binding immunoglobulin protein/Grp78
BSA – Bovine serum albumin
C9orf72 – Chromosome 9 open reading frame 72
ChAT – Choline acetyltransferase
CHOP – C/EBP homologous protein
CMAP – Compound muscular action potential
CNS – Central nervous system
DNA – Deoxyribonucleic acid
DMSO – Dimethyl sulfoxide
DTT – Ditiotreitol
ECL – Enhanced chemiluminescence
EDTA – Ethylenediaminetetraacetic acid
eIF2α – Eukaryotic initiation factor 2α
ER – Endoplasmic reticulum
ERAD – Endoplasmic reticulum-associated degradation
fALS – Familial ALS
FF – Fast fatigable
FR – Fast resistant
FTD – Frontotemporal dementia
FUS – Fused in sarcoma
GFAP – Glial fibrillary acidic protein
HRP – Horseradish peroxidase
Iba1 – Ionized calcium binding adaptor molecule 1
ICV – Intracerebroventricular
IL-2 – Interleukin 2
I.P. – intraperitoneal
iPSC – Induced pluripotent stem cell
IRE1α – Inositol-requiring enzyme 1α
KO – Knockout
mRNA – Messenger ribonucleic acid
NMJ – Neuromuscular Junction
Non-Tg – Non-transgenic
NP40 – Nonidet P-40
N.S. – Non-significant

OCT – Optimal cutting temperature
PBP – Progressive bulbar palsy
PBS – Phosphate-buffered saline
PCR – Polymerase chain reaction
PDI – Protein disulfide isomerase
PERK – PKR-like ER kinase
PFA – Paraformaldehyde
PLS – Primary lateral sclerosis
PMA – Progressive muscular atrophy
PMD – Protein misfolding disease
PNS – Peripheral nervous system
PVDF – Polyvinylidene fluoride
qPCR – Quantitative PCR
RNA – Ribonucleic acid
RPM – Revolutions per minute
RT-qPCR – Reverse transcription followed by quantitative PCR
sALS – Sporadic ALS
SD – Standard deviation
SDS – Sodium dodecyl sulphate
SDS-PAGE – Sodium dodecyl sulphate-polyacrylamide gel electrophoresis
SEM – Standard error of the mean
SIL1 – SIL1 Nucleotide Exchange Factor 1
SJL/BL6 – Swiss/Jackson Laboratory / Black six mixed mouse strain
SOD1 – Superoxide dismutase 1
TBS – Tris-buffered saline
TDP-43 - TAR DNA binding protein 43 kDa
TEMED - Tetramethylethylenediamine
TEN – Tris-Cl-EDTA-NaCl
UPR – Unfolded protein response
WT – Wild type
XBP1 – X-box binding protein 1
XBP1s – Spliced X-box binding protein 1

RESUMEN

La esclerosis lateral amiotrófica (ELA) es una enfermedad neurodegenerativa progresiva y fatal que afecta a las neuronas motoras en la corteza motora y en la médula espinal. A pesar de que ha sido estudiada por más de un siglo, los mecanismos celulares y moleculares que controlan su patogénesis y progresión permanecen poco comprendidos. La ELA se caracteriza por el mal plegamiento y la agregación en cuerpos de inclusión de proteínas ligadas a la enfermedad, lo que refleja una pérdida de la homeostasis proteica (proteostasis). La acumulación de proteínas mal plegadas dentro del retículo endoplasmático (RE) provoca una condición conocida como estrés de RE. Para reducir la carga de proteínas mal plegadas, se activa la respuesta a proteínas mal plegadas (UPR por su sigla en inglés) que promueve el incremento de los niveles de varias chaperonas de RE y de vías de degradación de proteínas, entre otras. Las proteínas disúlfuro isomerasas (PDIs) PDIA1 y ERp57 son blancos río abajo de la UPR y sus niveles proteicos están significativamente aumentados en tejido postmortem de pacientes con ELA y en modelos animales de la enfermedad. Hasta la fecha, no existen estudios que definan la posible contribución de las PDIs a la progresión de la ELA *in vivo*. En este trabajo, se estudió el rol de ERp57 en la patogénesis y progresión de la ELA usando el establecido modelo murino que sobrexpresa SOD1 con una mutación ligada a ELA (SOD1G93A), cruzándolo con un ratón transgénico que sobreexpresa ERp57 en el sistema nervioso central (SNC). Los resultados indican que al sobreexpresar ERp57 en el SNC desde etapas tempranas del desarrollo se retrasa el inicio de la enfermedad en ratones machos y hembras, y se protege el desempeño motor de ratones machos sin afectar la sobrevida del modelo SOD1G93A. Más aún, la agregación y oligomerización de SOD1 mutante disminuye en

la médula espinal de los ratones doble transgénicos. Los resultados sugieren una modulación de ERp57 sobre la conectividad de las neuronas motoras en etapas pre-sintomáticas que no es capaz de protegerlas en estadios avanzados de la enfermedad.

ABSTRACT

Amyotrophic lateral sclerosis (ALS) is a progressive fatal neurodegenerative disease that affects motor neurons at the motor cortex and spinal cord. Despite being study for more than a century, the cellular and molecular mechanisms that drive ALS pathogenesis and progression remain poorly understood. ALS is characterized by ALS-linked proteins misfolding and aggregation in large inclusions inside motor neurons that reflect loss of protein homeostasis (proteostasis). Protein misfolding accumulation inside endoplasmic reticulum (ER) causes a condition known as ER stress. To cope with misfolded protein load, the unfolded protein response (UPR) is activated which promotes the upregulation of several ER chaperones and protein degradation pathways, among others. Protein disulfide isomerases (PDIs) PDIA1 and ERp57 are downstream targets of the UPR and their protein levels are upregulated in ALS post mortem tissue and animal models of the disease. Until now, there were no studies addressing the contribution of PDIs *in vivo* to ALS progression. Here, the role of ERp57 in ALS pathogenesis and progression was study using the well-established ALS mouse model that overexpress SOD1 with an ALS-linked mutation (SOD1G93A), breeding it with a novel transgenic mouse that overexpresses ERp57 in the central nervous system (CNS). The results show that overexpressing ERp57 in CNS since early development delays disease onset of male and female mice, and protect motor performance of male mice without altering lifespan of SOD1G93A model. Moreover, mutant SOD1 aggregation and oligomerization is reduced in spinal cord of double transgenic animals. The results suggest a modulation of ERp57 on motor neuron connectivity in pre-symptomatic stages that is not able to protect them in later stages of the disease.

INTRODUCTION

Amyotrophic lateral sclerosis

Amyotrophic lateral sclerosis (ALS), also known as Lou Gehrig disease, "motoneurone" disease or Charcot disease, is a progressive and fatal late-onset neurodegenerative disease characterized by loss of spinal cord, brainstem and motor cortex somatic motor neurons. This leads to muscle twitching, lack of coordination, paralysis, respiratory failure and eventually death, typically 3-5 years after diagnosis (J. Paul Taylor, Brown, and Cleveland 2016). First symptoms could include tremors at hands, toes and difficulty to speak and swallow. Interestingly, motor neuron that control pelvic floor muscles, urinary and anal sphincters and eye movements are usually spared (Carvalho, Schwartz, and Swash 1995). ALS prevalence is estimated to be 5 per 100,000 people worldwide being more common in males that females in an estimated ratio of 1.2-1.5:1, respectively (J. Paul Taylor, Brown, and Cleveland 2016; Manjaly et al. 2010). In Chile, the mortality rate by ALS is 1.13 per 100,000 with a 1.2:1 male:female ratio (D. Valenzuela, Zitko, and Lillo 2015). ALS patients need constant care at home, kinesiology therapy, neurologist counseling, periodic examination and eye tracking systems to allow communication, all of which implies an economic cost to public health system and families (Caligari et al. 2013).

Although most of ALS cases arise from unknown factors, around 10% of them are inherited and termed familial ALS (fALS), while the remaining 90% have no familial records being referred to as sporadic ALS (sALS) (M. R. Turner et al. 2013). Importantly, genetic studies in ALS families led to identification of causative mutation in several genes. The most common mutations in ALS are the GGGGCC (G_4C_2)

hexanucleotide expansion in *C9ORF72*, and point mutations in superoxide dismutase 1 (*SOD1*), trans-active response (TAR) DNA-binding protein 43 (*TDP-43*), and fused in sarcoma (*FUS*) (reviewed in (M. R. Turner et al. 2013; J. Paul Taylor, Brown, and Cleveland 2016)) (Fig. 1).

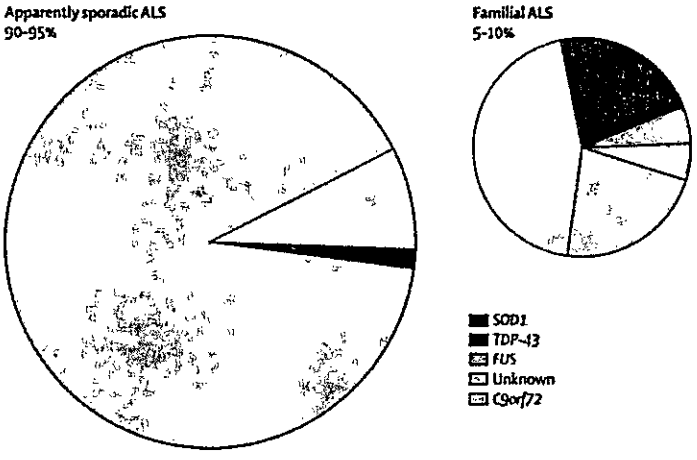

Figure 1. ALS cases and their associated genetic factors. Familial ALS cases are linked to mutations in several genes, being most prevalent *SOD1*, *TDP-43*, *FUS* and *C9ORF72*. These patients have familial clinical history. "Unknown" makes reference to patients with no association with known genetic factors. Sporadic cases can also be due mutations in these genes but without any known familial records. Percentages are related to total ALS cases. Adapted from (M. R. Turner et al. 2013).

Initially described by Jean-Martin Charcot in 1869 (Charcot and Joffroy 1869). ALS was characterized as motor disease with muscle atrophy (amyotrophic) and spinal cord rigidity (sclerosis) at its lateral portion (lateral). Now it is clear that this rigidity arises from a glial scar at the spinal cord along with motor neuron loss. Indeed, astrocyte and microglia activation at central nervous system (CNS) is a histological hallmark of sALS and fALS detected in post mortem tissue and a transversal feature of neurodegenerative diseases (reviewed in (Rizzo et al. 2014)).

The etiology of ALS has remained elusive despite decades of investigation. ALS-linked genes are involved in several and distinct cellular processes, therefore motor neuron malfunction can arise from multifactorial pathological events (J. Paul Taylor, Brown, and Cleveland 2016). Some of the most relevant processes affected in ALS comprise mitochondrial dysfunction, axonal transport defects, RNA metabolism alterations and protein homeostasis (proteostasis) loss due to autophagy impairment and endoplasmic reticulum (ER) stress (J. Paul Taylor, Brown, and Cleveland 2016). The net contribution of each process to motor neuron loss depends on the cellular or animal model used, being a barrier for translational efforts to the clinic. In fact, although more than one hundred years had passed since its discovery there are only two drugs approved by FDA to treat ALS patients: riluzole and, recently this year, edaravone. Riluzole blocks sodium channels, inhibiting motor neuron hyperexcitability and mildly extending lifespan (Lamanauskas and Nistri 2008; Fritz et al. 2013). Edaravone acts as a free radicals scavenger and its efficacy has only been proved in Japan and warrants further validation (Martinez et al. 2017). Thus, more basic research and complementary models are still needed to understand ALS pathogenesis and progression.

At cellular level, ALS has been proposed as a cell non-autonomous disease, where glial cells modulate disease onset and progression on ALS mouse models (reviewed in (B. J. Turner and Talbot 2008)). Indeed, astrocyte, microglia and oligodendrocyte modulate motor neuron function in health and disease (Reemst et al. 2016; Barres 2008). Using mouse models, targeting ALS-linked mutations on glial cells do not prevent disease but prolongs survival or delays disease onset (reviewed in (Rizzo et al. 2014) and (Nijssen, Comley, and Hedlund 2017)). Furthermore, muscle cells and axon terminals have also been shown to contribute to disease, promoting motor neuron degeneration in a retrograde fashion by a process called "dying back". This phenomenon consists in the loss of healthy neuromuscular junction (NMJ) interactions, thus disassembling them and promoting axonal degeneration due loss of neurotrophic signals from the post-synaptic terminal. Finally, motor neuron soma is compromised at the spinal cord and degenerate (Dadon-Nachum, Melamed, and Offen 2011). These evidences show that intrinsic and cell non-autonomous factors participate in ALS disease course.

Another histological hallmark is the presence of protein inclusions inside motor neurons at spinal cord (lower motor neurons), brainstem and motor cortex (upper motor neurons) (Fig. 2). This key feature of ALS differentiates it from other motor neuron disease (MND) like spinal muscular atrophy (SMA), progressive muscular atrophy (PMA), primary lateral sclerosis (PLS), among others, where a solely component of the CNS (lower or upper motor neurons) or the peripheral nervous system (PNS) (axons or myelin sheets) are affected without protein inclusion pathology (Nijssen, Comley, and Hedlund 2017; Statland et al. 2015; Al-Chalabi and Hardiman 2013).

These protein inclusions have been reported in sALS and fALS post mortem tissue and are positive for Ubiquitin, SOD1, TDP-43 or FUS staining, highlighting the role of protein misfolding and aggregation in pathophysiology (Neumann et al. 2006; Vance et al. 2009; Bosco et al. 2010; H.-X. X. Deng et al. 2010; Pokrishevsky et al. 2012). Remarkably, SOD1 inclusions have been found not only in SOD1-related fALS, but also in sALS with no SOD1-related mutations (Bosco et al. 2010). This evidence shows a wide role of protein misfolding in disease. Indeed, most of ALS-linked mutant proteins are prone to misfold and aggregate disrupting several cellular processes by direct interaction with other proteins (reviewed in (J. Paul Taylor, Brown, and Cleveland 2016)). Protein misfolding is a conspicuous and common characteristic of several neurodegenerative diseases like Alzheimer's disease, Parkinson's disease and Prion related disorders (Hetz and Mollereau 2014). All of these neurological diseases can be classified as protein misfolding disorders (PMDs), highlighting neuronal vulnerability to proteostasis loss.

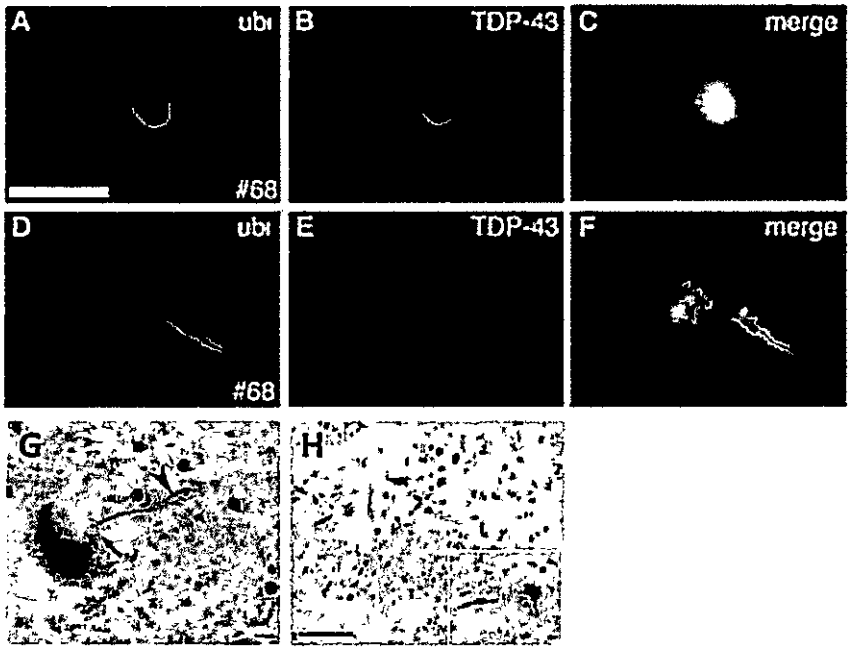

Figure 2. Protein inclusions is a histological hallmark of ALS. A to F) Ubiquitin (A and D) and TDP-43 (B and E) inclusions in sporadic ALS (sALS) co-localize in motor neurons (C and F) seen by immunofluorescence. #68 is sample number. Scale bar: 25 μm. Adapted from (Neumann et al. 2006). **G)** FUS inclusions at somas (large arrow) and neurites (arrowhead) seen by immunohistochemistry in sALS spinal cord. Scale bar: 25 μm. Adapted from (H.-X. X. Deng et al. 2010). **H)** SOD1 inclusions in swollen spinal axons and motor neurons (inset) of SOD1-related familial ALS (fALS). Scale bar: 60 μm. Adapted from (Pokrishevsky et al. 2012).

In order to study ALS pathogenesis and progression, a myriad of models have been used. *In vitro* models usually take advantage of fast screenings using immortalized cell cultures, mainly the motor neuron-like NSC34 cell line (Cashman et al. 1992) overexpressing ALS-linked mutant proteins. In the recent years, inducible pluripotent stem cells (iPSCs) derived from ALS patients have become an important tool to analyze disease mechanisms at motor neuron level (Kiskinis et al. 2014; Wainger et al. 2014), showing that neuronal degeneration can be abolished by genetic correction of mutant *SOD1* in fALS-derived iPSCs (Kiskinis et al. 2014). Despite being personalized models, iPSCs lack cell-non-autonomous disease components, ageing factor, neuron-muscle connection, and microenvironmental elements at spinal cord and motor cortex. These characteristics can be assessed using *in vivo* models. Following this idea, the most studied ALS models are genetically modified mice that overexpress ALS-linked mutant proteins like SOD1, TDP-43 or FUS, or have bacterial artificial chromosome bearing *C9ORF72* repetitions (Gurney et al. 1994; Wegorzewska et al. 2009; Peters et al. 2015; O'Rourke et al. 2015; Y. Liu et al. 2016). *In vivo* models recapitulate part of ALS clinical features and have been proved useful in unraveling pathogenic mechanisms.

ALS mouse models

Since discovery of *SOD1* as the first gene linked to ALS in 1993 (Rosen et al. 1993), several disease models have been developed to study the molecular and cellular mechanisms that underlay disease progression. Mice overexpressing distinct ALS-linked mutant SOD1 develop a progressive motor impairment phenotype with different degrees of severity depending on the specific mutation and transgene copy number (Alexander et al. 2004). Mutation changing glycine for alanine at position 93 (SOD1G93A) is one of the most well-characterized ALS-linked mutation. SOD1G93A

mice develop late onset paralysis resembling key features of ALS progression (Gurney et al. 1994). These features include progressive decrease of motor performance, neuromuscular junction (NMJ) denervation, loss of spinal motor neurons concomitantly with astrogliosis and microgliosis, organelles dysfunction and presence of intracellular mutant SOD1 inclusions (Fig. 3) (B. J. Turner and Talbot 2008). Hence, this model is a useful genetic tool to perform pharmacological and/or genetic approaches to assess ALS disease biology and find therapeutic targets.

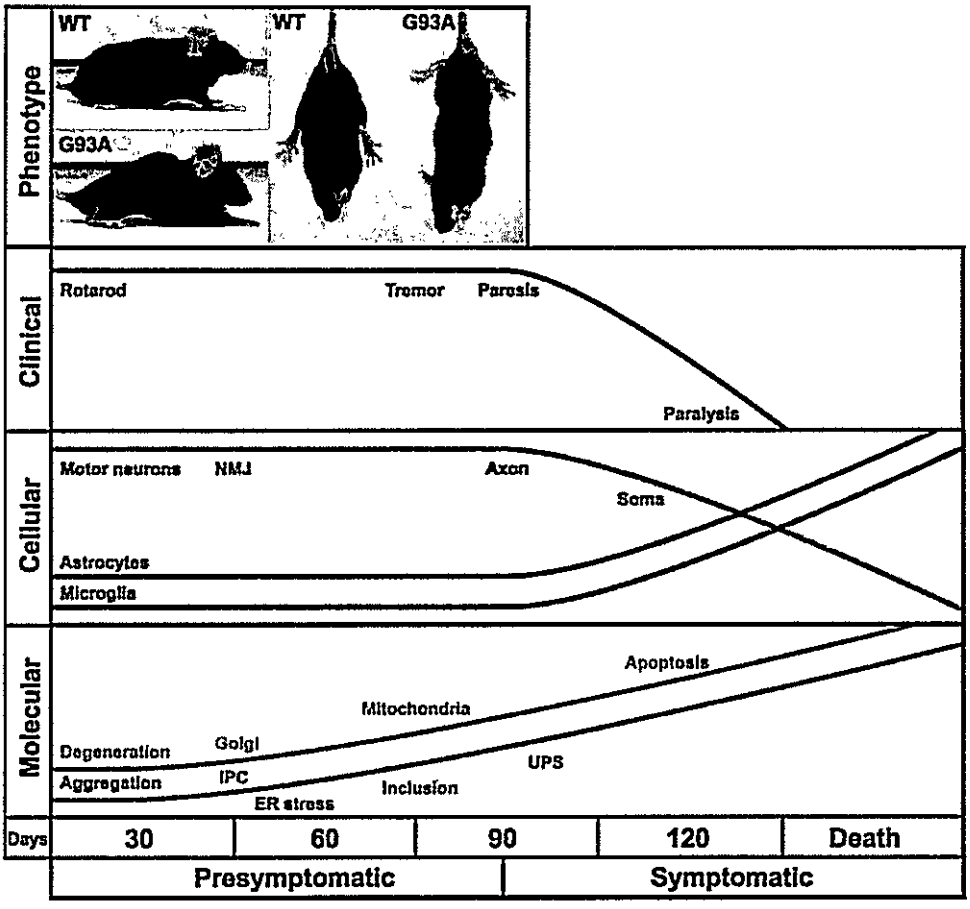

Figure 3. SOD1G93A ALS mouse model features. Mice that overexpress human mutant SOD1G93A develop progressive motor impairment and recapitulate key features of ALS at phenotypic, cellular and molecular levels. Phenotype includes kyphosis (spine curvature), absence of grooming and clasping reflex (unable to extend hind limbs when grabbed by the tail). Clinical signs include tremor and progressive paralysis. At cellular level, alterations include motor neuron loss at spinal cord and glial activation. Molecular hallmarks include SOD1G93A protein aggregation, ER stress, cytosolic protein inclusions, activation of UPS and apoptosis. Presymptomatic and symptomatic stages are defined by onset of motor impairment measured by motor tests such as Rotarod. NMJ: neuromuscular junction. IPC: insoluble protein complexes. UPS: ubiquitin proteasome system. ER: endoplasmic reticulum. Adapted from (B. J. Turner and Talbot 2008).

A major breakthrough in ALS field was achieved in 2006. TDP-43 was identified as the main component of protein inclusions in sALS and fALS post mortem tissue and also of Fronto Temporal Dementia (FTD) cases, a neurological disease that share common clinical and histopathological features with ALS, molecularly linking these diseases for the first time (Neumann et al. 2006). It was shown later that TDP-43 inclusions are present in almost 97% and 45% of total ALS and FTD cases, respectively (Ling, Polymenidou, and Cleveland 2013). Moreover, TDP-43 positive inclusions are consistently present in *c9orf72* cases (DeJesus-Hernandez et al. 2011). TDP-43 is a RNA-binding protein involved in RNAs processing. Its mislocalization to the cytosol has been proposed as a nuclear loss-of-function pathogenic mechanism, while acquiring a toxic gain-of-function by forming ubiquitin-positive cytosolic aggregates in ALS (Neumann et al. 2006). Mice overexpressing ALS-linked mutant TDP-43 (TDP-43A315T) in CNS develop a progressive and fatal neurodegenerative disease with ubiquitinated TDP-43 inclusions in spinal motor neurons and cortical pyramidal neurons (Wegorzewska et al. 2009). Nevertheless, this model has been subject of controversy since another group shown that premature dead was attributed to gastrointestinal problems (Esmaeili et al. 2013).

The most common genetic cause of ALS is the intronic G4C2 hexanucleotide expansion in *C9ORF72*. This gene is transcribed into RNA molecules that can aggregate inside the nucleus forming RNA "foci", an overlapping feature of ALS and FTD (O'Rourke et al. 2015; J. Liu et al. 2017). Moreover, a paradigm shift has been made in the past recent years, understanding these diseases as part of a spectrum of a neurodegenerative disease (FTD/ALS spectrum) with common pathogenic mechanisms (Swinnen and Robberecht 2014; Ling, Polymenidou, and Cleveland 2013). Recently, in

2015 and 2016, three independent genetic mouse models were developed that carry G4C2 expansions using bacterial artificial chromosome (BAC) strategy due to the size of the expansion constructs (Peters et al. 2015; O'Rourke et al. 2015; Y. Liu et al. 2016). Cognitive problems and RNA foci are common characteristic of these models. However, only one of them do develop motor problems and premature dead along with spinal motor neuron loss (Y. Liu et al. 2016).

Interestingly, *C9ORF72* undergoes repeat associated non-ATG dependent translation (RAN translation). RAN translation of *C9ORF72* produce five types of dipeptide repeats called RAN peptides. These peptides are found in intracellular neuronal inclusions, a histological signature of some cases of FTD/ALS spectrum (Ash et al. 2013). Furthermore, RAN peptides can also induce neuronal toxicity by inhibiting the proteasome in primary cultures (Flores et al. 2016; Gupta et al. 2017), highlighting detrimental effects of inhibiting protein degradation systems, such as proteasome and macroautophagy, on neuronal physiology. The protein encoded by *C9ORF72* has functions that are beginning to be described. Mice lacking *C9ORF72* homologue die around 500 days old due immune alterations without motor phenotype, suggesting a toxic gain-of-function of hexanucleotide repeats rather than a toxic loss of function in ALS context (Sudria-Lopez et al. 2016). Functionally, it has recently been shown that C9ORF72 protein is involved in autophagy acting as a GDP/GTP exchange factor of Rabs proteins involved in autophagy flux (Sellier et al. 2016).

Viral delivery of (G4C2) repetitions in CSF of newborn mice constitutes a non-genetic model of *C9ORF72* FTD/ALS (Chew et al. 2015). This approach achieves an age-dependent protein inclusion pathology, astrogliosis and, importantly, motor deficit and

behavioral alterations. All of these phenotypes are linked to cortical neurons and Purkinje cells loss.

Several other models have been developed targeting other ALS-linked genes like *FUS* or *Ubiquilin-2* (reviewed in (Picher-Martel et al. 2016)). The availability of various tools provides an advantage to study distinct etiologies and features of ALS. However, trouble arises in order to unify translational efforts to the clinic. Hence the importance of testing hypothesis in more than one model and/or focus therapeutic interventions in the model that fits best to the aim of study. For example, despite *C9ORF72* models offers a new avenue of research in the most common genetic mutation in ALS, the established SOD1G93A model keeps being the one that recapitulates best the motor aspects of the FTD/ALS spectrum. Moreover, the spinal motor neuron dysfunction in this model is well-characterized and involves a complex crosstalk of several cellular mechanisms that compromise ER stress as one of the earliest events in early presymptomatic stages (Saxena, Cabuy, and Caroni 2009).

ER stress and the unfolded protein response in ALS

Misfolded protein accumulation at the ER causes a condition known as ER stress, triggering an adaptive response aimed to restore proteostasis termed unfolded protein response (UPR). Under mild ER stress, this response promotes clearance of misfolded proteins by ER-associated degradation (ERAD), inhibition of protein synthesis, up-regulation of chaperones and foldases, among other pathways (reviewed in (Hetz, Chevet, and Oakes 2015)) (Fig. 4). Adaptive UPR is implicated in many physiological processes, especially in professional secretory cells such as pancreatic beta cell, plasma cell, osteoblast and hepatocytes, ageing; and nervous system development and

function (Moore and Hollien 2012; Hetz 2012). On the other hand, ER stress and UPR activation have been characterized as relevant events in several diseases, including cancer, diabetes, PMDs and CNS or peripheral nervous system (PNS) injuries (Estefanie Dufey, Urra, and Hetz 2015; E. Dufey et al. 2014; Martínez et al. 2017). Under chronic ER stress, UPR shifts to signaling pathways that induce apoptosis (Hetz, Chevet, and Oakes 2015) (Fig. 4).

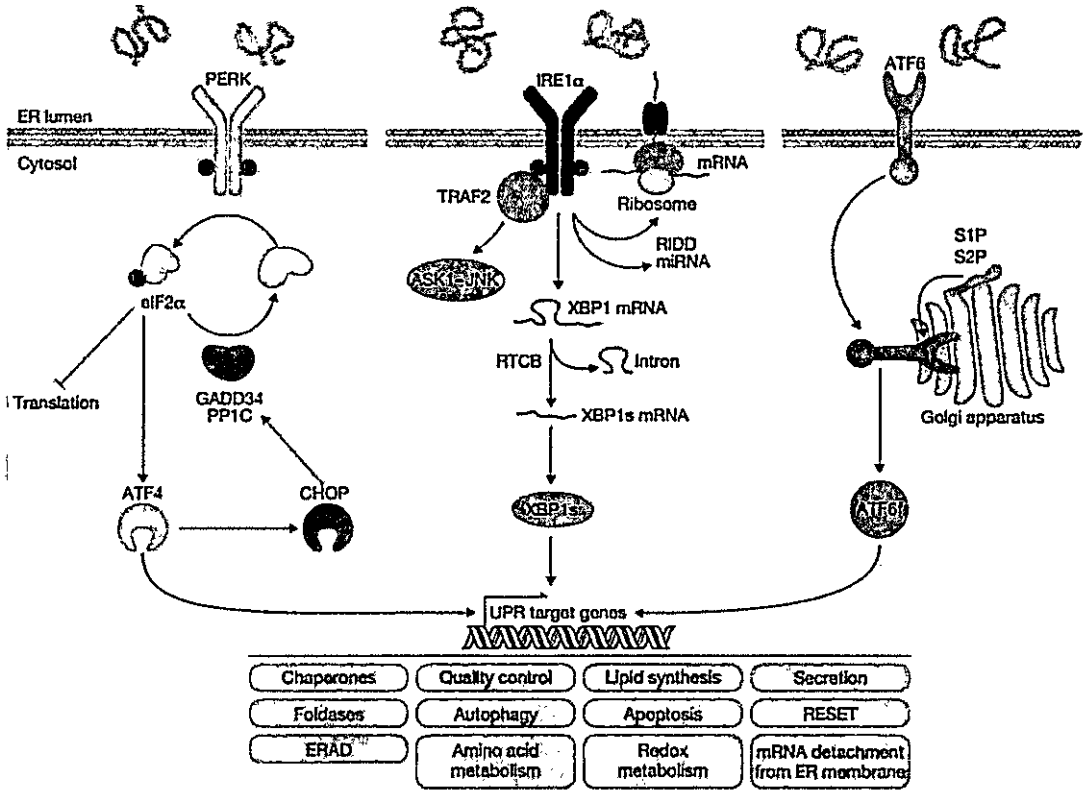

Figure 4. Unfolded protein response (UPR) is triggered by ER stress. Three branches of the UPR exist in mammalian cells, characterized by the activation of the transducers PERK, IRE1alpha and ATF6. These transmembrane proteins transduce information of protein (mis)folding status within ER lumen to cytosol and nucleus through effector proteins that regulate translation and transcription, in addition to modulate cytosolic pathways. The transcription factors ATF4, XBP1s and ATF6f are master effectors of PERK, IRE1alpha and ATF6 branches, respectively. ATF4 is selectively induced downstream of PERK activation. XBP1s is produced by splicing of *XBP1* mRNA by IRE1alpha. ATF6f is produced by ATF6 processing at Golgi apparatus. If the intensity of stress is sublethal, UPR triggers an adaptive response aimed to restore proteostasis by transiently inhibiting protein synthesis, degrading misfolded proteins and up-regulating chaperones, among others. If intensity of stress increases or if stress is sustained over time, UPR triggers an apoptotic response. ERAD: ER-associated degradation; RESET: rapid ER stress-induced export; RIDD: regulated IRE1-dependent decay of mRNA and microRNA. Taken from (Hetz, Chevet, and Oakes 2015).

ER stress in ALS has been largely described in literature occurring in patients, animal models and *in vitro* models. Independent groups have shown ER stress signs in post mortem spinal cord tissue of sALS and fALS patients (J. Atkin et al. 2008; Hetz et al. 2009; Ilieva et al. 2007). These findings have also been described in animal models of fALS at different disease stages showing activation of different UPR branches, autophagy, ERAD and upregulation of ER chaperones (J. Atkin et al. 2006; Kikuchi et al. 2006; Nishitoh et al. 2008; Hetz et al. 2009). Importantly, ER stress is an early event in SOD1G93A mouse model being detectable in pre-symptomatic stages at p37, much earlier than first phenotypic features (Saxena, Cabuy, and Caroni 2009). Using ribosome profiling, a cell-population resolution technique, Sun and collaborators reported chronic PERK pathway activation at pre-symptomatic stages, specifically in spinal cord motor neurons of fALS mouse model (Sun et al. 2015). In line with this cell-type specific phenotype, iPSCs-derived motor neurons from *C9ORF72* or *SOD1* patients develop intrinsic ER stress compared to other cell types (Dafinca et al. 2016; Kiskinis et al. 2014; Wainger et al. 2014). Of note, this intrinsic ER stress has been linked to motor neuron hyperexcitability, placing ER stress at the intersection of proteostasis impairment and neuronal dysfunction (Matus, Medinas, and Hetz 2014; Wainger et al. 2014). Despite most studies are focused on lower motor neurons, recent evidence also shows that upper motor neurons are also susceptible to ER stress (Jara et al. 2015). How ER stress disrupts motor neuron function is not fully understood. However, it is an intrinsic property of motor neurons manifested in a transversal manner in ALS cases with different etiology.

ER stress and motor neuron vulnerability

Susceptibility to ER stress differs within different subpopulations of motor neurons that coexist in the same region of the spinal cord (Saxena, Cabuy, and Caroni 2009). These populations diverge on their target muscles, referred as connectivity, and transcriptional and translational profiles, determining their electrophysiological properties (Hadzipasic et al. 2014). Motor neuron-muscle fibers unit is termed motor unit (Nijssen, Comley, and Hedlund 2017). Patients and mutant mouse models of fALS show different rates of muscle denervation and degeneration of motor units (Hadzipasic et al. 2014). The fast-fatigable (FF) motor units are the first to become denervated in fALS mice at presymptomatic stages, and are termed "vulnerable". Then, the fast fatigue-resistant (FR) motor units become denervated determining disease onset location (spinal or bulbar depending on the muscles affected). Finally, slow motor units (S), which are responsible for muscular tone, denervate only at end stage of the disease and are termed "resistant" motor neurons (reviewed in (Saxena and Caroni 2011)). This particular spatial and temporal course of motor neuron degeneration reveals selective vulnerability within motor neurons subpopulations (Fig. 5). How specific pools of motor neurons degenerate first given the same genetic background? What are the molecular bases for this selective vulnerability?

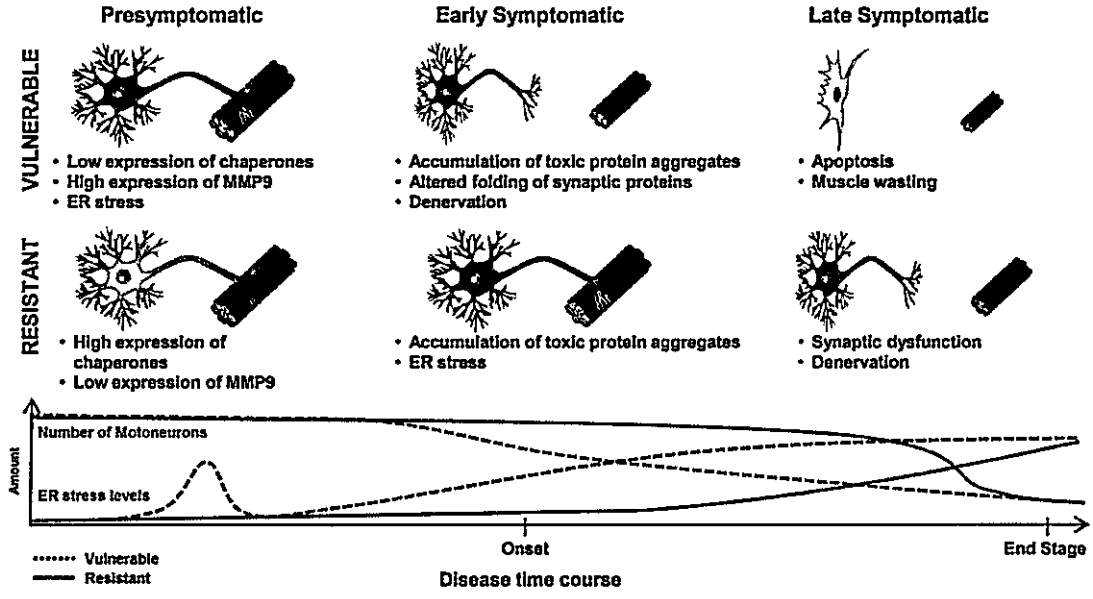

Figure 5. ER stress signatures in motor neuron selective vulnerability. Vulnerable motor neurons express lower levels of ER chaperones compared to resistant motor neurons. They also express higher levels of MMP9, related to increased levels of ER stress. This stress occurs (depicted as blue motor neurons) early during presymptomatic stages on vulnerable motor neurons of mutant SOD1 mouse (Saxena, Cabuy, and Caroni 2009). Vulnerable motor neurons denervate their target muscles (depicted as red fibrils) initiating disease onset. At late symptomatic stages, vulnerable motor neurons are degenerated already and resistant motor neuron starts to denervate from muscles (Rozas et al. 2017).

ER stress has emerged as early and transversal pathogenic mechanism driving motor neuron degeneration in ALS and also in spinal muscular atrophy (SMA), another motor neuron disease (reviewed in (Rozas et al. 2017)). A landmark study by Saxena and collaborators performed laser capture of resistant and vulnerable motor neurons in lumbar spinal cord stained with retrograde tracers injected in soleus (mainly resistant motor units and tibialis anterior (mainly vulnerable) muscles for global analysis of factors underlying selective vulnerability in ALS. Temporal gene expression profiling of resistant and vulnerable motor neurons of mutant SOD1 mice identified early ER stress specifically in vulnerable motor neurons (Saxena, Cabuy, and Caroni 2009). This is one of the earliest alterations of the fALS mouse model, even before muscle denervation, highlighting the relevance of proteostasis disturbance to ALS pathogenesis. Following this report, several other groups have demonstrated proteostasis alterations in vulnerable motor neurons (Kaplan et al. 2014; Nathalie Bernard-Marissal et al. 2015; de L'Etang et al. 2015; Jara et al. 2015; Sun et al. 2015).

How these ER stress signatures in vulnerable motor neurons translate into selective vulnerability? Downstream of the UPR, the protein folding quality control network becomes upregulated. This network comprises chaperones, co-chaperones and foldases acting in an orchestrated response to restore proteostasis (Rozas et al. 2017). This chaperone network has been proved of critical relevance to neuromuscular system and also ALS progression (Fig. 6). The role of this chaperone network starts at protein synthesis inside de ER. BiP is the main chaperone that binds nascent polypeptide chains inside ER lumen. Knock-in mice that lack ER retrieval sequence of BiP develop age-dependent motor problems, degeneration of spinal motor neurons, and aggregation of SOD1 reminiscent of sALS (Jin et al. 2014). Moreover, BiP co-chaperone SIL1 was

found to be expressed in resistant compared to vulnerable motor neurons in mutant SOD1 mice (de L'Etang et al. 2015). Remarkably, using a gene therapy approach to overexpress SIL1 in spinal neurons de L'Etang and collaborators achieved motor neuron protection concomitantly with reduced SOD1 aggregation. This was correlated with increased ER stress buffering capacity, delayed muscle denervation and, importantly, prolonged survival in SOD1G93A mice. On the other hand, deleting one *sil1* gene copy accelerates ALS pathology in this model (de L'Etang et al. 2015).

Furthermore, ribosome profiling of motor neurons, astrocytes and oligodendrocytes in spinal cord showed that protein disulfide isomerase (PDI), a major ER chaperone that catalyze disulfide bonds within ER, is ten-fold less expressed in motor neurons compared to surrounding glial cells (Sun et al. 2015), suggesting decreased folding capacity as an intrinsic vulnerability factor of spinal motor neurons. This observation is in close relation with RNA-seq data in iPSCs-derived motor neurons from fALS patients showing up-regulation of several chaperones and intrinsic ER stress in fALS motor neurons leading to alterations in electrical activity (Kiskinis et al. 2014; Wainger et al. 2014). Remarkably, an unbiased proteomic approach was recently published showing that early-onset of ALS patients have decreased levels of chaperones and foldases, including BiP, compared to late-onset patients. Also, the reduction of these targets involved in protein quality control system were also decrease in early-onset fALS mice (Filareti et al. 2017).

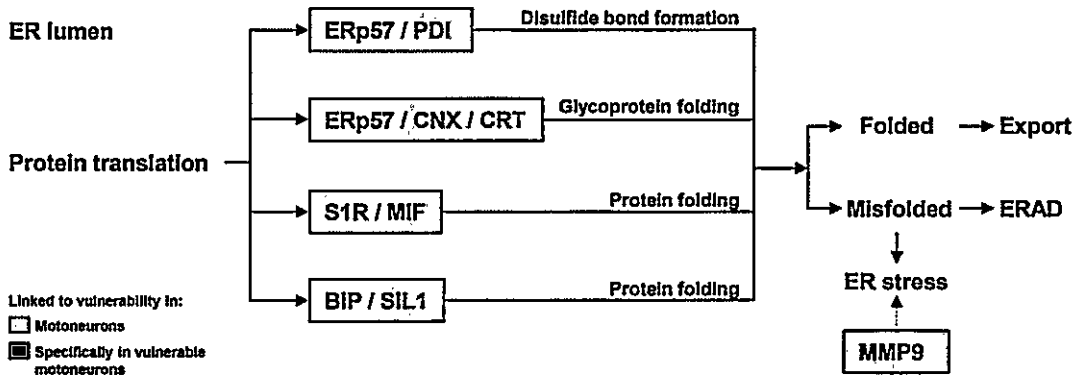

Figure 6. ER chaperone network is involved in ALS. Several ER chaperones have been linked to motor neuron vulnerability. Altering these protein functions disrupts several folding processes that directly impact on ER stress. Chaperones involved in: disulfide bond formation - ERp57 and protein disulfide isomerase (PDI); glycoprotein folding - ERp57, calnexin (CNX) and calreticulin (CRT); protein folding - sigma-1-receptor (S1R), macrophage migration inhibitory factor (MIF), binding immunoglobulin protein (BiP) and SIL1. MMP: matrix metalloproteinase 9. Taken from (Rozas et al. 2017).

How could reduced levels of chaperones and foldases impact on motor neuron functionality and viability? Many of the ion channels and synaptic proteins directed to cell membrane and axon terminals are glycosylated and traffic through the secretory pathway (Scott and Panin 2014). Folding of glycosylated proteins is assisted by the calnexin/calreticulin cycle, two critical molecular chaperones and Ca^{+2} buffering proteins within the ER (Tannous et al. 2015) (Fig. 6). It has been observed that calreticulin levels are decreased in FF motor neurons of fALS mice (N Bernard-Marissal and Moumen 2012). Remarkably, deleting one gene copy of *Calreticulin* leads to acceleration of NMJ denervation in mutant SOD1 mice at early pre-symptomatic stages (Nathalie Bernard-Marissal et al. 2015). Together, the accumulated evidence supports that impairment of the ER chaperone network is associated to motor neuron vulnerability and ALS progression.

Protein disulfide isomerases in ALS

Proteomic studies of spinal cord of rat and mouse ALS models have identified two protein disulfide isomerase family members (PDIs), PDIA1 and ERp57 (also known as PDIA3 or GRP58) as main hits up-regulated at different disease stages at spinal cord, suggesting major dysregulation of redox folding in the ER of affected tissue (J. Atkin et al. 2006; Massignan et al. 2007). In 2006, Atkin and collaborators showed that PDIA1 and ERp57 protein levels were increased in rat spinal cord at pre-symptomatic stages using two-dimensional gel electrophoresis followed by MALDI-TOF-MS analysis. This was further confirmed at disease end stage in rat and mouse ALS models by Western blot (J. Atkin et al. 2006). An independent group showed in 2007, that PDIA1 was up-regulated in pre-symptomatic ALS mouse model spinal cord with a similar proteomic approach (Massignan et al. 2007). Importantly, PDIA1 and ERp57 were found up-

regulated in post mortem spinal cord of sALS patients by two independent groups (J. Atkin et al. 2008; Hetz et al. 2009). Moreover, protein inclusions positive for PDIA1 were found in spinal motor neurons of sALS patients. These observations suggest a possible neuroprotective role of PDIs in ALS (J. Atkin et al. 2008). Increased levels of PDIA1 were also seen in cerebrospinal fluid (CSF) of sALS patients (J. Atkin et al. 2008). Remarkably, another proteomic study performed in peripheral blood mononuclear cells (PBMC) of sALS patients showed ERp57 as a reliable blood biomarker for disease progression and the most associated hit with disease severity (Nardo et al. 2011).

Protein disulfide isomerase family members (PDIs) are major downstream targets of the UPR and part of ER chaperone network (Andreu et al. 2012; Matus et al. 2013) (Fig. 6). These proteins catalyze the reduction, isomerization and formation of disulfide bonds of several substrates within ER lumen, promoting their folding. Mechanistically, impairment of PDIs function in oxidative folding may be important for ALS pathogenesis. Inactivation of PDIA1 by S-nitrosylation has been found in spinal cord of ALS mouse models and post mortem tissue of sALS and fALS patients (A. K. Walker et al. 2010; Jeon et al. 2014). This inactivation promotes the aggregation of mutant SOD1 *in vitro* and in spinal cord of mouse ALS models (Chen et al. 2013; Jeon et al. 2014). Aggregation of mutant SOD1 also occurs when silencing PDIA1 expression in neuronal cell culture. On the other hand, overexpressing PDIA1 decreases mutant SOD1 aggregates (A. K. Walker et al. 2010). Moreover, PDIA1 co-localize with ALS-linked mutant proteins like SOD1, FUS, VAPB and TDP43 aggregates (Aliaga et al. 2013; J. Atkin et al. 2006; Honjo et al. 2011; Farg et al. 2012) suggesting a role of PDIs in folding interactions of these ALS-linked proteins. PDIs up-regulation in ALS could serve

as a neuro-protective mechanism aimed to decrease misfolded protein overload, however, this has not been proved *in vivo*.

Recently, our laboratory in collaboration with Robert H. Brown at University of Massachusetts identified mutations in *PDIA1* and *ERp57* genes as risk factors to develop ALS (Gonzalez-Perez et al. 2015). Our group described a role for these PDIs in promoting motor neuron neuritogenesis using several models, including cell lines, primary spinal cord cultures and zebra fish (Woehlbier et al. 2016). Importantly, these mutations do not alter protein structure of these PDIs but lead to functional alterations as revealed by the impaired capacity of mutant chaperones to promote motor neuron outgrowth in cell culture and altered interaction with calnexin and calreticulin. ALS-linked PDIs mutants cause aberrant motor neuron branching and motor deficits in zebra fish (Woehlbier et al. 2016), thus implicating altered motor neuron connectivity as an early pathogenic mechanism in ALS.

To corroborate the role of PDIs in regulating motor neuron connectivity, we developed conditional knockout mouse for *Erp57* in CNS (Woehlbier et al. 2016), in addition to transgenic mouse lines that overexpress wild-type (Torres et al. 2015; Castillo et al. 2015) or ALS-linked mutant *ERp57* (Sepúlveda 2015). Deficiency of *Erp57* as well as expression of ALS-linked mutations led to altered NMJs and impaired motor functions reminiscent of early ALS stages (Woehlbier et al. 2016; Sepúlveda 2015). Moreover, the impaired motor function is associated with decreased levels of certain synaptic proteins, suggesting that ERp57 function in motor neurons is important for proper maintenance of connectivity of motor units. Furthermore, we also determined that ERp57 interacts and assists the folding of Prion protein in CNS, which has a relevant

role in synaptic functions (Torres et al. 2015; Sepulveda et al. 2016). Interestingly, mice overexpressing wild type ERp57 show improved peripheral nerve regeneration after sciatic nerve injury whereas they do not show improved resistance to neurodegeneration of dopaminergic neurons in a pharmacological model of Parkinson's disease (Castillo et al. 2015). Taking into account the fact that *Erp57* deficiency does not result in motor neuron loss or paralysis (Woehlbier et al. 2016), the accumulated evidence suggests that ERp57 is involved in early ALS stages and its mutant forms are risk factors to develop the disease.

Whether PDIs up-regulation in ALS mice and patient post-mortem tissue is a neuro-protective mechanism, an epiphenomenon of disease progression, or even a pathogenic event, remains to be addressed. Importantly, PDIs could have a detrimental effect on motor neuron survival. Supporting this idea, it has been shown that PDI has a pro-apoptotic role in other PMDs related proteins, such as in mutant huntingtin or Aβ toxicity (Hoffstrom et al. 2010). This pro-apoptotic role is due aberrant interactions at mitochondrial-associated-ER-membranes, while inhibiting reductase PDI activity rescues cell from apoptosis, showing that increasing PDIs activity is not always neuroprotective (Hoffstrom et al. 2010).

Despite the accumulating evidence linking PDIs ALS pathogenesis, thus far no pharmacological or genetic study has directly investigated PDIs functional role in disease onset and progression. Although genetic approaches have been performed overexpressing ALS-linked mutants of ERp57 *in vivo* (Sepúlveda 2015), if this PDI has a neuroprotective effect by targeting toxicity of other ALS proteins remains an open question. For instance, it could be reasoned that pathogenic mutant SOD1 aggregates

crosslinked through intermolecular disulfide bonds could be dismantled by thiol reductase activity of PDIs, relieving ER stress. On the other hand, the sequestration of PDIs by mutant SOD1 aggregates may lead to toxicity due to PDI loss-of-function as occurs for PDI nitrosylation (Chen et al. 2013). Undoubtedly, further studies addressing the relationship of mutant SOD1 aggregates, PDI function, and ER stress could contribute to understand ALS pathogenic mechanisms and pave the way to the development of novel therapeutic targets to treat this fatal disease

In order to address the *in vivo* role of ERp57 in ALS context, in this thesis we have studied the effects of overexpressing the wild type form of ERp57 mainly in CNS in the SOD1G93A ALS mouse model through the generation of double transgenic mice for human *ERp57* and *SOD1G93A* (Fig. 7). The ERp57 transgenic mouse line (ERp57-Tg) overexpresses the human chaperone containing a FLAG tag conjugated to the C-terminus of ERp57 under the control of Prion protein promoter (Fig. 7). The FLAG tag is used to detect the exogenous protein by anti-FLAG immunofluorescence or WB analysis. Prion protein promoter is expressed during embryonic development and mainly in CNS with leaky expression in other tissues like lungs, heart and kidney among others, being higher in CNS (whole brain and spinal cord) by at least one order of magnitude (Borchelt et al. 1996; J. Wang et al. 2005; Castillo et al. 2015). Thus, we crossed the ERp57-Tg transgenic mouse line previously generated in Dr. Hetz laboratory (Torres et al. 2015; Castillo et al. 2015) with the mutant SOD1G93A mice and characterized F1 generation at phenotypic, histological, and molecular levels. Using this genetic strategy, we aimed to define the impact of ERp57 on ALS disease pathogenesis and progression.

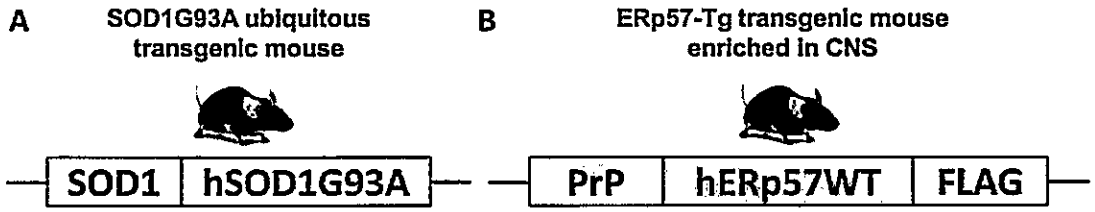

Figure 7. Scheme of transgenic mouse lines used in this study. A) SOD1G93A ALS mouse model (Jackson Laboratory Number 004435) expresses human SOD1 with G93A mutation. This line is in C57Bl6 background and corresponds to the "transgene high copy number" SOD1G93A model, harboring 25 transgene copies, approximately (Jackson Laboratory). Each copy has human *SOD1* promoter sequence that assures ubiquitous expression in mouse. **B)** ERp57-Tg mouse line expresses human ERp57 wild type (hERp57wt) under command of Prion protein promoter that is expressed mainly in CNS with leaky expression in other tissues (Borchelt et al. 1996; J. Wang et al. 2005; Castillo et al. 2015). ERp57-Tg is conjugated to a FLAG tag at C-terminal domain. This line is also in C57Bl6 background (characterized in this work and in (Castillo et al. 2015; Torres et al. 2015)). SOD1G93A (red) and ERp57-Tg (green) color nomenclature is used throughout this study unless otherwise stated.

HYPOTHESIS

ERp57 overexpression in CNS delays disease onset and progression in SOD1G93A mouse model of ALS.

AIM

To investigate the effects of overexpressing ERp57 in CNS on experimental ALS.

Specific aims:

1) Define the impact of overexpressing ERp57 in CNS on disease progression and lifespan of SOD1G93A mice
2) Determine the effects of overexpressing ERp57 in CNS on histopathological features of SOD1G93A mice.
3) Investigate the effects of ERp57 overexpression in CNS on proteostatic alterations of SOD1G93A mice.

MATERIAL AND METHODS

Cell culture neuritogenesis assay

NSC34-SOD1 cell lines

Cell culture assay were performed in collaboration with Juan Pablo Henriquez's Lab at Universidad de Concepción, Concepción, Chile. Mouse motor neuron-like NSC34 cell line expressing wild-type SOD1 (SOD1WT) or mutant SOD1 (SOD1G93A) in a stable form, were maintained in proliferation medium (DMEM, 4.5 g/L Glucose, 8 mM L-Glutamine (HyClone), 1X Penicillin-Streptomycin (Biological Industries), 15% fetal bovine serum and 0.4 mg/mL G418 (Merck) as selection antibiotic for the stable transgene.

Cells transient transfection

For immunostaining, NSC34 cells were grown on 18 x 18 mm glass coverslips and incubated in OptiMEM medium (Invitrogen) and transfected using a Lipofectamine Plus Reagent mix (Invitrogen), according to the indications of the manufacturer, for 24 h. The amounts of plasmid DNAs used were: 0.8 μg of YFP as control or 0.8 μg of human ERp57WT-V5 tagged. Both plasmids are in pcDNA3.1 backbone.

Immunofluorescence microscopy

To identify transfected cells, anti V5 immunostaining was performed. The medium was removed and cells were rinsed with cold PBS, fixed with 4% paraformaldehyde for 30 min, at 4°C and subsequently permeabilized with 0.1% Triton X-100 in Tris-buffered saline (TBS). Cells were rinsed with Tris-phosphate buffer and then incubated with

1:1000 anti-V5 primary antibody (Thermo Fisher, R960-25) diluted in blocking solution (1% BSA in TBS), for 15 h at 4°C. Corresponding Alexa-488 conjugated secondary immunoglobulins (Invitrogen) were incubated for 2 h at room temperature. After washes, nuclei were labeled with DAPI and coverslip mounted with Faramount mounting medium (Dako). Images were acquired with a laser confocal LSM780 Zeiss microscope at the Centro de Microscopía Avanzada (CMA) Bio–Bio facility (Universidad de Concepción, Concepción, Chile).

Image analysis

Acquired images were analyzed using ImageJ software. The number of differentiated cells and the length of their neurites were determined in cells having at least one neurite with a minimum size equal to the cell soma diameter. For each condition, 10 fields from 3 different experiments were evaluated. The mean ± SEM was plotted.

ERp57-Tg mice characterization

Mice from C57BL/6 strain that overexpress human form of wild type ERp57 (termed ERp57-Tg) were generated in Centro de Estudios Científicos (CEC), Valdivia. These mice were characterized previously in (Torres et al. 2015; Castillo et al. 2015) at CNS and PNS levels. This transgenic line use Prion protein promoter to express human ERp57 conjugated with a FLAG tag at C terminus (Fig. 7B). Motor system characterization was performed for this thesis in collaboration with Juan Pablo Henriquez's Lab at Universidad de Concepción, Concepción, Chile. All ERp57-Tg mice used were heterozygous to avoid artifacts of homozygous strategy because of random insertion of the transgene. Insertion site and transgene copy number has not been

characterized for this line. Previous characterizations from our lab were also performed in heterozygous mice (Castillo et al. 2015; Torres et al. 2015).

Diaphragm muscle dissection and immunofluorescence

Eight months old mice were euthanized using isoflurane and freshly dissected. Diaphragm muscle were dissected and fixed with 4% paraformaldehyde in PBS pH 7.4 at 4°C for 1 h. Muscles were washed and permeabilized using 0.5% Triton X-100 in PBS several time for 10 min each during 2 h in a shaking platform. Then, muscles were washed with 0.15 M glycine in PBS for 15 min followed by two washes with 0.5% Triton X-100 in PBS and incubated with 10 mg/mL $NaBH_4$ in distilled water for 5 min. Then, muscles were washed thrice in 0.5% Triton X-100 in PBS for 10 min each and blocked with blocking buffer (2% horse serum, 0.025% BSA, 0.5% Triton X-100 in PBS) at 4°C overnight. Then, muscles were incubated with 1:1000 anti-neurofilament antibody (Abcam, ab8135) in blocking buffer at 4°C overnight. Next day, tissues were washed ten times using 0.5% Triton X-100 in PBS and then incubated with 1:300 secondary antibody conjugated with Cy3 (Jackson) and 1:500 αBungarotoxin-Alexa 488 (Molecular Probes) at 4°C overnight. Finally, muscles were washed several times with 0.5% Triton X-100 in PBS for 10 min each during 2 h followed by one wash with distilled water and mounted in a slide with Faramount mounting medium (Dako). Neuromuscular junction (NMJ) images were acquired using confocal microscopy (Zeiss LSM 780) with 1 μm confocal plane setting and Z-stack.

Neuromuscular junction morphological analysis

NMJ images were 3D reconstructed using ImageJ software and analyzed to determine different NMJ shapes distribution. "Pretzel" shape consist in NMJs separated in four or more fragments; "O" and "C" shapes have less complex densities. "Dismantled" shape has no internal lines. Morphology of > 200 structures were manually quantified and showed as percentage from total. Volume, surface and swelling of NMJs were quantified from 3D reconstructed images using 3D object counter plugin for ImageJ software (Bolte and Cordelières 2006) adjusting fluorescence threshold and excluding selected objects at the edges of the z-stack because they contain incomplete NMJs. Approximately, 40-50 postsynaptic apparatus from five animals per genotype were quantified. Total endplates were quantified using 3D reconstructed images using 3D object counter plugin for ImageJ software.

Tibialis anterior muscle dissection and fiber type analysis

Eight months old mice were euthanized using isoflurane and freshly dissected. Tibialis anterior muscles were dissected, washed in PBS and snap frozen in isopentane on liquid nitrogen for 2 to 3 min. Frozen muscle were embedded in Optimal Cutting Temperature medium (OCT) (Sakura) and stored at -80°C. Transversal sections at 20 µm thickness were obtained using a cryostat. For fiber area and integrity analysis, tissues were hydrated using 100% ethanol toward 50% ethanol battery. Then, sections were washed with distilled water and incubated in Harris hematoxilin for 2 min. After a wash step in tap water, sections were dehydrated using 50% ethanol toward 80% ethanol. At this point, tibialis anterior muscles were incubated with 0.25% eosin Y in 95% ethanol. Finally, sections were dehydrated in 100% ethanol and xilol, and mounted in slides using Entellan mounting medium (Merck). For oxidative fiber type, cryosections

were incubated with NADH-NBT in Tris-PO_4 pH 7.4 (0.08% w/v reduced NADH, 0.1% w/v Nitro Blue Tetrazolium (NBT)) for 45 min. Then, sections were washed in several steps with acetone solutions (30, 60, 90, 60 and 30% v/v) for 5 min each. Finally, sections were washed in distilled water and mounting in aqueous medium. Fiber type percentage and area of slow (dark blue staining) and fast (light blue) fibers were quantified using ImageJ software.

Systemic induction of ER stress

To assess if ERp57 overexpression conferred differential susceptibility to ER stress at CNS, ERp57-Tg and non-Tg mice were injected intraperitoneally (i.p.) once with ER-stress-inducing drug tunicamycin at 5 μg per g of body weight in 5% DMSO vehicle solution. Mice were euthanized by CO_2 inhalation 24 h post i.p. injection and spinal cord was dissected on ice and frozen at -80°C until analysis using reverse transcription and real time PCR (see "Biochemical analyses" section in Material and Methods).

Mouse models, breeding and genotyping

The ALS mouse model SOD1G93A high copy number in C57BL/6 background from Jackson Laboratory (Jackson laboratory, strain number: 004435) was employed. SOD1G93A transgene has human *SOD1* promoter and has approximately 25 copies inserted in tandem at mouse non-sexual chromosome 12 (Achilli et al. 2005; Alexander et al. 2004; Gurney et al. 1994). This promoter assures ubiquitous expression of human SOD1G93A. Importantly, this transgenic line is used in a heterozygous fashion recapitulating ALS features described previously (Fig. 3) (B. J. Turner and Talbot 2008). All mice were housed in cages supplied with water and pellet food *ad libitum* in a

light/dark cycle of 12 h/12 h at 22 ± 2°C. Symptomatic mice were provided with pellet food on the floor of the cages in order to facilitate food intake. This was performed to reduce noise in disease progression parameters such as body weight and clinical score.

Heterozygous female mice from ERp57-Tg colony were bred with heterozygous male mice from SOD1G93A line. This strategy was used to avoid motor problems of female SOD1G93A during pregnancy and delivery. Litters were weaned at post natal day 21 (p21), identified with metal tags in one ear, and submitted to tail biopsy for genotyping. For DNA extraction, tails were digested with 10mg/mL proteinase K in lysis buffer (50 mM Tris pH 8.0, 100 mM EDTA, 100 mM NaCl and 1% SDS) for 16 h at 55°C. After 5 min centrifugation at 13000 g, supernatant was mixed with 100% isopropanol by inverting the tubes. DNA was pelleted by centrifugation at 13000 g for 5 min. DNA was washed with 70% ethanol and resuspended in TE buffer (10 mM Tris-Cl pH 7.5, 1 mM EDTA). PCR was performed using 12.5 μL of Go Taq Master Mix (Promega), 1 μL of genomic DNA and 1 μM of each primer to a finally volume of 25 μL. For SOD1G93A transgene detection, thermal profile used was: 1 denaturing cycle of 95°C for 3 min; 36 amplification cycles of 95°C for 30 s, 60°C for 30 s, 72°C for 45 s; 1 final elongation cycle of 72°C for 2 min. . Primers used were: *hSOD1* forward: CATCAGCCCTAATCCATCTGA; *hSOD1* reverse: CGCGACTAACAATCAAAGTGA; *IL-2* (used as an internal loading control) forward: CTAGGCCACAGAATTGAAAGATCT; *IL-2* reverse: GTAGGTGGAAATTCTAGCATCATCC. For hERp57 transgene detection, thermal profile used was: 1 denaturing cycle of 95°C for 5 min; 20 amplification cycles of 95°C for 30 s, 65°C for 30 s, 72°C for 50 s; 16 second amplification cycles of 95°C

for 50 s, 65°C for 30 s, 72°C for 50 s; a final elongation cycle of 72°C for 5 min. Primers used were: *hERp57* forward: TCTGCTTGTCATCGTCGTCCTTGT; *hERp57* reverse: AATTCCTGGATGCTGGGCACAAAC. Amplicons were resolved using 2% agarose gel electrophoresis stained with SYBR Safe (Invitrogen). Male and females from all four genotypes expected (Table II) were used for phenotypic, biochemical, histological and electrophysiological characterization.

Animal care and housing, including genotyping and experiments were performed according to procedures approved by the Committee of Bioethics of the Faculty of Medicine of the University of Chile (approved protocol CBA #0821-FMUCH).

Phenotypic characterization: body weight, clinical score and motor tests

Disease progression, in terms of onset and lifespan, was analyzed using four parameters: body weight, Clinical Score, Rotarod test and Hanging wire test. Disease onset was determined for each parameter using the criteria described below. Disease end point was considered as the time point when the mouse is unable to right itself within 10 seconds when put on its side.

Body weight analysis

SOD1G93A ALS model is characterized by progressive loss of body weight due to muscle atrophy and impairment of muscles involved in feeding (chewing and swallowing, mainly) (B. J. Turner and Talbot 2008). Body weight was measured once a week starting at p35 until end point. Disease onset by body weight was defined as the time point when mice lose 5% of their maximum weight.

Clinical Score analysis

Clinical score used in this work consisted in an arbitrary scale observing four parameters: A) Hind limb clasping: under healthy conditions: mice fully extend their hind limbs when hold by the tail. A symptomatic mice moves its hind limbs toward the body (Fig. 15D); B) Kyphosis: i.e. curvature of the spine; C) Absence of grooming: observed as dirty fur and eyes; D) Paralysis: starting as difficulty to move hind limbs. For each parameter, the score was assigned depending on the severity: 0: absence of sign; 1: mild sign; 3: moderate sign; 5: severe sign. Clinical score was measured once a week starting at p35. Mouse final score for each day was the sum of each parameter. Clinical Score onset was defined as the up-ward inflection point of the curve as long as it was above "noise". Noise was defined as the maximum value obtained by non-Tg or ERp57-Tg single transgenic mice.

Rotarod test

Rotarod test consist of placing the mouse in a rotating cylinder (Fig. 16A) using an acceleration protocol from 4 to 40 rpm in 2 min. Latency to fall from the cylinder to the base platform was recorded as measure of motor performance. This protocol assures the fall of mice due to limb problems and not for stamina draining. One week before Rotarod test, mice were trained for 5 days walking on the cylinder at a constant speed of 4 rpm for 1 minute followed by 10 rpm for another minute. Rotarod test was performed in 3 trials in a single session once a week starting at p42. Mice that did not learn to keep walking on the rotating rod at basal speed (4 rpm) were excluded for analysis. Disease onset by Rotarod test was defined as the down-ward inflection point of the curve.

Hanging wire test

Hanging wire test consists on placing the mouse by its fore paws in a horizontal metal wire suspended by two vertical plastic bars 30 cm above the table surface (floor) (Fig. 17A). Hanging test score was determined as a function of mouse performed in trying to reach one of the vertical bars and then climbing down reaching the floor within 30 seconds. The scale used to score mouse performance was: 0: mouse falls on the floor before the first 10 seconds; 1: the mouse stays hanging through forelimbs only without moving; 2: the mouse tries to reach the horizontal bar using the hind limbs without success; 3: the mouse reaches the horizontal bar with at least one of the hind limbs; 4: the mouse reaches the horizontal bar with all limbs including the tail; 5: the mouse reaches one of the vertical bars; 6: the mouse reaches the floor. Hanging wire test was performed in 3 trials in a single session once a week starting at p42. Disease onset by Hanging wire test was defined as the down-ward inflection point of the curve.

Histological analysis

Spinal cord dissection and cryosectioning

Mice were perfused transcardially with 0.9% NaCl followed by 4% paraformaldehyde. Laminectomy was performed to dissect whole spinal cord. Using sciatic nerve as reference, L5 segment was sectioned with a blade followed by a second sectioning 5mm rostral-ward the first section in order to obtain L5 to L2 region (Fig. 21A and B). Spinal cords were post-fixed in 4% paraformaldehyde for 24 h at 4°C. Gastrocnemius and tibialis anterior muscles were dissected using tweezers and post-fixed in 4% paraformaldehyde for 30 minutes at RT. Tissues were dehydrated in sucrose gradient (7.5%-15%-30% sucrose in PBS for 1 h each at RT). Dehydrated tissues were embedded in OCT and cryosectioned (Leica CM 1510S cryostat) at 25 μm per section.

Motor neuron count and gliosis analysis

For spinal motor neuron count, serial sections were used assuring 3.2 mm coverage of lumbar segment starting at L5 (one section every 200 μm).

For gliosis analysis, four sections per animal were used assuring 0.8 mm coverage of lumbar segment starting at L5 (one section every 200 μm).

For motor neuron count, anti-ChAT immunohistochemistry (IHQ) was performed treating spinal cord sections with 3% H_2O_2 - 10% MeOH in TBS for 15 min at RT to inhibit endogenous peroxidases. After one wash step with TBS, epitope retrieval was performed using citrate buffer (10 mM sodium citrate, 0.05% Tween 20, pH 6.0) for 5 min at 95°C. After one wash with TBS, spinal cord cryosections were mounted on super frost slides (VWR International). Sections were blocked using 5% donkey serum and 0.2% Triton x-100 in TBS for 1 h at RT and then incubated with 1:250 anti-ChAT (MerckMillipore, AB144P) antibody in blocking buffer 48 h at RT. Sections were then washed with TBS six times for 15 min each and incubated with anti-goat HRP-conjugated antibody (MerckMillipore, AP180P) in blocking buffer for 3 h at RT and then washed with TBS six times for 15 min each. Chromogenic reaction was performed using DAB kit (Vector Lab) following manufacturer instructions. ChAT positive cells were manually counted using bright field microscopy.

For astrocyte and microglia activation, anti-GFAP or anti-Iba1 immunofluorescence (IF) were performed, respectively. Epitope retrieval was performed using citrate buffer (10mM sodium citrate, 0.05% Tween 20, pH 6.0) for 5 min at 95°C. After one wash with

Phosphate-buffered saline (PBS), spinal cord cryosections were mounted on super frost slides (VWR International). Sections were blocked using 1% BSA and 0.025% Triton x-100 in PBS for 2 h at RT and then incubated with 1:500 anti-GFAP (Abcam, ab7260) or 1:500 anti-Iba1 (Wako, 019-19741) in 1% BSA in PBS over night at 4°C. Sections were then washed four times for 5 min each and incubated with 1:1000 Alexa-488 conjugated secondary antibody (Molecular Probes) and 1:5000 Hoechst 33342, for nuclear staining, in 1% BSA in PBS for 2 h at RT. After four washes in PBS, sections were cover with coverslips using Fluoromount-G (Thermo Fisher Scientific) as mounting medium. Confocal microscopy (Nikon eclipse C2+) was used to obtain pictures of both ventral horns per section. Alexa-488 staining area in ventral horn was quantified using ImageJ (NIH, Bethesda, Maryland) using the same background subtraction macro for all GFAP or Iba1 set of images. Automatic background subtraction was performed using ImageJ custom macro. This macro was set up using symptomatic SOD1G93A and non-Tg technical control L5 sections.

Biochemical analyses

Animals were euthanized using CO_2. Brain and spinal cord were dissected on ice and immediately stored at -80°C. Tissues were homogenized in TEN buffer (10 mM Tris-HCl, 1 mM EDTA, 100 mM NaCl, pH 8.0) with proteases and phosphatases inhibitors (Sigma Aldrich). Tissue homogenates were separated into two fractions: 1) for protein analysis, tissue homogenates were diluted in TEN buffer with proteinase and phosphatase inhibitors plus 1% NP-40 and 50 mM iodoacetamide (to inhibit artificial disulfide bond formation); 2) for RNA analysis, tissue homogenates were diluted in TRIzol reagent (Thermo Fisher). Protein fractions were sonicated for 15 sec and quantified using BCA protein assay (Thermo Fisher).

SDS-PAGE and western blot

For SDS-PAGE and WB analysis, protein samples were prepared using 100 mM DTT or nanopure H_2O (to assess the effect of disulfide bonds on protein aggregates) in 5X loading buffer (0.2 M Tris-HCl pH 6.8, 10% SDS, 0.05% bromophenol blue and 20% glycerol). Protein samples were incubated at 95°C for 5 min before SDS-PAGE.

Polyacrylamide gel electrophoresis was performed under denaturing conditions. For SOD1 western blot, polyacrylamide gels under reducing and non-reducing conditions were incubated in running buffer containing 50 mM DTT for 30 min at RT after electrophoresis to ensure equal transfer of SOD1 monomer and high-molecular-weight species in both gels. Proteins were transferred to PVDF membranes and blocked in 5% non-fat dry milk in PBS. Primary antibodies were diluted in blocking solution and incubated over night at 4°C. The following primary antibodies and dilutions were used: sheep anti-SOD1 1:3000 (Merck, 574597); rabbit anti-ERp57 1:2000 (Santa Cruz Biotechnology, H-220); mouse anti-β actin 1:20000 (MP Biomedicals, C4). Membranes were washed thrice in 0.1% Tween in PBS (PBS-T) for 5 min each and incubated with 1:2000 HRP-conjugated secondary antibodies (Life Technologies) in blocking buffer for 2 h at RT. After washing thrice in PBS-T, HRP signal was developed using ECL method (Thermo Fisher) following manufacturer instructions. HRP signals and protein ladder images were acquired using ChemiDoc Imaging System (BioRad).

Filter trap

For filter trap, sonicated protein fractions were treated or not with 100 mM DTT for 30 min on ice and then diluted in PBS plus 1% SDS (PBS-SDS). Final protein

concentration in PBS-SDS was 0.25 μg/μL to avoid artificial clumping of the membrane pores. Protein samples were vacuum filtered through a cellulose acetate membrane with 0.22 μm pore size. Membrane was then washed once with PBS-SDS and twice with PBS-T for 5 min at RT each and blocked with 5% non-fat dry milk in PBS for 30 min at RT. Membrane was incubated with sheep anti-SOD1 1:3000 (Merck, 574597) primary antibody over night at 4°C diluted in blocking buffer. Membranes were washed thrice in PBS-T for 5 min each and incubated with 1:2000 HRP-conjugated secondary anti-sheep antibody (Life Technologies) in blocking buffer for 2 h at RT. After washing in PBS-T, filter trap was developed using ECL method (Thermo Fisher) following manufacturer instructions. HRP signals images were acquired using ChemiDoc Imaging System (BioRad).

RNA isolation, reverse transcription and real time PCR

For RT-qPCR, a total of 1 μg RNA was prepared from tissue using TRIzol reagent (Thermo Fisher) following manufacturer instructions. cDNA was synthesized with SuperScript III (Thermo Fisher) using random primers p(dN)6 (Roche) according to manufacturer instructions. Quantitative real-time PCR reactions employing EvaGreen™ reagent (Biotium) in a mix of 4 μL of 1:20 cDNA: nuclease-free water dilution, 0.5 μL of 10 μM primers, 10 μL of EvaGreen™ and 7.5 μL of nuclease-free water in a final volume of 20 μL. qPCR was performed in Stratagene Mx3000P system (Agilent Technologies). Thermal profile used for real time PCR was: 1 denaturing cycle of 95°C for 10 s; 40 amplification cycles of 95°C for 15 s, 60°C for 18 s, 72°C for 15 s; 1 final amplification cycle of 95°C for 15 s, 25°C for 1 s, 70°C for 15 s and 95°C for 1 s. The relative amounts of mRNAs were calculated from the values of comparative threshold

cycle by using *Actin* mRNA as control. RT-qPCR primers used in this work are detailed in Table I.

Table I. Primers used in RT-qPCR and genotyping.

Gene	Sequence	Application	Reference
SOD1G93A transgene	Forward: 5'-CAT CAG CCC TAA TCC ATC TGA-3' Reverse: 5'-CGC GAC TAA CAA TCA AAG TGA-3'	Genotyping and RT-qPCR	(Alexander et al. 2004)
Sod1 mouse	Forward: 5'-AAC CAG TTG TGT TGT CAG GAC-3' Reverse: 5'-CCA CCA TGT TTC TTA GAG TGA GG-3'	RT-qPCR	This work
IL-2	Forward: 5'-CTA GGC CAC AGA ATT GAA AGA TCT-3' Reverse: 5'-GTA GGT GGA AAT TCT AGC ATC ATC C-3'	Genotyping	(Alexander et al. 2004)
ERp57 transgene	Forward: 5'-AAT TCC TGG ATG CTG GGC ACA AAC-3' Reverse: 5'-TCT GCT TGT CAT CGT CGT CCT TGT-3'	Genotyping	(Castillo et al. 2015; Torres et al. 2015)
ERp57 human/mouse	Forward: 5'-GTC ATA GCC AAG ATG GAT GCC-3' Reverse: 5'-TTA ATT CAC GGC CAC CTT CAT A-3'	RT-qPCR	This work
Xbp1s	Forward: 5'-TGC TGA GTC GGC AGC AGG TG-3' Reverse: 5'-GAC TAG CAG ACT CTG GGG AAG-3'	RT-qPCR	This work
Chop	Forward: 5'-TGG AGA GCG AGG GCT TTG-3' Reverse: 5'- GTC CCT AGC TTG GCT GAC AGA -3'	RT-qPCR	This work

Electromyography (Compound Muscle Action Potential)

For electrophysiological analysis of gastrocnemius and tibialis anterior muscles, mice were anesthetized using isoflurane/oxygen mixture supplied by the precision vaporizer RC2 Rodent Circuit Controller Anesthesia System (VetEquip Inc.). These muscles are well known to show denervation in mutant SOD1 mice models corresponding to the first symptoms of motor problems (Mancuso, Osta, and Navarro 2014). Mice were laid on a

non-conductive plastic procedure bed. A laptop and the Power lab 26T data acquisition system with LabChart software for data analysis (ADInstruments, New South Wales, Australia) were used. Two electrode pairs were used. One pair for recording and the other one for delivering the electrical stimulus. Recording electrode pair: a positive needle electrode was inserted intramuscularly to record Compound Muscle Action Potential (CMAP). Its ground electrode was placed subcutaneously in the ipsilateral paw. Stimulus electrode pair: ground electrode for the stimulus was inserted in the perianal region. The positive electrode for stimulation was manually placed on the surface of the skin (without insertion) at the lumbar spine region (Fig. 19A). The stimulation protocol consisted in a single stimulus of 20 mA given at the fifth second after protocol initiation. This latency time was used to ensure correct position of stimulation electrode because is the only electrode held by hand. CMAP was calculated as the total amplitude of the sinusoidal recording (half period voltage amplitude) (Fig. 19B). At least two sinusoidal responses were recorded at two different regions for each muscle. For CMAP time course experiment, the right hind limb was assessed over time. Final CMAP value for each muscle at each time point was defined as the maximum value obtained in that session, since it is interpreted as the maximum electrical response capacity of the motor units.

Statistical analysis

Data were compared using One-way ANOVA or Two-way ANOVA for unpaired groups followed by multiple comparison post-test (Bonferroni's *post hoc* Test) to compare more than two groups, as stated in each figure. Student's *t*-test was performed for unpaired group comparison between two groups; Log-rank test was performed to evaluate significance in Kaplan-Meier survival curves. In all plots, *p* values are shown as

indicated: * $p < 0.05$, ** $p < 0.01$, and *** $p < 0.001$; **** $p < 0.0001$; **** < 0.0001 and were considered significant.

RESULTS

Characterization of ERp57-Tg transgenic mice

The development of this thesis contributed to the characterization of the transgenic mouse line overexpressing human wild-type ERp57 (ERp57-Tg mice) at phenotypic and histological levels, leading to original papers describing physiopathological roles of ERp57 in the CNS and PNS that complemented our study in the SOD1G93A ALS model (Torres et al. 2015; Castillo et al. 2015) (see discussion section for further details). Moreover, ERp57-Tg mice were further characterized at histological motor unit level due its relevance in ALS context.

ERp57-Tg construct (Fig. 8A) is expressed in spinal cord, a central component of ALS pathology. In this tissue, *ERp57* is 9- and 2-fold overexpressed at mRNA and protein levels, respectively, compared to non-Transgenic (non-Tg) littermates (Fig. 8B and C). Human and mouse ERp57 have the same length (505 aa) and FLAG tag is 8 aa adding 1 kDa approximately. This difference cannot be resolved in 10% SDS-PAGE used in this analysis (Fig. 8C). Moreover, immunofluorescence analysis revealed ERp57 overexpression in motor neurons of the spinal cord ventral horn (Fig. 8D) as discriminated by morphology (Fig. 8D inset). ERp57-Tg is also expressed in muscle cells of the tibialis anterior muscle (Fig. 8E) as can be discerned by the pattern of FLAG staining.

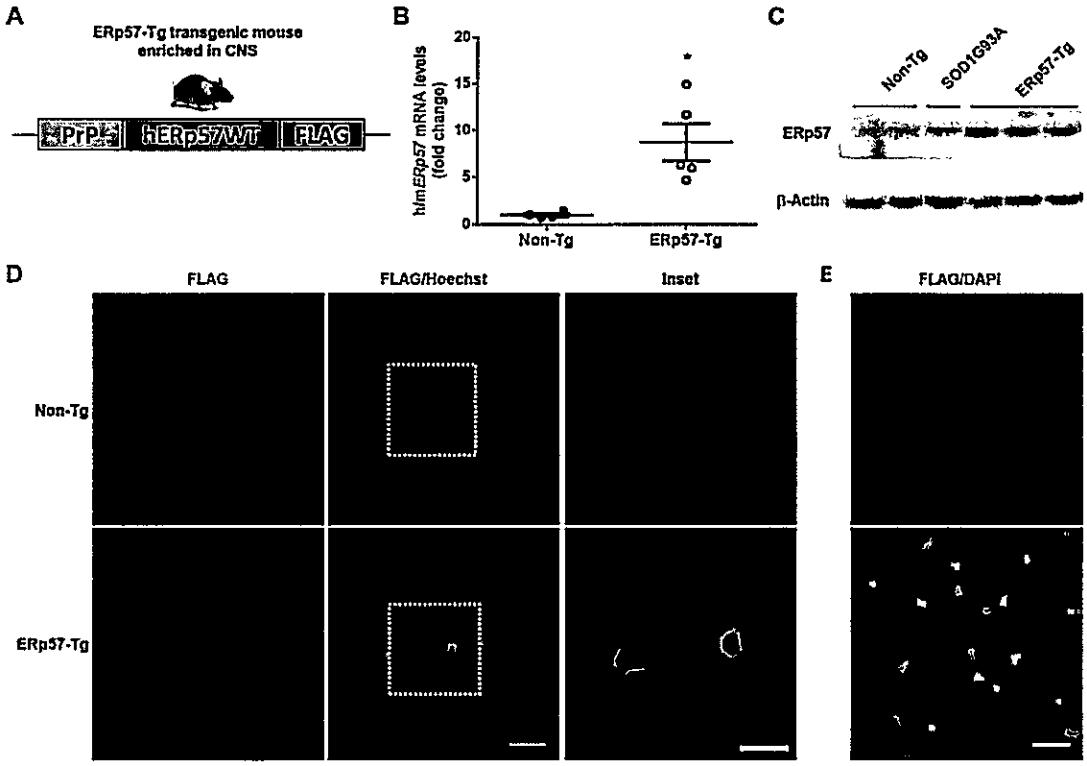

Figure 8. ERp57 transgene expression in spinal cord and muscle. A) ERp57-Tg transgene scheme. Human wild-type ERp57 is expressed under the control of Prion protein promoter to assure central nervous system enrichment. **B)** RT-qPCR analysis of human and mouse *ERp57* (h/mERp57) mRNA in lumbar spinal cord. Primers used amplify both the mouse endogenous *Erp57* and human transgenic *ERp57* by hybridization on a conserved region (100% identity) between both forms. *ERp57* mRNA is expressed as fold change compared to non-Tg. Mean ± SEM. t-test with *p* value: * < 0.005. **C)** Western blot analysis of lumbar spinal cord protein samples using anti-ERp57 or anti-β-Actin as indicated. Each lane corresponds to an independent mouse of the indicated genotype. There is no expected difference in apparent molecular weight between endogenous and human ERp57 with FLAG tag because of the length of FLAG tag (8 aa) and the resolving capacity of 10% gels SDS-PAGE used in this analysis. **D)** Anti-FLAG staining (red) shows ERp57 transgene expression in transversal sections of spinal cord of ERp57-Tg mice. FLAG/Hoechst merged images indicate FLAG staining in motor neurons plus Hoechst nuclear staining. Scale bar: 100 μm. Inset is digital zoom of dotted white boxes. Inset scale bar: 50 μm. **E)** Anti-FLAG staining (green) shows ERp57 transgene expression in transversal sections of tibialis anterior muscle along with DAPI nuclear staining (blue). Scale bar: 50 μm.

Several studies have shown ER stress in spinal cord of SOD1G93A ALS mouse model (Sun et al. 2015; Saxena, Cabuy, and Caroni 2009; de L'Etang et al. 2015; Hetz et al. 2009; J. D. Atkin et al. 2006). Thus, we investigated whether ERp57 overexpression alters susceptibility to ER stress in spinal cord tissue of mice treated with the ER stressor tunicamycin. Acute tunicamycin treatment via intraperitoneal injection induces robust ER stress in spinal cord as detected by induction of *Xbp1s* and *Chop* mRNA, markers for adaptive and terminal UPR, respectively. ERp57 overexpression, however, did not modulate susceptibility to ER stress in this pharmacological model (Fig. 9). To determine the possible involvement of ERp57 in SOD1 expression, we measured endogenous mouse *Sod1* mRNA levels. Despite the trend of *Sod1* upregulation in ERp57-Tg mice, there is no statistically significant difference comparing ERp57 transgenic mice to non-transgenic littermates at basal and ER stress conditions (Fig. 9).

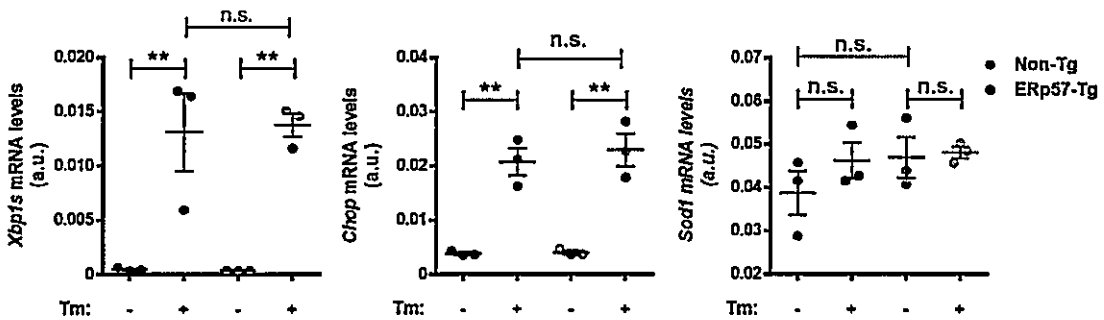

Figure 9. ER stress response and SOD1 expression in ERp57 transgenic mice. mRNA levels of Xbp1s (adaptive UPR marker), Chop (terminal UPR marker) and endogenous mouse *Sod1* were analyzed in spinal cord of mice 24 h after one treatment i.p. with 5 µg/g tunicamycin. Each dot represents one animal. Tm: Tunicamycin treatment (+) or 5% DMSO treatment as vehicle (-). Mean ± SEM. One-way ANOVA with Bonferroni's *post-hoc* test was performed. *p* value: ** < 0.01. n.s: non-significant.

Mice expressing ALS-linked mutant forms of ERp57 as well as *Erp57* conditional knockout in the CNS develop NMJ alterations (Sepúlveda 2015; Woehlbier et al. 2016). Thus, NMJs were analyzed to verify integrity of motor units in ERp57-Tg mice. Diaphragm muscle, a closely flat muscle, was investigated due to its technical advantage for NMJs morphometric analysis (Fig. 10). NMJ shapes were classified as healthy (pretzel-like) or altered (fragmented, O shaped, C shaped or dismantled) (Fig. 10B). There was no difference in NMJ number and shape between ERp57-Tg mice and non-transgenic littermates (Fig. 10C and D).

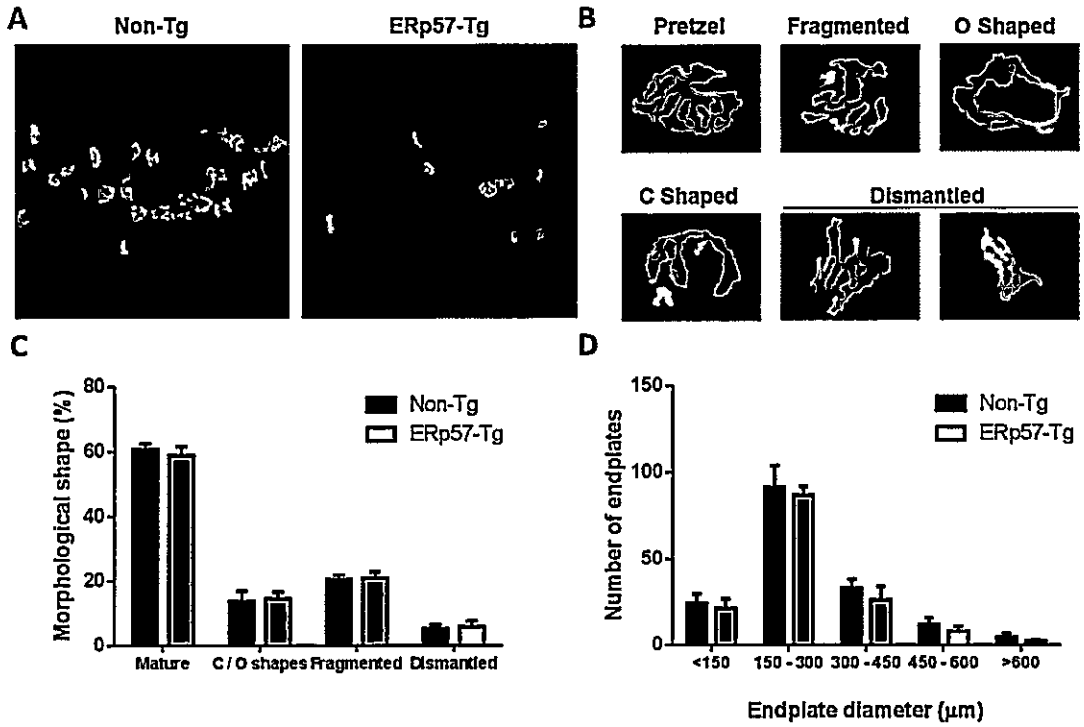

Figure 10. Morphometric analysis of diaphragm endplates. A) Example images of acetylcholine enriched muscle endplates stained with α-bungarotoxin-Alexa480 (green) from non-Tg or ERp57-Tg eight months old mice. **B)** Examples of possible endplate morphologies analyzed ranging from healthy and functional (pretzel shape) to transitional/unhealthy shapes (fragmented, O shaped, C shaped and dismantled). "Pretzel" shape consist in NMJs separated in four or more fragments; "O" and "C" shapes have less complex densities. "Dismantled" shape has no internal lines. Adapted from (Woehlbier et al. 2016). **C)** Endplates shape distributions of non-Tg and ERp57-Tg mice as percentage of total. **D)** Endplate histograms in function of diameter. For each animal, morphology of > 200 structures were manually quantified for morphological shape (C) and number (D) analyses. Five animals per genotype were analyzed for each parameter. Mean ± SEM. One-way ANOVA with Bonferroni's *post-hoc* test was performed. There is no difference between genotypes. This analysis was performed in collaboration with Dr. Juan Pablo Henriquez's Laboratory at Universidad de Concepción, Chile.

To obtain detailed information of NMJ endplates, different morphometric parameters were analyzed after 3D reconstruction of α-bungarotoxin signal at the diaphragm (Fig. 11A). There were no differences in volume, area, axonal swelling or number of clusters between non-Tg and ERp57-Tg mice (Fig. 11B, C, D and E) indicating that ERp57 overexpression in motor neurons and muscle does not alter the structure of the NMJ endplate.

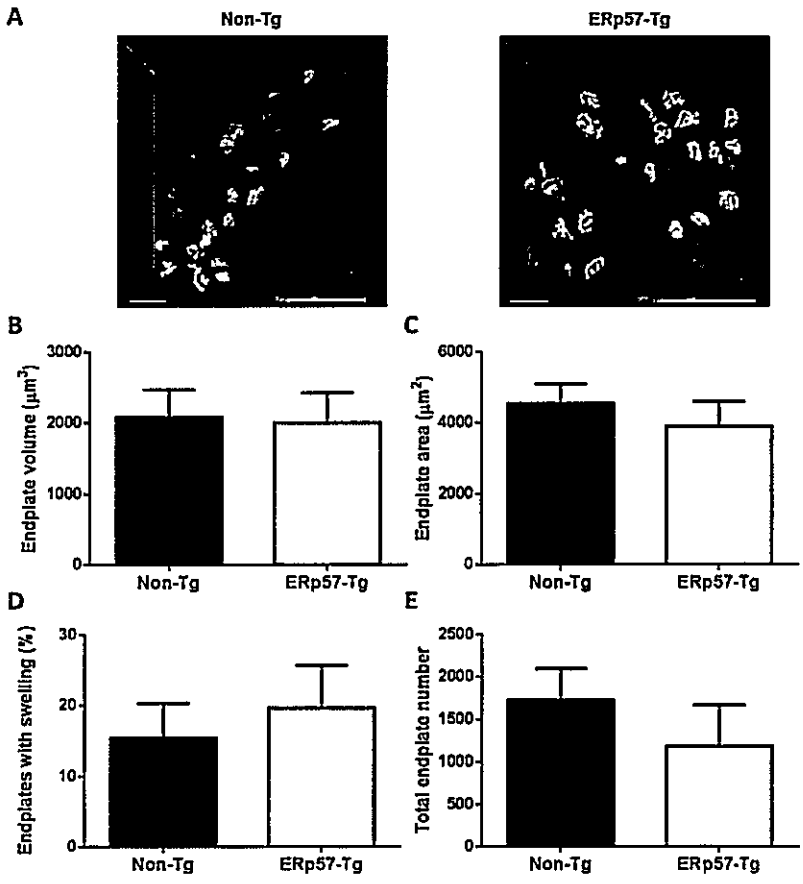

Figure 11. Diaphragm endplates 3D reconstruction and morphological analysis. A) Example images for diaphragm endplate 3D reconstructions using ImageJ software with heat map ranging between higher (red) and smaller (blue) volumes from non-Tg and ERp57-Tg eight months old mice. Scale bar: 50 µm. **B)** Endplates volume and **C)** area analysis. **D)** Percentage of total endplates with swelling. **E)** Total number of endplates in analyzed diaphragms. A total of 40 to 50 endplates were analyzed for each animal in B), C) and D). Total endplate number for each animal was count using 3D object counter plugin for ImageJ software in E). Five animals per genotype were analyzed for each parameter. Mean ± SEM. Student t-test was performed. There are no differences between genotypes in B), C), D), and E). This analysis was performed in collaboration with Dr. Juan Pablo Henriquez's Laboratory at Universidad de Concepción, Chile.

Tibialis anterior muscle, largely innervated by fast-fatigable (FF) motor neurons, is one of the first muscles denervated in SOD1G93A mice (Mancuso, Osta, and Navarro 2014) and was analyzed for histological integrity and fiber type composition (Fig. 12). There was no overt change in muscle fibers integrity (Fig. 12A) or surface area analyzed in transversal sections of the muscle (Fig. 12B). Fast- and slow-fatigable muscle fibers were analyzed using *in situ* enzymatic reaction of nicotinamide adenine dinucleotide tetrazolium reductase (NADH-TR) to assess they oxidative metabolism (Fig. 12C). The ratio of fast to slow fibers was shifted to higher content of slow fiber type in ERp57-Tg mice (Fig. 12D).

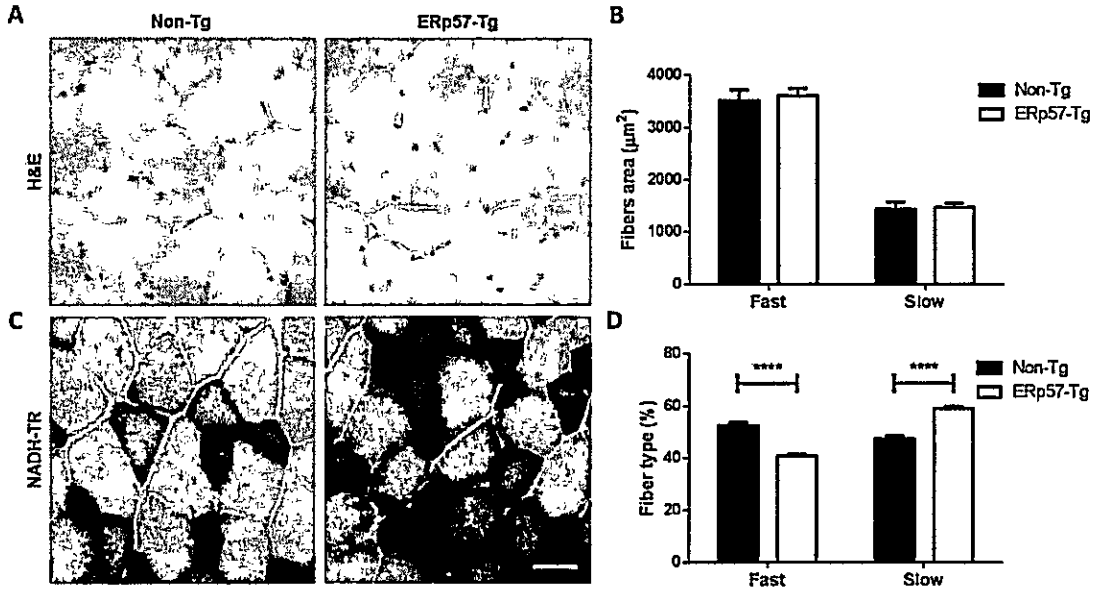

Figure 12. Tibialis anterior muscle fibers analysis. A) Representative hematoxylin and eosin (H&E) staining of transversal sections of tibialis anterior muscle from non-Tg or ERp57-Tg eight months old mice. **B)** Quantification of fibers area using H&E staining. **C)** Representative NADH-TR *in situ* oxidative reaction staining of transversal sections of tibialis anterior muscle. Slow fiber types are more oxidative than fast type and develop dark blue staining by NADH-TR staining. **D)** Quantification of fibers type as percentage of total using NADH-TR staining. Five animals per genotype were analyzed for B) and D). Mean ± SEM. One-way ANOVA with Bonferroni's *post-hoc* test was performed. *p* value: **** < 0.0001. Scale bar for (A) and (C): 50 µm. This analysis was performed in collaboration with Dr. Juan Pablo Henriquez's Laboratory at Universidad de Concepción, Chile.

Taken together, these data show ERp57-Tg construct expression in both main components of the motor unit, i.e. the spinal motor neuron and muscle cells; and this overexpression induces change in muscle fiber type composition in tibialis anterior muscle without affecting fiber integrity. Number and morphology of diaphragm's NMJ endplates are also not modulated by ERp57-Tg transgene. Whether ERp57 expression in muscle is contribution of fibroblast or presynaptic terminals is not known. The levels of overexpression compared to non-Tg muscles remains to be addresses at mRNA and protein levels.

Analysis of ERp57 contribution to disease progression in mutant SOD1 mouse model

In order to address the impact of modulating the levels of ERp57 in ALS pathogenesis and progression, ERp57-Tg mice were breed with SOD1G93A ALS model mice (see Materials and Methods for further strain details). SOD1G93AxERp57-Tg double transgenic mice were obtained by breeding SOD1G93A male with ERp57-Tg female mice to avoid potential muscular problems interfering with pregnancy in SOD1G93A females. Double transgenic mice were viable and born on Mendelian rate (Table II) with no overt deleterious phenotype.

Table II. Animals generation rate from SOD1G93A and ERp57-Tg breeding.

		Non-Tg		ERp57-Tg		SOD1G93A		SOD1G93AxERp57-Tg		Total
	Gender	Males	Females	Males	Females	Males	Females	Males	Females	
Observed	No.	17	17	9	11	15	10	11	18	108
	%	15,7	15,7	8,3	10,2	13,9	9,3	10,2	16,7	100
	Total %	31,5		18,5		23,1		26,9		100
Expected	%	12,5	12,5	12,5	12,5	12,5	12,5	12,5	12,5	100
	Total %	25		25		25		25		100

The SOD1G93A and double transgenic mice (12 and 21 animals cohort, respectively) were closely monitored over the disease course until end-stage to determine lifespan. The ERp57-Tg and non-transgenic (non-Tg) littermates were also monitored over the entire period as control. It has been reported that C57BL/6 background mice have a median lifespan of 73 months approximately (around 2.4 years) (Neff et al. 2013). Despite initial predictions, the lifespan of double transgenic male (158 ± 4.6) or female (164 ± 9.8, mean ± SD) mice were the same as the SOD1G93A model (161 ± 7.3 and 163 ± 10.1 for male and female mice, respectively (mean ± SD)) (Fig. 13A). There were no differences between genders within genotypes (Fig 14A). The average lifespan per genotype was 162 ± 8.3 and 162 ± 9.3 for SOD1G93A and double transgenic mice, respectively (mean ± SD) (Fig. 14B). As expected, Non-Tg and ERp57-Tg mice did not die during this time course and were euthanized at same age of end stage SOD1G93A and double transgenic mice (around 180 days) as age-matched control groups.

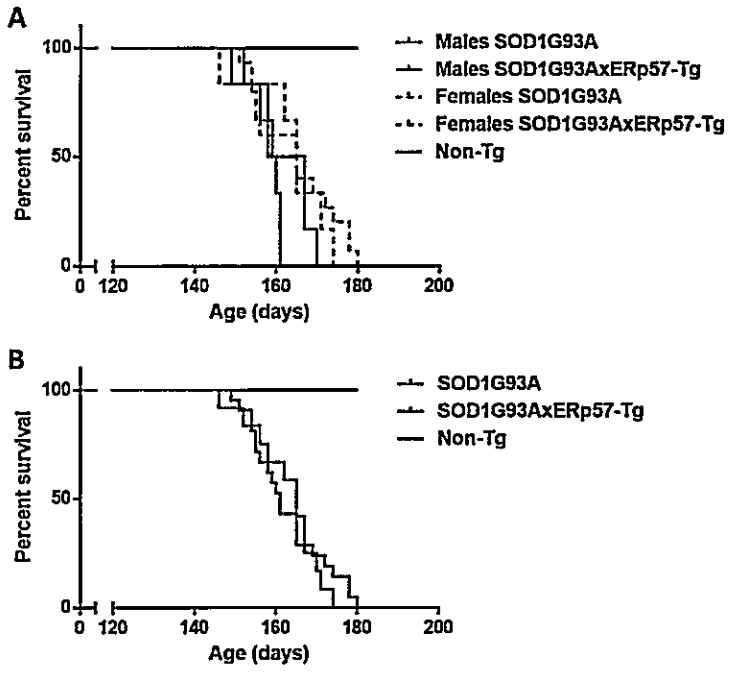

Figure 13. Survival analysis of SOD1G93A and double transgenic animals. End point was considered as the time point when the mouse is unable to right itself within 10 seconds when put on its side. **A)** Kaplan-Meier survival plot of male (N: SOD1G93A: 6; double transgenic: 6) and female mice (N: SOD1G93A: 6; double transgenic: 15). **B)** Kaplan-Meier survival plot of total animals per genotype. Log-rank test was performed to analyze survival curves. There is no difference between genotypes. Control non-Tg line in A) and B) is used as reference of survival and were euthanized around 180 days as an age-matched control group.

Disease course in SOD1G93A mice is characterized by the progressive loss of body weight (B. J. Turner and Talbot 2008). Mice from all genotypes gained body weight normally until 3 months of age when female mice expressing SOD1G93A (single and double transgenic) showed reduced gain of weight compared to control littermates (Fig. 14). Disease onset, defined by 5% loss of the maximum body weight, was not altered in double transgenic mice compared to SOD1G93A littermates (& in Fig. 14).

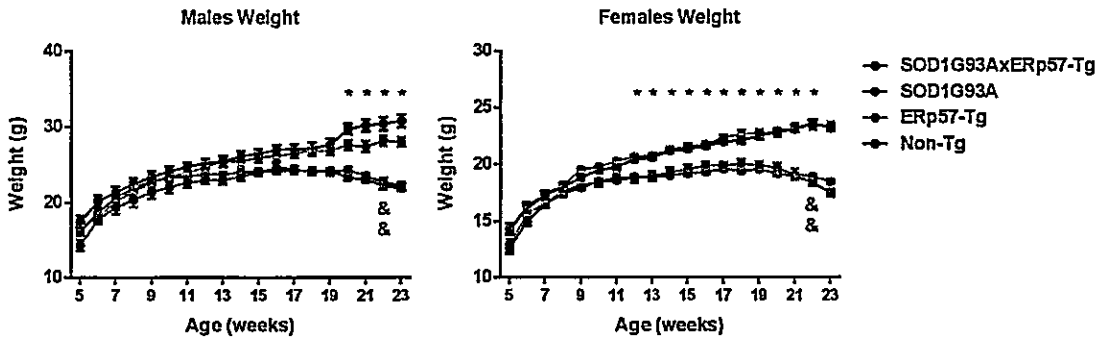

Figure 14. Mouse body weight by genotype and gender. Male and female mouse body weight was measured once a week over the entire lifespan (n = 6-17). Mean ± SEM. Two-way ANOVA followed by Bonferroni's *post hoc* test for multiple comparisons. *: indicates significant difference between mutant SOD1G93A (single or double transgenic) to non-Tg and ERp57-Tg control littermates with p value < 0.001. &: indicates disease onset by body weight criteria, i.e. a 5% drop of maximum body weight reached.

The visual aspect of double transgenic mice was followed by one lab partner observer blinded to the genotype once a week over the entire lifespan assigning a "Clinical Score" for each mouse (Fig. 15) (see Material and Methods section for Clinical Score details). This score takes into account four visual aspects of mice: kyphosis, absence of grooming, paralysis (Fig. 15A and B) and clasping reflex (Fig. 15C and D). Clinical Score starts with value equals to zero when SOD1G93A mice are indistinguishable from non-Tg littermates and progressing up-ward over disease course (Fig. 15E and F). Non-Tg and ERp57-Tg sometimes were assigned a score of 1 due to blinded observations, considered as experimental "noise". Disease onset by Clinical Score analysis (& in Fig. 15E and F) was defined as the up-ward inflection point above the noise (the highest value of non-Tg or ERp57-Tg, i.e. a score of 0.8). Disease onset for SOD1G93A was 128 ± 1.3 and 116 ± 2.1 days of age for male and female mice, respectively (mean ± SEM); whereas for double transgenic it was 128 ± 0.4 and 123 ± 2.1 days of age for male and female mice, respectively (mean ± SEM). Overall, male SOD1G93A (single and double transgenic) mice showed the same disease onset defined by Clinical Score, but double transgenic female mice showed a delay by one week compared to SOD1G93A littermates (& in Fig. 15 E and F).

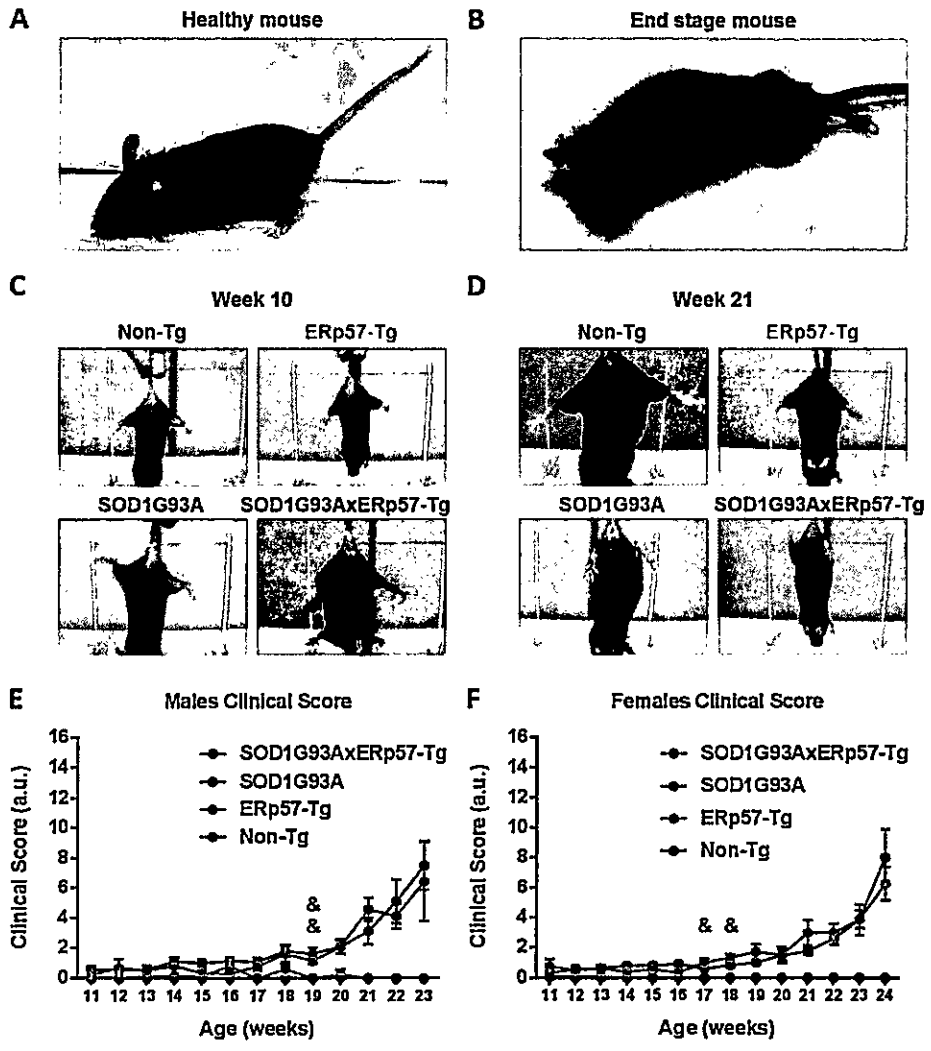

Figure 15. Clinical disease progression in SOD1G93A and double transgenic mice. A) Healthy non-Tg mice display normal curvature of the spine, clean fur and normal gait. **B)** SOD1G93A mice at end stage display kyphosis, dirty fur and paralysis (as can be seen in hind limb dragging). **C)** At pre-symptomatic stage (10 weeks old) SOD1G93A and double transgenic mice display healthy clasping reflex (fully extending hind limbs when grabbed by the tail) similar to non-Tg and ERp57-Tg mice. **D)** At symptomatic stage (21 weeks old), SOD1G93A and double transgenic mice cannot extend their hind limbs, while non-Tg and ERp57 still have normal clasping reflex. **E)** and **F)** Clinical score progression in male and female mice, respectively. Disease onset (&) is defined as the time point when clinical score is above 0.8 points with an up-ward trend (see Material and Methods for details). n = 6-13. Mean ± SEM.

Motor performance was assessed using Rotarod (Fig. 16) and Hanging wire test (Fig. 17). On Rotarod, each mouse is placed on a rotating rod and challenged by an accelerated protocol (see Material and Methods for details). The latency time to fall from the rotating rod on the platform below is a measure of motor coordination and equilibrium (Fig. 16A). The time point corresponding to the downward inflection of the curve marks disease onset (see Material and Methods for details). There was a progressive decline in motor performance of SOD1G93A and double transgenic male mice (Fig. 16B left panel) with a disease onset at 74 ± 1.7 and 73 ± 1.7 days, respectively (mean ± SEM). On the other hand, double transgenic female mice (Fig. 16B right panel) had a delayed decline in Rotarod performance by one week compared to SOD1G93A with 73 ± 1.8 and 66 ± 2.3 days old, respectively (mean ± SEM). There were no differences between non-Tg and ERp57-Tg in male and female mice (Fig. 16B).

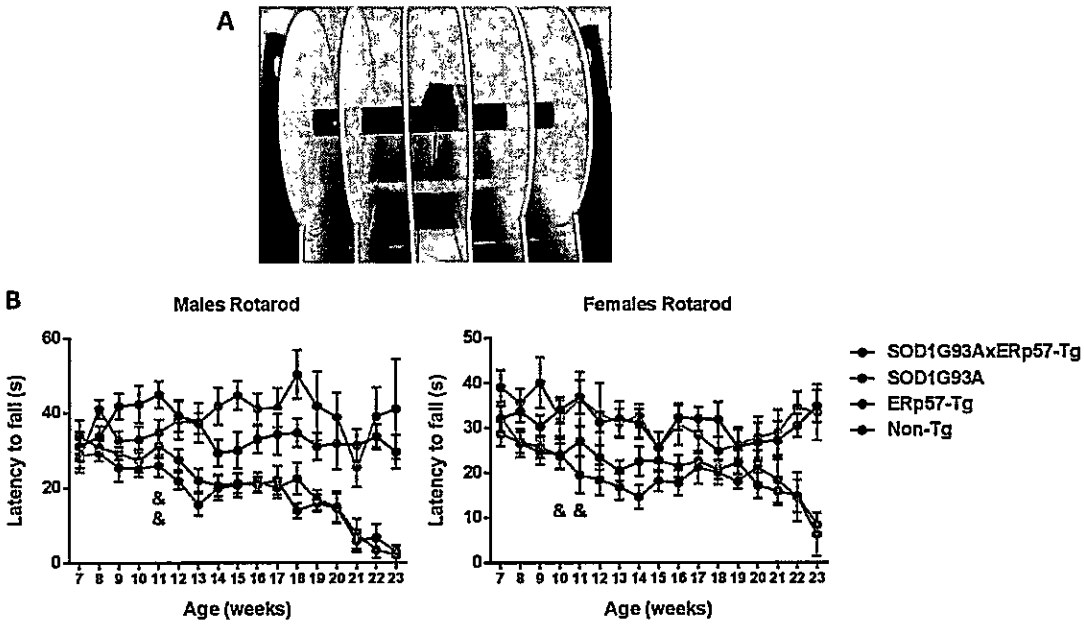

Figure 16. Rotarod motor performance. A) Rotarod test was used placing a mouse on a rotating rod at constant accelaration. Latency to fall corresponds to the time between mouse falls onto a platform after beginning of acceleration. **B)** Male and female motor performance over disease course. Rotarod test was performed once a week over entire lifespan since 7 weeks old. Disease onset (&) is define as the time point of the downward inflection of the curve (see Material and Methods for details). n = 6-14. Mean ± SEM.

Hanging wire test score is a measure for motor coordination, equilibrium and motor strength. Each mouse is placed on a horizontal bar and challenged to reach a vertical pole and then the floor within 30 seconds (Fig. 17A). An arbitrary score is assigned in function of mouse performance with a score of 6 as the maximum taking into account the use of fore limbs, hind limbs and the tail (see Material and Methods for details). As expected, mice harboring SOD1G93A had a progressive motor decline (Fig. 17B). Disease onset was defined as the downward inflection point of the curve. Male and female double transgenic mice had an approximately one week delay in disease onset compared to SOD1G93A mice (Fig. 17B). For SOD1G93A and double transgenic male mice onset was at 58 ± 0.5 and 68 ± 1.1 days old, respectively (mean ± SEM) (Fig. 17B left panel). For SOD1G93A and double transgenic female mice onset was at 94 ± 1.1 and 100 ± 0.6 days old, respectively (mean ± SEM) (Fig. 17B right panel). Interestingly, double transgenic male mice performed significantly better in Hanging wire test than SOD1G93A mice during symptomatic period, indicating an adaptive advantage of enforcing ERp57 expression in ALS (# in Fig. 17B left panel, weeks 17 and 18). Remarkably, differences were also found between ERp57-Tg and non-Tg male mice, where ERp57-Tg presented higher Hanging wire test score for several weeks under basal conditions (* in Fig. 17B left panel).

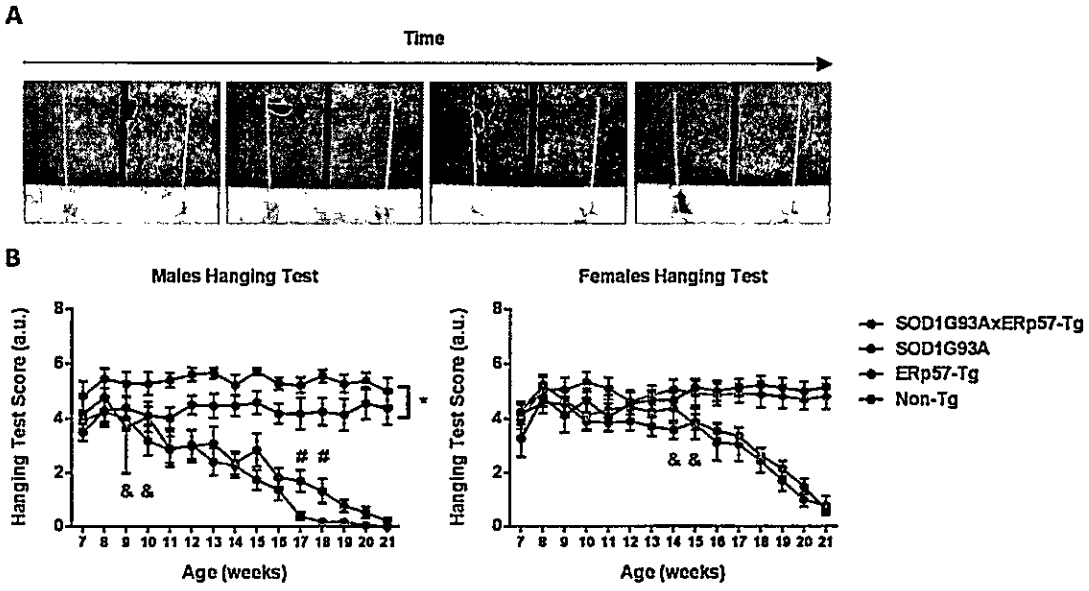

Figure 17. Hanging wire test motor performance. A) Hanging wire test consists in placing a mouse on a horizontal bar and recording the escape response to reach the floor within 30 seconds. An arbitrary score is assigned in function of use of forelimbs and hind limbs and capacity to reach the vertical pole and descend to the floor within 30 sec (see material and methods for details). Time depicts the performance of a healthy mouse that successfully completes the task. **B)** Male and female mice motor performance over disease course. Disease onset (&) is define as the downward inflection point of the curve. n = 6-16. Mean ± SEM. Two-way ANOVA followed by Bonferroni's *post hoc* test for multiple comparisons. There is significant difference of overall performance between non-Tg and ERp57-Tg mice with *p* value: *< 0.05. There is significant difference in motor performance between male double transgenic and SOD1G93A mice (#) at weeks 17 and 18 with *p* value: # < 0.05.

A summary of disease onset by gender for each parameter analyzed is shown in (Fig. 18). Despite there are not differences in body weight onset between genotypes (Fig. 18A), there was a significant delay of one week in disease onset of double transgenic female mice by Clinical Score, Rotarod and Hanging wire test (Fig. 18B, C and D, respectively). As assessed by Hanging wire test, there was a significant delay of seven to ten days in disease onset of double transgenic mice of both genders. Motor performance tests give earlier disease onset compared to visual Clinical Score and body weight measurements.

Together, our assessment of disease onset and progression by different parameters reveals that ERp57 overexpression delays motor decline of SOD1G93A mice without altering lifespan or body weight loss and confers two weeks protection to male mice in Hanging wire test motor performance during symptomatic stage.

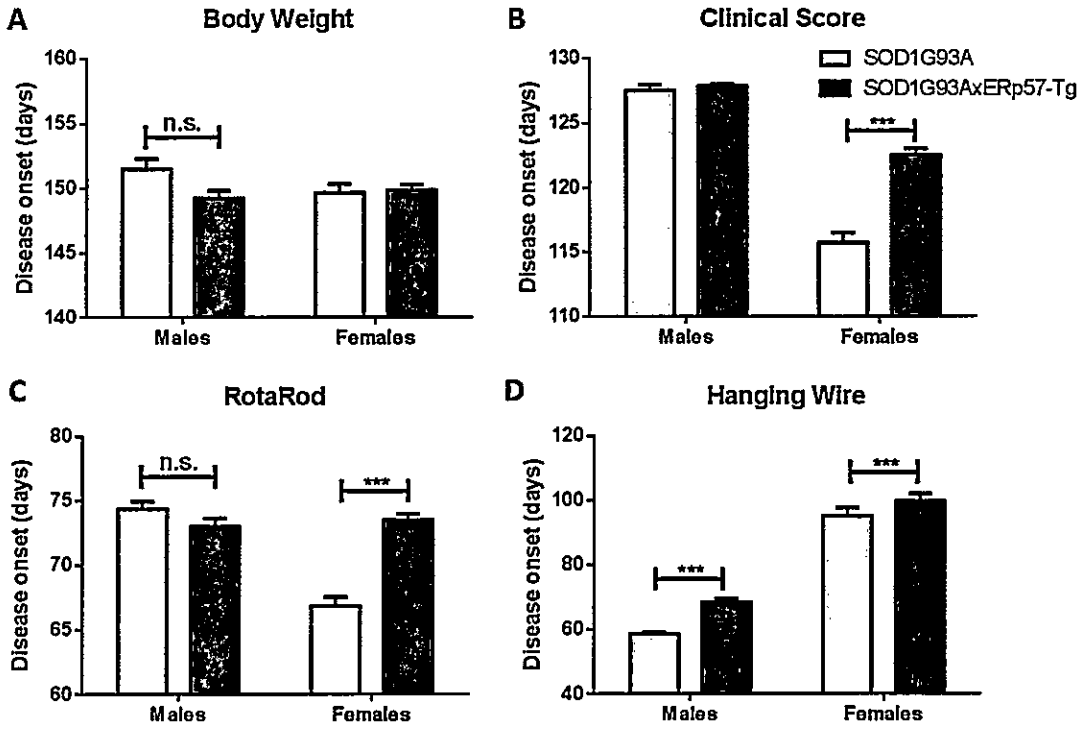

Figure 18. Summary of disease onset as defined by each parameter. Disease onset for each parameter analyzed in this thesis defined as: **A)** Body weight, when body weight dropped 5% from the maximum reached; **B)** Clinical score, when mice score above the threshold level of 1.8 points and upward trend of the curve; **C)** Rotarod, the time point corresponding to the downward inflection point of Rotarod curves; **D)** Hanging wire test, the time point corresponding to the downward inflection point of the Hanging wire curves. n: 6 to 16 animals per genotype per gender were analyzed. Mean ± SD. One-way ANOVA followed by Bonferroni's *post hoc* test for multiple comparisons. *p* value: *** < 0.001. n.s: non-significant. Genotype label in (B) applies for all parameters.

Electrophysiological analysis of SOD1G93AxERp57-Tg mice

Loss of NMJ integrity due to motor neuron denervation is a common characteristic of human ALS and mouse models. This denervation occurs before the symptomatic stage and translates in reduced action potential of muscles (Mancuso, Osta, and Navarro 2014). SOD1G93AxERp57-Tg mice showed a delay in disease onset using motor tests that could be related to pre-symptomatic protective roles of ERp57. For this reason, compound muscle action potential (CMAP) was measured at primary affected muscles (gastrocnemius and tibialis anterior) in early stages of pre-symptomatic period (from 38 to 72 days old). CMAP is an intramuscular measurement of the sum of action potentials at the muscle in response to non-invasive spinal cord electrical stimulation (Fig. 19A). Lower CMAP values reflect motor axons denervation (Fig. 19B). Male and female mice were grouped in order to achieve a significant number for statistical analysis. There is a decline in CMAP values of both muscles before motor test disease onsets in SOD1G93A model (Fig. 19C and D). Importantly, compared to non-Tg mice, double transgenic mice started their denervation one week later than SOD1G93A mice (58 days old compared to 51 days old, respectively) (Fig. 19C and D). Interestingly, there is a longitudinal trend of higher CMAP values in double transgenic compared to SOD1G93A mice that, however, it is not significant (Fig. 19C and D). This data shows that ERp57 overexpression delays denervation of motor units.

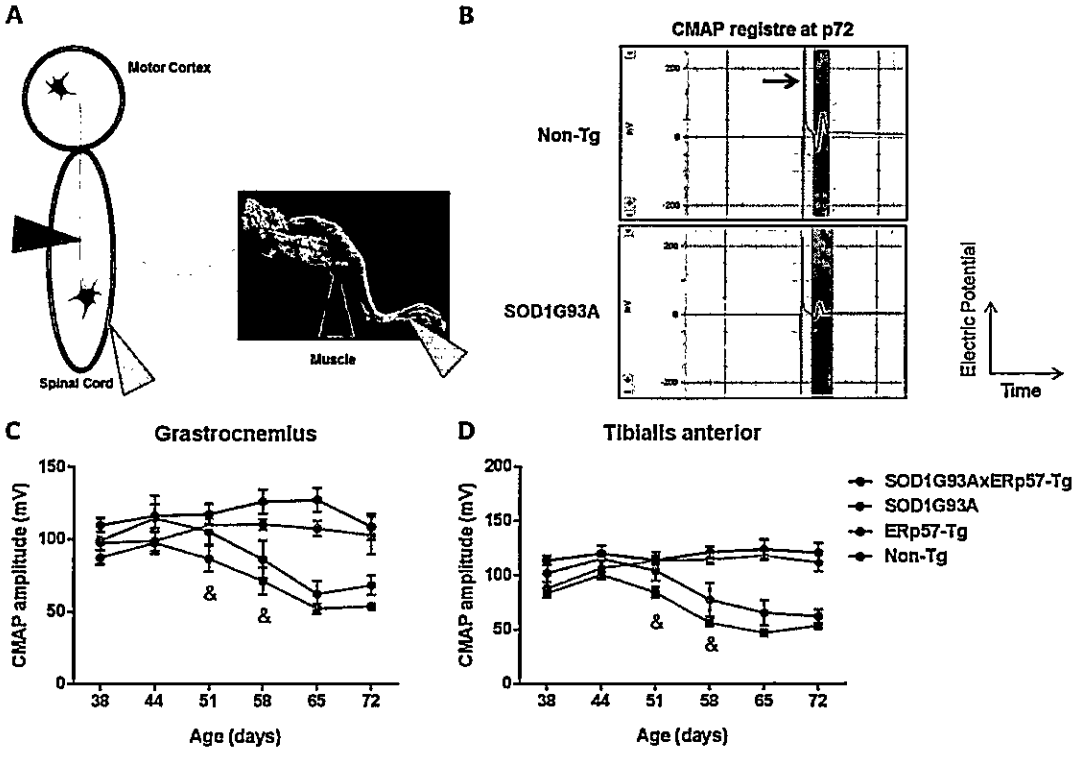

Figure 19. Electromyography analysis of hind limb muscles. **A)** Electromyography set up for compound muscle action potential (CMAP) amplitude recording. Black cells within blue boundaries represent upper and lower motor neurons of motor cortex and spinal cord, respectively. Recording electrode (depicted as solid blue arrowhead (adapted from (Charles et al. 2016)) is placed intramuscularly in gastrocnemius or tibialis anterior muscle. Ground electrode (depicted as dashed blue arrowhead) is placed subcutaneously in the paw. Stimulation electrode (depicted as solid red arrowhead) is placed non-invasively over mouse's column on the lumbar region. Ground electrode for stimulation (dashed red arrowhead) is placed intramuscularly near the perianal region. **B)** Electric potential recording examples. X axis is time. Stimulation protocol consists in a pulse of 20 mA (pointed by black arrow) followed by depolarization and hyperpolarization within the muscle (red line inside grey shadow). CMAP amplitude is calculated as the amplitude between minimum and maximum values of the curve inside grey shadow. Recording of SOD1G93A mouse at p72 shows decreased amplitude compared to non-Tg mouse. CMAP amplitude values from gastrocnemius **(C)** and tibialis anterior **(D)** muscles were measured at pre-symptomatic stages (from p38 to p72) of grouped male and female mice. n = 4-7. Mean ± SEM. Two-way ANOVA followed by Bonferroni's post hoc test for multiple comparisons. There are significant differences

between SOD1G93A or double transgenic mice compared to non-Tg mice starting at (&) with p value < 0.05. There is no significant difference between SOD1G93A and double transgenic mice or between non-Tg and ERp57-Tg mice across time.

Effect of ERp57 on neuritogenesis of NSC34 cell line expressing mutant SOD1

ERp57 has been proposed to be involved in motor neuron neuritogenesis and connectivity. This process is promoted by wild-type ERp57 while abrogated by its ALS-linked mutants (Woehlbier et al. 2016). Furthermore, mutant SOD1 also disrupts this process (Juan Pablo Henríquez's Lab, University of Concepción, unpublished results). Here, the mouse motor neuron-like NSC34 cell line was used to assay how ERp57 could modulate neuritogenesis under mutant SOD1 context. NSC34 expressing human mutant SOD1 (NSC34-SOD1G93A) or human wild-type SOD1 (NSC34-SOD1WT) in a stable fashion were transiently transfected with human wild-type ERp57 (ERp57) or YFP as control (Fig. 20A). Neuritogenesis was induced by serum deprivation for 24 h and percentage of cells with neurites and neurite length were analyzed using ImageJ software (Fig. 20B). Mutant SOD1G93A decreased the number of cells with neurites compared to SOD1WT. Remarkably, ERp57 increases basal neuritogenesis in SOD1WT cells and fully rescues SOD1G93A phenotype (Fig. 20B left panel). Neurite length is not altered by mutant SOD1 or ERp57 expression (Fig. 20B right panel).

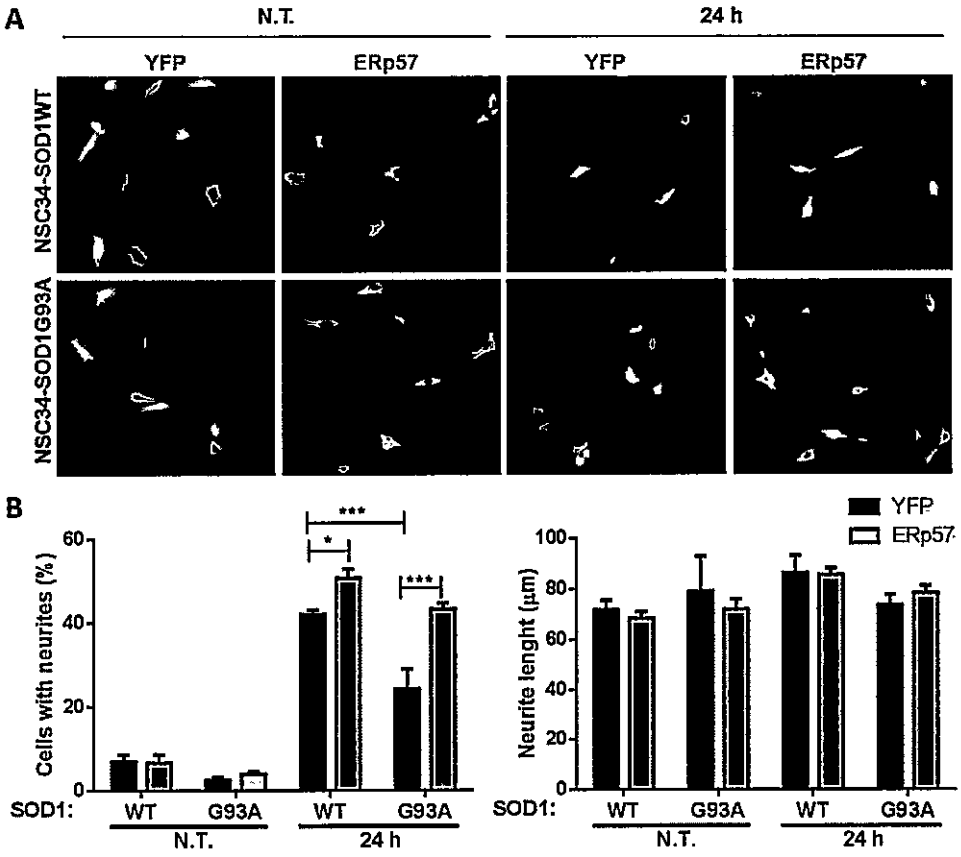

Figure 20. NSC34 neuritogenesis is modulated by ERp57. NSC34 cells expressing human wild-type SOD1 (NSC34-SOD1WT) or mutant SOD1 (NSC34-SOD1G93A) in a stable fashion were transiently transfected with YFP or human wild-type ERp57 coupled to V5 tag (ERp57). Neuritogenesis was induced by serum deprivation for 24 h. Immunofluorescence against V5 was performed to quantify ERp57 transfected cells. N.T: non-treated cells. **A)** Representative microphotograph of NSC34 cells before (N.T.) and after (24 h) serum deprivation visualized using DAPI nuclear staining (blue) and YFP fluorescence or anti-V5 immunofluorescence (green). Scale bar: 20 µm. **B)** Percentage of cells with neurites and mean neurite length from SOD1WT (WT) or SOD1G93A (G93A) expressing cells. For each condition, ten fields from three different experiments were evaluated before (N.T.) and after (24 h) serum deprivation. Cells with neurite were considered as cells having at least one neurite larger than soma diameter. ImageJ software was used for neurite length quantification. Mean ± SEM. One-way ANOVA with Bonferroni's *post-hoc* test was performed. *p* value: * < 0.05; *** < 0.001. There are no differences in (C). This analysis was performed in collaboration with Dr. Juan Pablo Henriquez's Laboratory at Universidad de Concepción, Chile.

Histopathological analysis of SOD1G93AxERp57-Tg mice

Spinal motor neurons loss is a critical histopathological feature of ALS. Motor neuron number was assessed at the lumbar segment of the spinal cord specifically between L5-L2 regions (Fig. 21A and B). This is the neuroanatomical niche of motor neurons that innervate hind limbs and, thus, is the primary affected zone in this mouse model (Lalancette-Hebert et al. 2016). Anti-choline acyltransferase (ChAT) staining specifically label motor neurons and was used to determine motor neuron number (Fig. 21C). SOD1G93A mice had a reduced number of motor neurons in the 1.5 mm of L5 section at end stage (23-24 weeks old) (Fig. 21C and D). This corresponds to around 50% motor neuron loss in this region (Fig. 21D). The remaining motor neurons generally had reduced surface compared to non-Tg or ERp57-Tg motor neurons (Fig. 21C and Fig. 22B). These phenomena occur indistinguishably in male and female mice in this model (Mancuso et al. 2012).

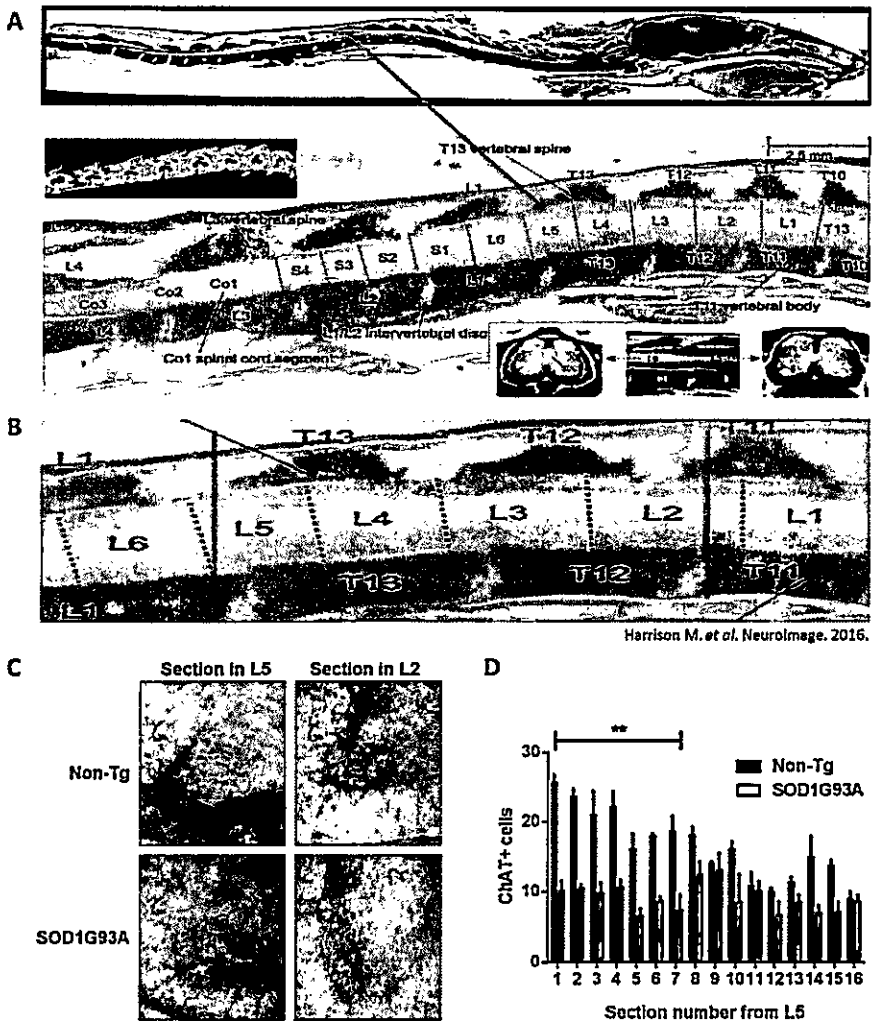

Figure 21. Motor neuron number analysis by serial sections. A) Magnetic resonance imaging of mouse central nervous system with a zoom to spinal cord (pointed by red arrow). Spinal cord segments and vertebras are named T for thoracic, L for lumbar, S for sacral, and Co for coccyx regions. **B)** Lumbar spinal cord showing the cryosectioned region for motor neuron count (L5 to L2 between red vertical bars). Motor neurons innervating hind limbs are located in this region. A) and B) are adapted from (Harrison et al. 2013). **C)** Motor neurons from end stage male mice were stained by anti-ChAT immunohistochemistry on lumbar spinal cord transversal cryosections. **D)** Motor neurons from male mice were counted from section 1 at L5 until section 16 in L2 separated 200 µm from each other, covering a 3.2 mm total region. Three animals per genotype were analyzed. Mean ± SEM. Two-way ANOVA followed by Bonferroni's *post hoc* test for multiple comparisons. **: p value < 0.01.

Spinal cord sections from grouped male and female end stage double transgenic mice were analyzed along with control mice (Fig. 22). Anti-ChAT staining was employed in serial sections from L5 to L2 (Fig. 22A). ERp57-Tg mice had the same number of motor neurons than non-Tg mice (Fig. 22B). SOD1G93A and double transgenic mice had around 50% motor neuron loss compared to non-Tg and ERp57-Tg mice in the first portion of L5 region (Fig. 22C). Total neuron number per section considering whole L5 to L2 region showed the same percentage of motor neuron loss (Fig. 22D). By visual inspection, soma diameter had reduced surface in SOD1G93A and double transgenic mice compared to non-Tg and ERp57-Tg mice (Fig 22A, arrows). ChAT-positive processes were also decreased in density in SOD1G93A and double transgenic mice compared to non-Tg and ERp57 mice (Fig. 22A, arrowheads).

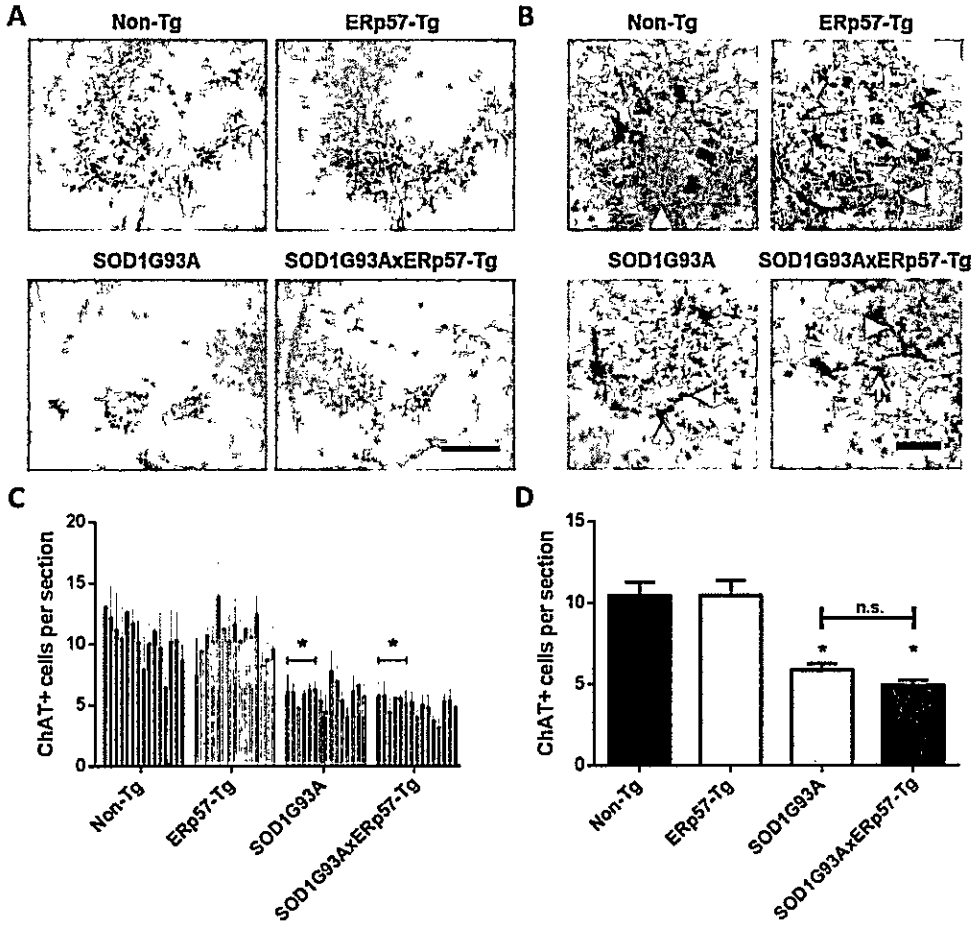

Figure 22. Motor neuron count analysis in SOD1G93AxERp57-Tg mice. A) Representative microphotographs of serial anti-ChAT immunostaining of lumbar spinal cord sections from end stage mice (SOD1G93A and double transgenic) and age-matched controls (non-Tg and ERp57-Tg). Scale bar: 250 μm. **B)** Digital zoom of ventral zone of spinal cords in (A). Arrows point motor neuron somas as example of motor neuron morphology. Arrowheads point ChAT positive processes of motor neurons. Scale bar: 50 μm. **C)** Motor neuron serial count from L2 to L5 (left to right within each genotype) with 200 mm section separation from each other. 3-8 animals per genotype were analyzed. Mean ±SEM. Two-way ANOVA followed by Bonferroni's *post hoc* test for multiple comparisons. *: p value < 0.05. **D)** Motor neuron total count grouping all sections from L2 to L5. Mean ± SEM. One-way ANOVA followed by Bonferroni's *post hoc* test for multiple comparisons. *: p value < 0.05. n.s: non-significant.

Astrogliosis and microgliosis are common histopathological features of ALS and symptomatic stages of SOD1G93A model (M. R. Turner et al. 2013; J P Taylor, Brown Jr., and Cleveland 2016). These two parameters were assessed in grouped male and female end stage mice using anti-GFAP and anti-Iba1 staining, respectively (Fig. 23A and C). There was an increase of astrogliosis and microgliosis in SOD1G93A and double transgenic mice spinal cord measured as percentage of ventral horn area stained with glial marker (Fig. 23B and D). There were no differences in glial activation between these genotypes despite the trend of lower GFAP burden in double transgenic mice (Fig. 23B and D). This gliosis was not restricted to the ventral horn, as white and grey matter of ventral and dorsal portions of the spinal cord were affected too (Fig. 23A and C). Interestingly, basal levels of GFAP or Iba1 staining were not modulated by ERp57-Tg overexpression (Fig. 23B and D).

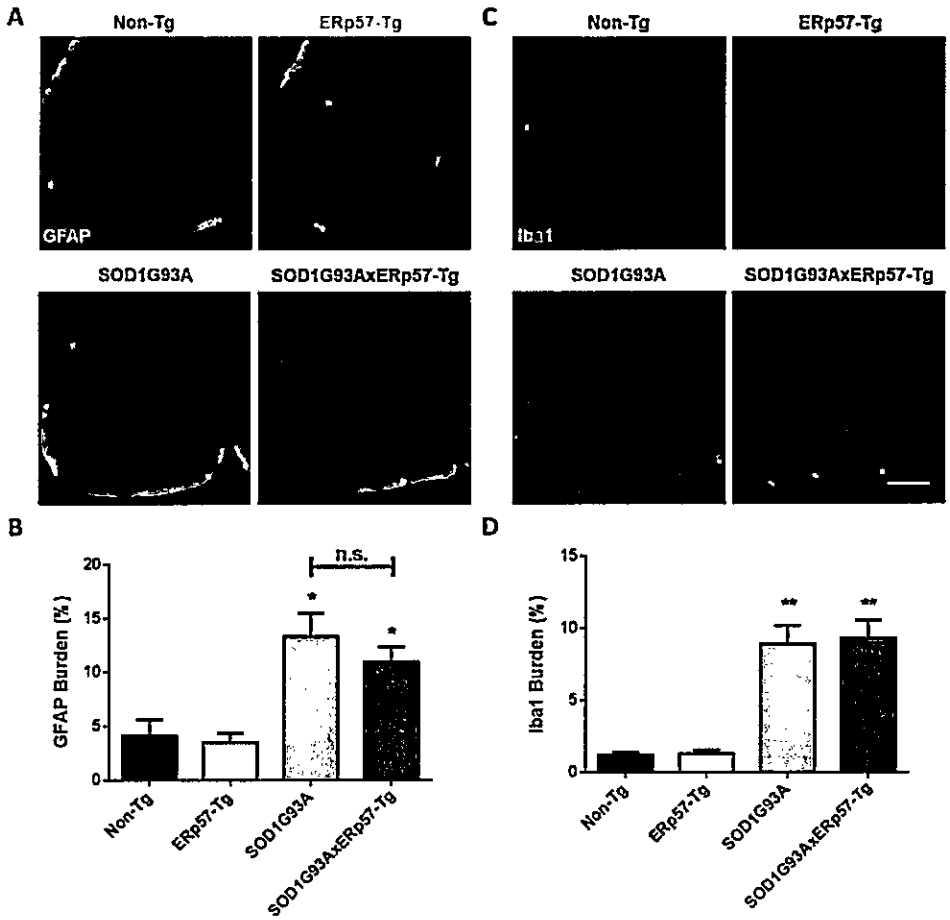

Figure 23. Astrogliosis and microgliosis analysis at lumbar spinal cord. A) Representative microphotographs of anti-GFAP immunostaining of L5 to L2 spinal cord sections from end stage mice (SOD1G93A and double transgenic) and age-matched controls (non-Tg and ERp57-Tg) for astrogliosis analysis. B) GFAP burden quantification after digital noise reduction. GFAP burden is expressed as percentage of GFAP surface staining from total ventral horn grey matter. C) Representative microphotographs of anti-Iba1 immunostaining of L5 to L2 spinal cord sections from end stage mice (SOD1G93A and double transgenic) and age-matched controls (non-Tg and ERp57-Tg) for microgliosis analysis. D) Iba1 burden quantification after digital noise reduction. Iba1 burden is expressed as percentage of Iba1 surface staining from total ventral horn grey matter. 3-8 animals per genotype were analyzed in (B) and (D). Mean ± SEM. One-way ANOVA followed by Bonferroni's *post hoc* test for multiple comparisons. *: p value < 0.05. **: p value < 0.01. * and ** are compared to non-Tg controls. n.s: non-significant. Scale bar applies for (A) and (C): 250 μm.

Biochemical analysis of stress response and SOD1 aggregation in SOD1G93AxERp57-Tg mice

Molecular level characterization was performed to assess whether ERp57 modulates stress response and protein aggregation in mutant SOD1 model. First, transgene expression levels were measured to control genetic interactions between SOD1 and ERp57 (Fig. 24). Cerebral cortex and lumbar spinal cord were analyzed to account for possible differences between the primary ALS affected tissues. Human wild-type *ERp57* mRNA overexpression levels in ERp57-Tg mice are not influenced by the overexpression of *SOD1G93A* in both tissue (Fig. 24 A and C). Human mutant *SOD1* overexpression levels are not altered by *ERp57* overexpression despite the trend of increased levels in spinal cord (Fig. 24B and D). Then, adaptive and terminal UPR were assessed by measuring the gold-standard markers *Xbp1s* and *Chop*, respectively (Fig. 24E and F). There was no difference in the level of these markers between genotypes at disease end stage despite the trend of increased levels in double transgenic animals.

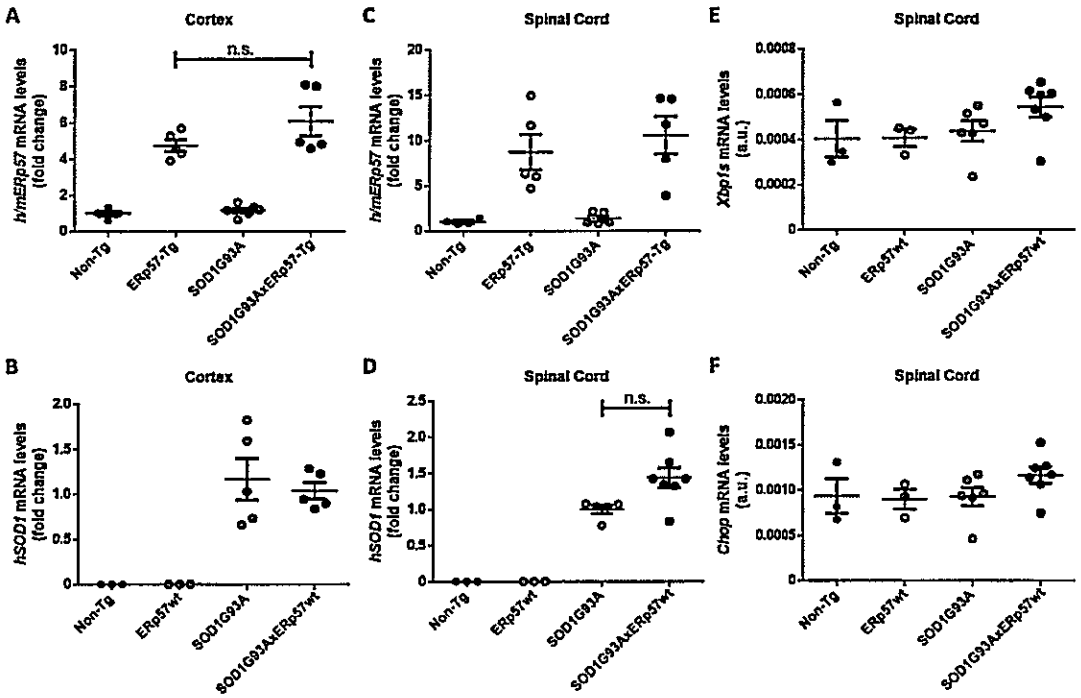

Figure 24. Transcriptional profile analysis of CNS tissue by RT-qPCR. Human and mouse *ERp57* mRNA expression (h/m*ERp57*) in cortex **(A)** and spinal cord **(C)** from end stage mice (SOD1G93A and double transgenic) and age-matched controls (non-Tg and ERp57-Tg). Human *SOD1* mRNA expression in cortex **(B)** and spinal cord **(D)** from end stage mice (SOD1G93A and double transgenic) and age-matched controls (non-Tg and ERp57-Tg). Adaptive **(E)** and terminal **(F)** UPR markers mRNA expression in spinal cord of end stage mice (SOD1G93A and double transgenic) and age-matched controls (non-Tg and ERp57-Tg). 3-7 animals per genotype were analyzed. Each dot represents an independent animal. Mean ± SEM. One-way ANOVA followed by Bonferroni's *post hoc* test for multiple comparisons. n.s: non-significant.

ERp57 protein levels were assessed to find possible modulations of ERp57 overexpression in mutant SOD1 context. As expected for Prion protein promoter, ERp57 is overexpressed in spinal cord (Fig. 25A) and cortex (Fig. 25C) in ERp57-Tg mice compared to non-Tg and SOD1G93A mice. Importantly, ERp57 is further upregulated in lumbar spinal cord from double transgenic mice compared to ERp57-Tg mice (Fig. 25A and B), despite unchanged h/m*ERp57* mRNA levels in double transgenic mice (Fig. 24A and C). Nonetheless, this change in ERp57 protein levels is not replicated in cerebral cortex (Fig. 25C and D), suggesting tissue specific effects of SOD1 and ERp57 interactions. SOD1G93A single transgenic mouse was included as a control, showing an upregulation of ERp57 protein levels at spinal cord, as reported (Hetz et al. 2009; J. D. Atkin et al. 2006), but not in cortex.

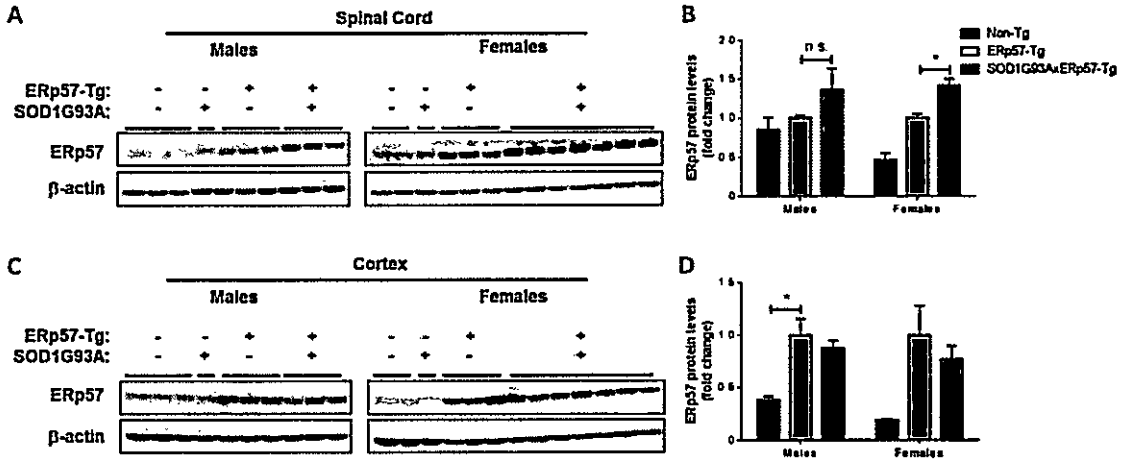

Figure 25. ERp57 protein levels in CNS tissue from end stage mice. A) Western blot analysis of lumbar spinal cord using anti-ERp57 and anti-β-Actin antibodies. **B)** Western blot quantification of (A) using β-actin as loading control. **C)** Western blot analysis of cortex. **D)** Western blot quantification of (C) using β-actin as loading control. Each lane corresponds to an independent animal. Samples order is the same for spinal cord and cortex WBs. All ERp57-Tg and double transgenic mice in (A) and (C) were used for quantification in (B) and (D). Non-Tg animals are quantified as reference too. Mean ± SEM. Student t-test. *: p value < 0.05. n.s: non-significant.

Mutant SOD1 is prone to misfold and form oligomers (high molecular weight (HMW) species), large aggregates (larger than 0.22 μm) and intracellular inclusions (Rotunno et al. 2014; Kikuchi et al. 2006; H.-X. Deng et al. 2006; J. Wang, Xu, and Borchelt 2002). These are hallmarks of mutant SOD1-linked fALS and some sALS cases. An important population of these mutant SOD1 aggregated forms is detergent insoluble and/or disulfide crosslinked (Chen et al. 2012; H.-X. Deng et al. 2006). Large aggregated species of SOD1 (larger than 0.22 μm) and HMWs were measured by filter trap (FT) and western blot (WB), respectively, in the presence and absent of the thiol reducing reagent (DTT) to analyze disulfide crosslink-dependent aggregates (Fig. 26). FT method consists in filtering the protein sample through 0.22 μm pores of a cellulose acetate membrane under denaturing conditions (1 % SDS in FT loading buffer). With this approach, covalently bond protein aggregates are trapped on the membrane. Lumbar spinal cord samples of end stage SOD1G93A and double transgenic mice showed SOD1 aggregates sensitive and resistant to DTT (Fig. 26A). Samples from non-Tg and ERp57-Tg mice were included on the membrane as technical controls and had no SOD1 aggregates or background signal (Fig. 26A). For aggregates quantification, mutant SOD1 monomer determined by WB was used as a loading control (Fig. 26A). Remarkably, there was around 30% reduction of DTT-sensitive SOD1 aggregates in double transgenic compared to SOD1G93A mice (Fig. 26B). On the other hand, there is not reduction of DTT-resistant SOD1 aggregates in double transgenic mice (Fig. 26C), suggesting specific effects of ERp57 on controlling redox SOD1 folding.

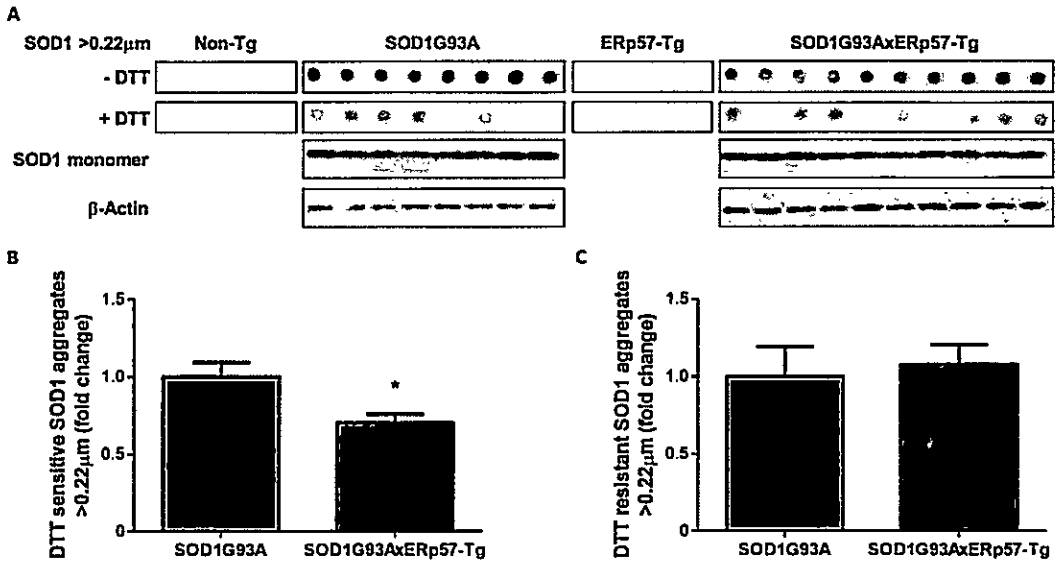

Figure 26. Disulfide-dependent SOD1 aggregates analysis of end stage lumbar spinal cord. A) Filter trap (FT) immunoblots for SOD1 aggregates in the absence (-DTT) or presence (+DTT) of the reducing reagent DTT. FT analysis consists in filtering the sample through a cellulose acetate membrane with pores of 0.22 µm diameter. Protein aggregates larger than 0.22 µm are retained in the membrane. Each dot represents an independent animal. SOD1 monomer is used as a loading control for total SOD1 in the sample running a parallel WB in presence of DTT. β-Actin is shown as a loading control for SOD1 monomer in WB (+DTT). Samples order is the same for lines –DTT, +DTT and WBs. **B)** and **C)** FT signal densitometric quantification for "DTT-sensitive" (B) or "DTT–resistant" (C) SOD1 aggregates. "DTT-sensitive" signal is the contribution of species that can be reduced by DTT plus non-disulfide bonded species of SOD1. All SOD1G93A or double transgenic mice in (A) were used for quantification. Mean ± SEM. Student t-test was performed. *: p value < 0.05.

Mutant SOD1 disulfide-crosslinked HMW species in lumbar spinal cord of end stage mice was analyzed by non-reducing WB (Fig. 27). Human SOD1 monomer levels were also analyzed (Fig. 27A and C) to further address the impact of ERp57 overexpression on human mutant SOD1 protein (Fig. 27). There was an increase of SOD1 protein levels in double transgenic male mice compared to SOD1G93A mice (Fig. 27B). Interestingly, HMWs seems to be at similar amounts between both genotypes (SOD1 - DTT gel in Fig. 27A), but SOD1 monomer levels are consistently increased in double transgenics (SOD1 monomer gel in Fig. 27A). This lead to a relative reduction of around 50% in SOD1 HMW species in double transgenic male mice (Fig. 27B). Importantly, double transgenic female mice also presented decreased relative levels of HMW species but in this case there is no modulation of mutant SOD1 monomer (Fig. 27C and D).

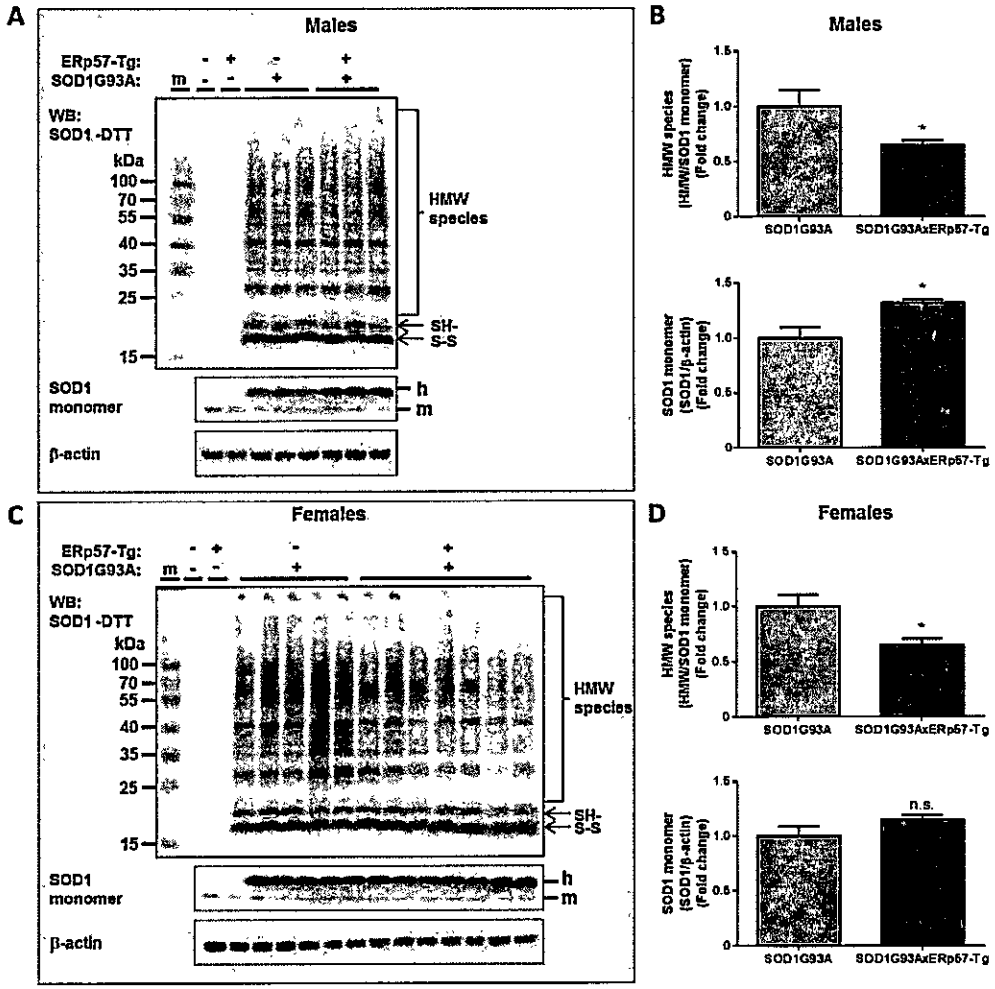

Figure 27. SOD1 high molecular weight species analysis of end stage lumbar spinal cord. A) and **C)** Western blot (WB) against SOD1 in male (A) and female (C) mice samples without DTT detected SOD1 oligomerization (high molecular weight (HMW) species) in SOD1G93A and double transgenic mice compared to age-matched controls (non-Tg and ERp57-Tg mice). m: molecular weight marker. SH- and S-S indicate reduced and oxidized forms of SOD1 monomer, respectively. SOD1 monomer is used as a loading control for total SOD1 in the sample using WB in presence of DTT. h- and m- indicate human SOD1 and mouse endogenous SOD1 monomers, respectively. **B)** and **D)** Densitometric quantification of SOD1 HMWs and SOD1 monomer in male (B) and female (D) mice. β-actin is used as a loading control for SOD1 monomer. Samples order is the same for all WBs within male and female boxes. All SOD1G93A or double transgenic mice were used for quantification. Mean ± SEM. Student t-test was performed. *: p value < 0.05. n.s: non-significant.

SOD1 HMW species were also analyzed in cerebral cortex to determine if SOD1 oligomerization is also modulated by ERp57 in other CNS tissue (Fig. 28). There was much less SOD1 oligomerization in cerebral cortex than in spinal cord of SOD1G93A and double transgenic mice (Fig. 28A), which was not modulated by ERp57 overexpression (Fig. 28B and C). Interestingly, total mutant SOD1 protein levels (SOD1 monomer gels) were also not altered by ERp57 overexpression in this tissue (Fig. 28A). Taking together, these data suggest that there is a tissue-specific differential modulation of mutant SOD1 in male double transgenic animals between spinal cord (Fig. 27A) and brain cortex (Fig. 28A).

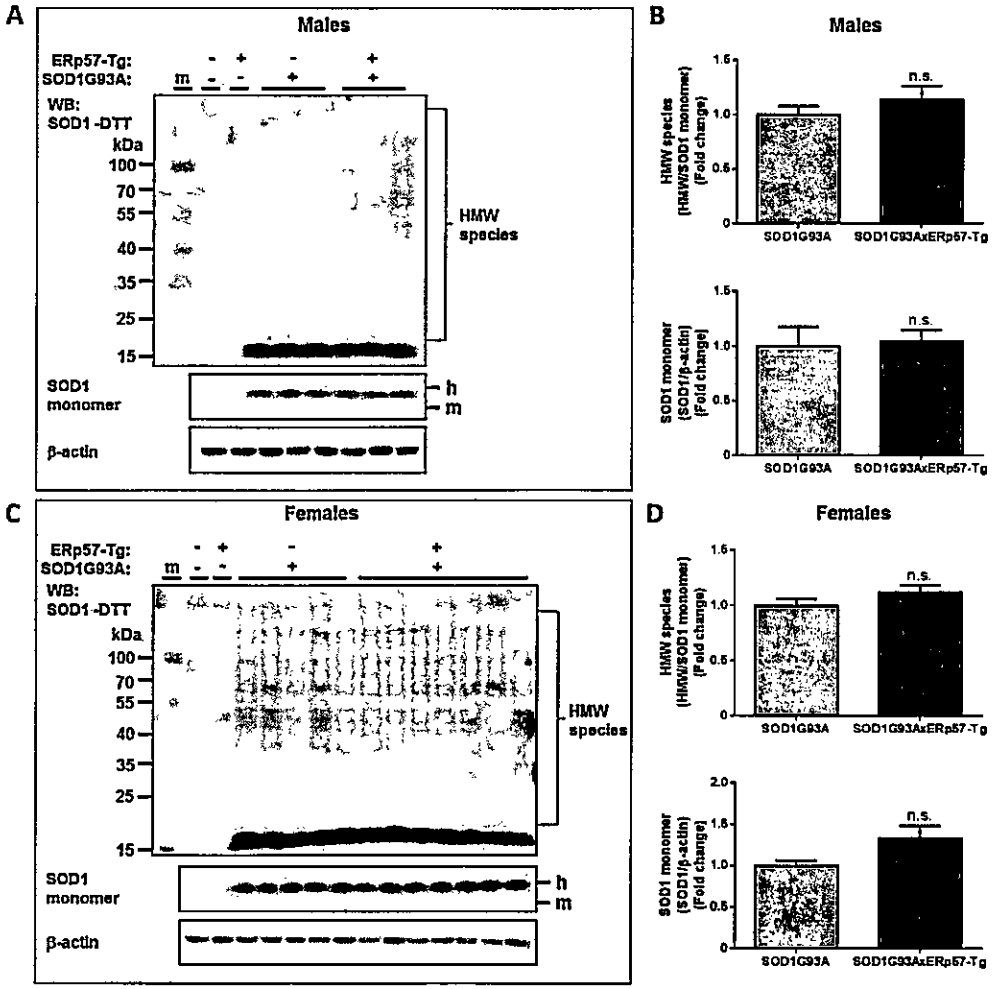

Figure 28. SOD1 high molecular weight species analysis of end stage brain cortex. A) and **C)** Western blot (WB) against SOD1 in male (A) and female (C) mice samples without DTT detected SOD1 oligomerization (high molecular weight (HMW) species) in SOD1G93A and double transgenic mice compared to age-matched controls (non-Tg and ERp57-Tg mice). m: molecular weight marker. SH- and S-S indicate reduced and oxidized forms of SOD1 monomer, respectively. SOD1 monomer is used as a loading control for total SOD1 in the sample using WB in presence of DTT. h- and m- indicate human SOD1 and mouse endogenous SOD1 monomers, respectively. **B)** and **D)** Densitometric quantification of SOD1 HMWs and SOD1 monomer in male (B) and female (D) mice. β-actin is used as a loading control for SOD1 monomer. Samples order is the same for all WBs within male and female boxes. All SOD1G93A or double transgenic mice were used for quantification. Mean ± SEM. Student t-test was performed. n.s: non-significant.

To analyze in further detail the impact of ERp57 on SOD1G93A misfolding, we employed immunofluorescence in transversal sections of the lumbar spinal cord using "conformational" antibodies (clones B8H10 and C4F6 antibodies) that recognize potentially toxic conformations of SOD1 (Fig. 29 and Fig. 30). These antibodies were raised against mutant SOD1 and have been used to discriminate misfolded SOD1 oligomers that do not necessarily form large inclusions (Rotunno et al. 2014). We observed immunoreactivity of B8H10 and C4F6 conformational antibodies in lumbar spinal cord of end stage SOD1G93A mice showing a punctate staining pattern (Fig. 29 and Fig. 30). This puncta pattern apparently co-localizes with ERp57-Tg construct inside FLAG positive cells, corresponding mainly to motor neurons as can be discriminate by morphology (Fig. 29 and Fig. 30, insets, arrows). Interestingly, there is also B8H10 and C4F6 staining in non-FLAG positive cells, suggesting mutant SOD1 misfolding in glial cells (Fig. 29 and Fig. 30, insets, arrowheads). Moreover, in line with differential vulnerability of spinal motor neurons, FLAG-positive motor neurons with B8H10 or C4F6 inclusions are smaller than other motor neurons devoid of inclusions in the same cellular environment (Fig. 30, insets, *), suggesting that B8H10 or C4F6 stain motor neurons undergoing soma degeneration.

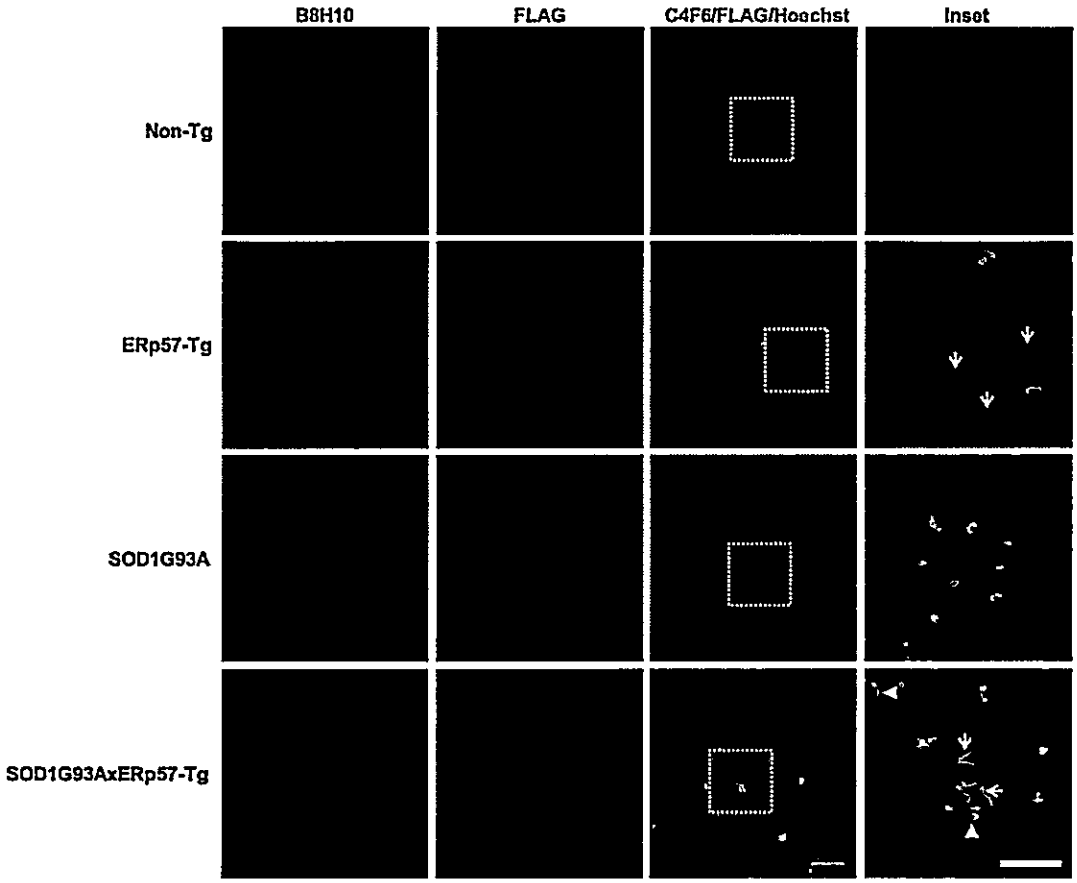

Figure 29. Misfolded SOD1 qualitative analysis in spinal motor neurons detected by B8H10 immunoreactivity. B8H10 conformational antibody detects misfolded forms of SOD1 that present punctate pattern. FLAG staining in large cells of spinal cord ventral horn mainly correspond to motor neurons as can be discriminated by morphology (arrows in insets) and co-localizes with misfolded SOD1 in double transgenic tissue. B8H10 puncta is also present in FLAG-negative cells, suggesting misfolded SOD1 in glia (arrowheads in insets). B8H10/FLAG/Hoechst: merged image of B8H10 and FLAG staining plus Hoechst nuclear staining. Scale bar of merged image: 100 μm. Insets are digital zooms from white dashed squares in merged images. Scale bar of inset: 50 μm.

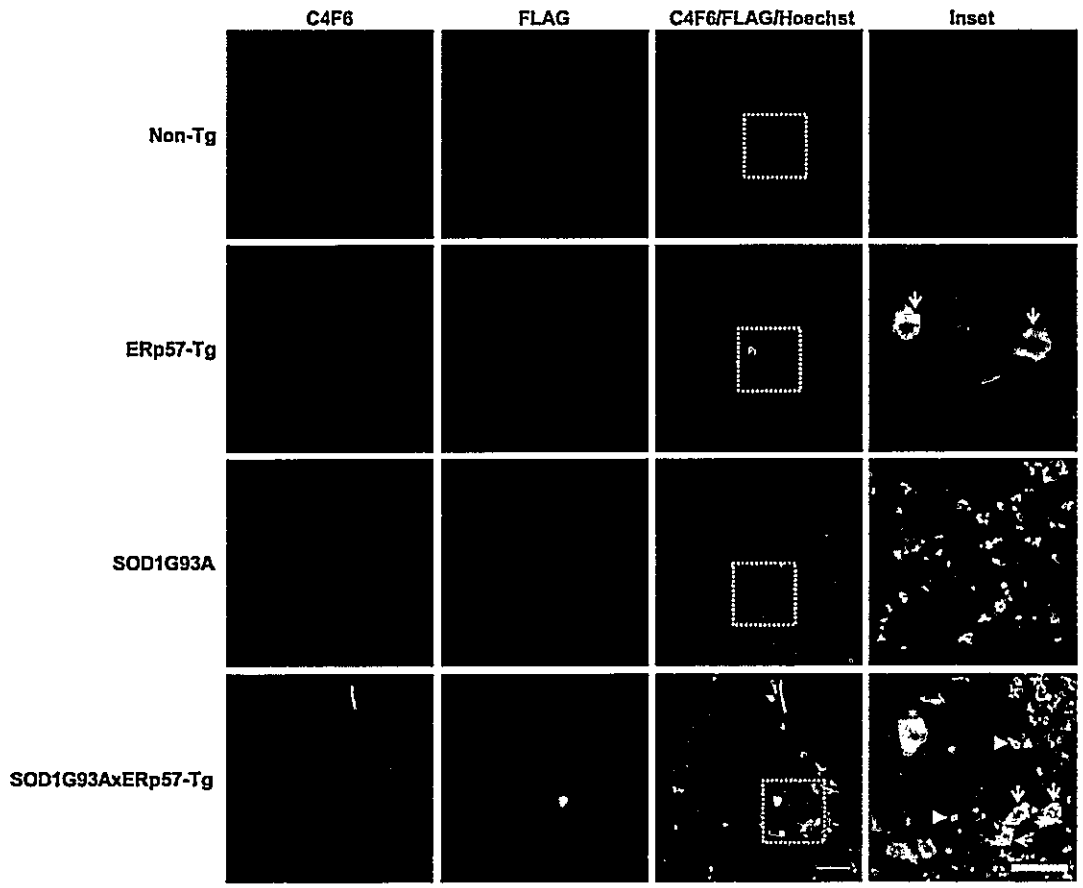

Figure 30. Misfolded SOD1 qualitative analysis in spinal motor neurons detected by C4F6 immunoreactivity. C4F6 conformational antibody detects misfolded forms of SOD1 that present punctate pattern. FLAG staining in large cells of spinal cord ventral horn mainly correspond to motor neurons as can be discriminated by morphology (arrows in insets) and co-localizes with misfolded SOD1 in double transgenic tissue. C4F6 puncta is also present in FLAG-negative cells, suggesting misfolded SOD1 in glia (arrowheads in insets). Some motor neurons do not have C4F6 inclusions and are larger than C4F6 positive cells (* in inset). B8H10/FLAG/Hoechst: merged image of B8H10 and FLAG staining plus Hoechst nuclear staining. Scale bar of merged image: 100 μm. Insets are digital zooms from white dashed squares in merged images. Scale bar of inset: 50 μm.

DISCUSSION

Proteostasis impairment is a salient feature of neurodegenerative diseases such as ALS, Prion-related disorders, Huntington's, Alzheimer's and Parkinson's diseases. ER stress has been proposed as an early mechanism involved in neuronal dysfunction and degeneration in these diseases, being proposed to underlie selective vulnerability of motor neurons and to ultimately trigger neuronal demise in ALS (reviewed in (Hetz and Mollereau 2014)). Protein disulfide isomerases (PDIs) are chaperones upregulated by the UPR upon ER stress. The discovery of PDIs, specifically PDIA1 and ERp57, as the main hits in proteomics studies of ALS mice and patients, in addition to association of missense mutations in these chaperones as disease risk factors, highlight their importance to ALS pathogenic mechanisms (J. Atkin et al. 2008; J. D. Atkin et al. 2006; Hetz et al. 2009; A. Walker et al. 2010; Gonzalez-Perez et al. 2015; Woehlbier et al. 2016). Surprisingly, functional studies addressing PDIs impact on ALS models *in vivo* are lacking in the literature. In this thesis, ERp57 contribution to disease progression was assessed using a genetic approach to overexpress the chaperone in the SOD1G93A ALS mouse model.

Characterization of ERp57-Tg mice

ERp57-Tg transgenic mouse line was developed by Dr. Hetz and collaborators (Castillo et al. 2015; Torres et al. 2015). During development of this thesis, ERp57-Tg mice were characterized at different levels to complement this and several other projects. This mouse line harbors human ERp57 with a FLAG tag conjugated at C-terminal domain of the protein (Fig. 7B), expressed under control of the Prion protein promoter to assure CNS enrichment (Borchelt et al. 1996). The ERp57 overexpression was confirmed in

several tissues such as brain cortex, *substantia nigra*, striatum, hippocampus, cerebellum, DRG neurons, Schwann cell (Torres et al. 2015; Castillo et al. 2015), spinal cord and tibialis anterior muscle (Fig. 8).

ERp57-Tg mice were previously used to study ERp57 role in neurodegeneration in peripheral and central nervous systems, using sciatic nerve transection and 6-OH dopamine Parkinson model, respectively (Castillo et al. 2015). ERp57-Tg transgenic mice regenerate peripheral nerves faster than non-Tg littermates while presenting no protection in the pharmacological Parkinson model. This shows a differential role of ERp57 in pathological context depending on neuronal subpopulation. Moreover, ERp57-Tg mice have increased levels of Prion protein in the CNS, showing a functional role of this transgenic construct (Torres et al. 2015).

Our double transgenic approach to study the impact of ERp57 on mutant SOD1G93A pathology yielded four experimental groups, named SOD1G93AxERp57-Tg, SOD1G93A, ERp57-Tg, and non-Tg. We performed full assessment of motor strength and coordination in both ERp57-Tg and non-Tg control groups to better understand possible beneficial effects of ERp57-Tg overexpression in the mutant SOD1G93A model. Interestingly, ERp57-Tg male mice have a better performance in Hanging wire test than non-Tg littermates at basal conditions (Fig. 17B). In parallel cohort, we investigated neuromuscular terminals of the ERp57-Tg mice by assessing several parameters. NMJ integrity, in terms of morphology, quantity, volume and area of endplates (acetylcholine receptor-positive postsynaptic terminals), is not altered in ERp57-Tg (Fig. 10 and Fig. 11). This is different from results from Hetz's laboratory characterizing transgenic mouse lines that overexpress ALS-linked mutant forms of

ERp57. These mutant lines have an increase of aberrant NMJ shapes and reduced number of end plate clusters (Sepúlveda 2015). Taking into account the similar overexpression of human ERp57 relative to endogenous chaperone levels (2-4 fold change in spinal cord) (Fig. 8 and (Sepúlveda 2015)), the phenotype seen in ALS-linked ERp57 mutant lines can be directly attributed to detrimental effects of the ALS-linked mutations on motor neuron proteostasis and connectivity, rather than overexpression artifacts.

Interestingly, fiber type composition in ERp57-Tg mice is shifted toward slow fiber types (Fig. 12D), i.e. muscle fibers that relay mainly on oxidative metabolism (Nijssen, Comley, and Hedlund 2017), without altering fiber integrity (Fig. 12B). Importantly, slow fiber types correspond to resistant-type of motor units (S motor unit type), i.e. motor units that are denervated in late symptomatic stages of ALS disease progression. This suggests that there might be more ALS-resistant motor units in ERp57-Tg mice, a hypothesis needed to be tested by electrophysiological experiments. Another possibility is that leaky overexpression of ERp57 in skeletal muscle modulates metabolic oxygen consumption. It is known that PDI activity is coupled to Ero1α, regulating the redox potential at ER lumen and cytosol (Poet et al. 2017; Oka, Yeoh, and Bulleid 2015). In addition, ERp57 is also located at mitochondria-associated membranes where it can impact calcium signaling and, therefore, cellular respiration (He et al. 2014; Li and Camacho 2004). Overall, these data show that ERp57 overexpression in CNS and tibialis anterior muscle can modulate muscle fiber type composition without altering NMJs integrity.

Analysis of SOD1G93AxERp57-Tg mice

PDIs activity has been proposed as a neuroprotective mechanism due to its interaction with mutant SOD1 and reduction of protein misfolding and aggregation (A. Walker et al. 2010; J. D. Atkin et al. 2006; Jeon et al. 2014). However, this hypothesis relay mainly on *in vitro* evidence. PDIA1, a close homologue of ERp57 (Andreu et al. 2012), is able to reduce mutant SOD1 aggregates in cell culture (A. Walker et al. 2010; Jeon et al. 2014). Interestingly, inactivation of PDIA1 disulfide isomerase activity by S-nitrosylation has been linked to protein misfolding and neurodegeneration (Uehara et al. 2006), and showed to drive accumulation of mutant SOD1 (A. Walker et al. 2010; Jeon et al. 2014). Moreover, PDIA1 co-localize with intracellular mutant SOD1 inclusions (J. D. Atkin et al. 2006). These evidences along with increased PDIs levels in ALS tissue led to the notion that ERp57 could delay mutant SOD1 pathogenesis and disease progression by diminishing the load of mutant misfolded protein, a therapeutic strategy that has never been tested in ALS mouse models. This idea was explored *in vivo* here using a combination of phenotypic, histological and biochemical approaches on SOD1G93AxERp57-Tg mice, hereafter "double transgenic mice".

Double transgenic mice are viable and born at Mendelian rates suggesting that both transgenes segregate independently (Table II). Also, they gain weight at similar rates compared to single transgenic mice (Fig. 14). In addition, neither human *ERp57* nor *SOD1G93A* expression alters the expression of each other at mRNA levels in both spinal cord and brain cortex, validating single transgenic littermates as control groups in terms of gene expression (Fig. 24).

As major result of this thesis, ERp57 overexpression in CNS at 2-4-fold the endogenous chaperone levels is not sufficient to alter lifespan of SOD1G93A mice (Fig. 13), with both genders reaching the disease end-stage at the age reported by Jackson Laboratory (Strain number: 004435). Nonetheless, ERp57 overexpression did modulate disease onset, measured by Clinical Score, Rotarod and Hanging wire test (Fig. 18). These different parameters consistently showed delayed disease onset in double transgenic female while Hanging wire test also revealed a significant difference in disease onset of males (Fig. 17). Noteworthy, Hanging wire test also revealed delayed disease progression of two weeks around 117-124 days old in double transgenic male mice (# in Fig. 17B left panel), a critical time window for deterioration of motor capacity in males when Rotarod and Hanging wire test performance sharply decline (Fig. 17B left panel) and clinical score starts to increase (Fig. 15B).

The difference in disease onset for each parameter analyzed reflects the physiological outputs most relevant for each task (Fig. 18). This is an interesting observation to ALS literature because usually disease onset and progression are determined using just one parameter where body weight or motor performance are employed. Comparing all four parameters tested (Fig. 18), Hanging wire test emerges as the best indicator of disease progression due to its low variability (Fig. 17B) and early detection power.

Overall, SOD1G93A and double transgenic male mice have earlier decline in Clinical Score, Rotarod and Hanging test than female counterparts (Fig. 18). This gender bias is not rare in familial or sporadic ALS context where more men than women are affected (D. Valenzuela, Zitko, and Lillo 2015; Manjaly et al. 2010) and disease in fALS mouse models tends to be more aggressive in males as seen in SOD1G93A and TDP43A315T

models in SJL/C57bl6 and C57bl6 backgrounds, respectively (Wegorzewska et al. 2009; Heiman-Patterson et al. 2005).

The fact that ERp57 enrichment in CNS delays symptoms onset despite having no impact on lifespan (Fig. 13) suggests that ERp57 exerts a neuroprotective role in pre-symptomatic disease stages. Indeed, clinical phenotype is the same between double transgenic and SOD1G93A mice at end-stage. Moreover, the end-stage phenotype correlates with histopathological alterations where both genotypes display the same spinal motor neuron loss in the lumbar region (Fig. 22), the primary affected spinal cord region in SOD1G93A fALS model (Fig. 21) (Lalancette-Hebert et al. 2016). In addition, astrocyte and microglia activation is the same between SOD1G93A and double transgenic mice (Fig. 23). This histopathological characterization together with phenotypic observation show that ERp57 overexpression delays motor unit dysfunction but is not able to prevent spinal gliosis and motor neuron demise that drives disease progression leading to paralysis and premature death (Fig. 18) (B. J. Turner and Talbot 2008).

To explore the idea of delayed motor unit dysfunction in double transgenic mice at pre-symptomatic stages of disease, CMAP was assessed (Fig. 19). This is an electrophysiological parameter that is directly associated to muscle denervation (Mancuso, Osta, and Navarro 2014). CMAP is a measure of the whole muscle response to supramaximal stimulation. In other words, it is the maximal electrical capacity of the muscle response when all motor axon are stimulated. Alterations in muscle innervation lead to decreased CMAP values. However, collateral axonal sprouting can partially restore CMAP amplitude despite NMJs are already altered

(Arnold et al. 2015). Remarkably, there is one week delay in CMAP drop of both muscles analyzed in grouped male and female double transgenic mice (& in Fig. 19). It would be necessary to add more animals to the experiment in order to assess if this delay is conserved in male and female mice, separately. It would be also important to analyze axonal sprouting and NMJ integrity at this pre-symptomatic time point in order to find possible mechanisms for motor unit protection.

Interestingly, the decrease in Rotarod and Hanging wire test performance (63-70 or more days old) (Fig. 16 and Fig. 17) occurs significantly later than gastrocnemius or tibialis anterior denervation (51 days old) (Fig. 19), suggesting that these motor tasks depend on more muscles than hind paw muscles and/or that the extent of denervation is not enough to deteriorate muscle function at this time. Indeed, motor performance decline correlates with 50% or more denervation of hind paw muscles at 63-70 days old. This delay between CMAP decrease and motor performance decline is consistent with other reports of muscular disease models where denervation of motor units is observed close before motor phenotype appears (Paganoni and Amato 2013; Dirren et al. 2015)

Analysis of pre-symptomatic stage reveals a longitudinal trend for preserved CMAP values upon ERp57 overexpression (Fig. 19). However, histological analysis to determine muscle innervation/denervation remains to be performed to corroborate this notion. The previous characterization of ERp57 function in CNS using conditional knockout mice showed that the chaperone does not modulate susceptibility to ER stress, but instead support function of motor neurons by assisting the folding of synaptic proteins such as synaptic vesicle protein 2, SV2 (Torres et al. 2015; Woehlbier et al.

2016). Indeed, the deficiency of ERp57 in the nervous system leads to impaired neuromuscular junction with electrophysiological alterations (Woehlbier et al. 2016).

Regarding motor neuron connectivity, ALS-linked mutant forms of ERp57 have a detrimental impact on neuritogenesis of motor neuron-like cell line NSC34 and spinal cord primary motor neurons (Woehlbier et al. 2016). Impaired neuritogenesis also occurs in NSC34 cells expressing SOD1G93A (Juan Pablo Henríquez's Lab. Universidad de Concepción. Unpublished results). Therefore, we set out to test the effect of ERp57 on NSC34 neuritogenesis under mutant SOD1 expression (Fig. 20). As expected, stable expression of SOD1G93A decreases neuritogenesis compared to SOD1WT. Remarkably, ERp57-Tg overexpression not only enhances neuritogenesis in SOD1WT cells but also fully rescues the phenotype in SOD1G93A line. This is consistent with ERp57 role in promoting neuritogenesis in this cell line and points toward possible protective effects of the chaperone at early disease stages involving muscle denervation. Whether mutant SOD1 and ALS-linked ERp57 mutants share molecular mechanisms affecting motor neuron neuritogenesis remain to be addressed. Taken these *in vitro* and *in vivo* data together, it is possible that ERp57-Tg protective effects on motor function can be explained in terms of improved neuromuscular junction maintenance.

To further explore the impact of ERp57 on SOD1G93A pathogenesis, protein misfolding, oligomerization and aggregation were assessed (Rotunno et al. 2014; Kikuchi et al. 2006; H.-X. Deng et al. 2006; J. Wang, Xu, and Borchelt 2002). Here, oligomers are referred as the species detected as high-molecular-weight bands by Western-blot analysis and to aggregates as the species that cannot be resolved in 4%

or denser polyacrylamide gels. Also, aggregate species are retained in the pores of 0.2 μm diameter cellulose acetate membranes using filter trap assay (Fig. 26). As expected, SOD1G93A mice accumulate oligomers and aggregates of SOD1 in spinal cord (Fig. 26 and Fig. 27). In addition, misfolded SOD1 can be detected in lumbar spinal cord apparently co-localizing with overexpressed ERp57 in motor neurons by immunofluorescence analysis with conformational antibodies recognizing buried epitopes in the wild type protein that become exposed to solvent upon misfolding of ALS mutants (Fig. 29 and Fig. 30) (Rotunno et al. 2014). Remarkably, DTT-sensitive mutant SOD1 oligomers and aggregates are selectively decreased in double transgenic mice (Fig 26 and Fig 27), suggesting that ERp57 probably prevents aberrant SOD1 disulfide crosslinks through its oxidoreductase activity as has been shown for PDIA1 *in vitro* (Jeon et al. 2014; A. Walker et al. 2010). Nevertheless, qualitative assessment of misfolded SOD1 levels detected with conformational antibodies staining suggests that SOD1 misfolding is unaltered by ERp57 (Fig. 29 and 30). The differential modulation of oligomeric and aggregated species of mutant SOD1 by ERp57 may be explained by the fact that ERp57 cannot interfere with the intrinsic property of mutant SOD1 to misfold in the cytosol where protein synthesis take place, but rather to the molecular events leading to protein disulfide crosslink which may be governed by SOD1 mislocalization to the ER lumen (Urushitani et al. 2008).

Mechanistically, reduced mutant SOD1 aggregation and oligomerization by ERp57 overexpression may be explained directly by reduction of aberrant intermolecular disulfide bonds at the ER. Nevertheless, investigation of this and other mechanisms were beyond the scope of this thesis. Indirect effects that could be associated to the impact of ERp57 on SOD1 aggregation could include changes in gene expression

responses. To further explore this critical question, it is necessary to analyze SOD1 aggregation in tissue from pre-symptomatic and early symptomatic disease stages. On the other hand, the toxicity of mutant SOD1 aggregates may be related to loss of function of molecular components such as chaperones that are entrapped within these proteinaceous structures (Bergemalm et al. 2010). Considering this panorama, obvious questions arise: What is the nature of chaperones sequestered into mutant SOD1 aggregates? Would this process happen in a stochastic or selective manner? Would there be a threshold for the accumulation of aggregates to translate into histopathological alterations and motor phenotypes? From correlative studies in the literature (J. Atkin et al. 2006; J. Atkin et al. 2008; Hetz et al. 2009; Jeon et al. 2014; A. K. Walker et al. 2010), ERp57 seems to be a strong candidate to be trapped into SOD1 aggregates.

Following this idea, from close examination of Hanging wire test of male mice, some conclusions emerge: 1) Overexpression of ERp57 improves motor performance compared to non-Tg mice, arguing for enhanced chaperone levels boosting the neuromuscular system under basal levels; 2) At pre-symptomatic stages, the improved motor performance caused by ERp57 overexpression is lost in double transgenic mice, supporting the notion that mutant SOD1 negatively impacts the chaperone activity (Fig. 17B). Thus, up-regulation of ERp57 in mouse and human ALS tissue could be interpreted in terms of compensatory response due to impaired folding of client proteins. This is an exciting concept to be explored in future studies comparing the effect of loss- and gain-of-function of ERp57 in motor neurons to ALS pathogenesis.

In summary, this thesis represents the first functional effort to study the role of ERp57 in an ALS mouse model. The results show that enforcing ERp57 expression in CNS can delay disease onset without increasing lifespan of the SOD1G93A model. Importantly, ERp57 overexpression is also able to reduce mutant SOD1 aggregation and oligomerization at lumbar spinal cord, even though the mechanistic implication of this finding to the neuroprotection observed remains obscure. These data encourages further investigation on the role of ERp57 in ALS by complementing the double transgenic approach with new genetic tools to manipulate ERp57 levels in motor neurons.

Future perspectives

ER stress and the UPR have emerged as attractive therapeutic targets to ALS. Several genetic and pharmacological attempts have been made to test this therapeutic potential with different outcomes. For example, pharmacological manipulation of UPR to sustain translation repression by inhibiting eIF2α phosphatase with guanabenz, sephin1 or salubrinal prolongs mutant SOD1 lifespan in mice (Das et al. 2015; L. Wang et al. 2014; Jiang et al. 2014). However, contrary effects have been obtained depending on the disease model and even gender studied (Vieira et al. 2015). For instance, genetic ablation of xbp1 leads to extended lifespan of mutant SOD1 mice, which was associated to increased autophagy and reduction of mutant SOD1 aggregates (Hetz et al. 2009). Surprisingly, overexpressing Xbp1s via intracerebroventricular AAV delivery in pups of SOD1G86R mouse model reduces SOD1 aggregates and extends lifespan (Valenzuela 2016). Remarkably, overexpressing ERp57 (this work) or Xbp1s via intraspinal AAV delivery (Valenzuela 2016) reduce SOD1G93A aggregation with no

impact on lifespan. Thus, it comes into question whether SOD1G93A aggregation in large insoluble species is indeed a pathogenic factor in ALS or a consequence of motor neuron proteostasis loss. These observations show that aggregation is not necessarily correlated with lifespan, or that the beneficial effects of ERp57 or Xbp1s overexpression on reducing SOD1 aggregation are restricted to (lumbar) spinal cord, which is insufficient to alter survival rates. Further investigation designing longitudinal studies with emphasis on pre-symptomatic and early symptomatic stages are needed to get a clear landscape of molecular pathways that lay beneath the clinical phenotype.

Regardless of the exact nature of the toxic mutant SOD1 misfolded or aggregated species, lowering SOD1 levels could define a therapeutic window as has been seen in gene silencing approaches against mutant SOD1 specifically in motor neurons or astrocytes (Dirren et al. 2015). In the case that mutant SOD1 exerts it toxicity by sequestering chaperones into proteinaceous aggregates, the overexpression of chaperones above a certain threshold could overcome mutant SOD1 pathogenesis. This can be achieved using gene therapy approach employing AAVs vectors with neuronal tropism, for instance. Indeed, neonatal neuronal delivery of Xbp1s via ICV injection using AAVs vectors has shown to reduce mutant SOD1 aggregates and extend lifespan of SOD1G93A mice associated with enhanced expression of ER protein quality control mechanisms (Valenzuela 2016). Thus, gene therapy aimed to overexpress ERp57 in CNS could be a useful strategy in order to enhance its protective effects. In addition, non-cell autonomous contribution of ERp57 coming from glial cells in ALS could be dissected using different AAVs serotype.

Another strategy to define ERp57 contribution to ALS pathogenesis and progression is genetic ablation of endogenous ERp57 specifically at CNS. Hetz and collaborators have previously showed that mice lacking one or two alleles of ERp57 in CNS have motor problems (Woehlbier et al. 2016). Assessing ERp57 loss-of-function in mutant SOD1 context would be a useful way to determine its involvement in ALS. Moreover, genetic tools are already available to knockout ERp57 specifically in motor neurons or glial cells, allowing to define the contribution of this chaperone in the neurodegenerative context.

Finally, it would be interesting to analyze the effect of ALS-linked ERp57 mutants in SOD1G93A mouse model. Considering the defects in neural connectivity and reduced motor performance caused by mutant ERp57 overexpression in model organisms (Woehlbier et al. 2016; Sepúlveda 2015), it is expected that mutant ERp57 would enhance disease severity. To test this idea, future studies will generate double transgenic SOD1G93AxERp57-ALS-linked mutations mice to follow disease progression and histopathological features. Overall, this work contributed to understand the functional role of ERp57 in ALS pathogenesis, highlighting its relevance to early disease stages by potentially supporting neuromuscular connections, in addition to reducing mutant SOD1 aggregates.

CONCLUSIONS

1. SOD1G93AxERp57-Tg mice are viable and overexpress ERp57 in central nervous system of SOD1G93A ALS mouse model.
2. ERp57 overexpression delays motor unit denervation and disease onset in double transgenic mice without altering body weight loss or survival.
3. There is no modulation of motor neuron loss or inflammation in end stage spinal cord of double transgenic mice.
4. ERp57 overexpression decreases SOD1 aggregates and high molecular weight species in end stage spinal cord of double transgenic mice.

REFERENCES

Achilli, Francesca, Shelagh Boyle, Dairin Kieran, Ruth Chia, Majid Hafezparast, Joanne E Martin, Giampietro Schiavo, Linda Greensmith, Wendy Bickmore, and Elizabeth M C Fisher. 2005. "The SOD1 Transgene in the G93A Mouse Model of Amyotrophic Lateral Sclerosis Lies on Distal Mouse Chromosome 12." *Amyotrophic Lateral Sclerosis and Other Motor Neuron Disorders: Official Publication of the World Federation of Neurology, Research Group on Motor Neuron Diseases* 6 (2): 111–14. doi:10.1080/14660820510035351.

Al-Chalabi, Ammar, and Orla Hardiman. 2013. "The Epidemiology of ALS: A Conspiracy of Genes, Environment and Time." *Nature Reviews Neurology* 9 (11): 617–28. doi:10.1038/nrneurol.2013.203.

Alexander, Guillermo M, Kirsten L Erwin, Nathaniel Byers, Jeffrey S Deitch, Brian J Augelli, Elizabeth P Blankenhorn, and Terry D Heiman-Patterson. 2004. "Effect of Transgene Copy Number on Survival in the G93A SOD1 Transgenic Mouse Model of ALS." *Molecular Brain Research* 130 (1–2): 7–15. doi:10.1016/j.molbrainres.2004.07.002.

Aliaga, Leonardo, Chen Lai, Jia Yu, Nikolai Chub, Hoon Shim, Lixin Sun, Chengsong Xie, et al. 2013. "Amyotrophic Lateral Sclerosis-Related VAPB P56S Mutation Differentially Affects the Function and Survival of Corticospinal and Spinal Motor Neurons." *Human Molecular Genetics* 22 (21): 4293–4305. doi:10.1093/hmg/ddt279.

Andreu, Catherine I., Ute Woehlbier, Mauricio Torres, and Claudio Hetz. 2012. "Protein Disulfide Isomerases in Neurodegeneration: From Disease Mechanisms to Biomedical Applications." *FEBS Letters* 586 (18): 2826–34. doi:10.1016/j.febslet.2012.07.023.

Appenzeller-Herzog, Christian, Jan Riemer, Brian Christensen, Esben Sørensen, and Lars Ellgaard. 2008. "A Novel Disulphide Switch Mechanism in Ero1alpha Balances ER Oxidation in Human Cells." *EMBO J* 27 (22): 2977–87. doi:10.1038/emboj.2008.202.

Arnold, W David, Kajri A Sheth, Christopher G Wier, John T Kissel, Arthur H Burghes, and Stephen J Kolb. 2015. "Electrophysiological Motor Unit Number Estimation (MUNE) Measuring Compound Muscle Action Potential (CMAP) in Mouse Hindlimb Muscles." *Journal of Visualized Experiments: JoVE*, no. 103(September). doi:10.3791/52899.

Ash, Peter, Kevin F Bieniek, Tania F Gendron, Thomas Caulfield, Wen-Lang Lin, Mariely DeJesus-Hernandez, Marka M van Blitterswijk, et al. 2013. "Unconventional Translation of C9ORF72 GGGGCC Expansion Generates Insoluble Polypeptides Specific to c9FTD/ALS." *Neuron* 77 (4): 639–46. doi:10.1016/j.neuron.2013.02.004.

Atkin, Julie D, Manal A Farg, Bradley J Turner, Doris Tomas, Judith A Lysaght, Janelle Nunan, Alan Rembach, et al. 2006. "Induction of the Unfolded Protein Response in

Familial Amyotrophic Lateral Sclerosis and Association of Protein-Disulfide Isomerase with Superoxide Dismutase 1." *The Journal of Biological Chemistry* 281 (40): 30152–65. doi:10.1074/jbc.M603393200.

Atkin, Julie, Manal Farg, Bradley Turner, Doris Tomas, Judith Lysaght, Janelle Nunan, Alan Rembach, et al. 2006. "Induction of the Unfolded Protein Response in Familial Amyotrophic Lateral Sclerosis and Association of Protein-Disulfide Isomerase with Superoxide Dismutase 1." *J Biol Chem* 281 (40): 30152–65. doi:10.1074/jbc.M603393200.

Atkin, Julie, Manal Farg, Adam Walker, Catriona McLean, Doris Tomas, and Malcolm Horne. 2008. "Endoplasmic Reticulum Stress and Induction of the Unfolded Protein Response in Human Sporadic Amyotrophic Lateral Sclerosis." *Neurobiology of Disease* 30 (3): 400–407. doi:10.1016/j.nbd.2008.02.009.

Barres, Ben A. 2008. "The Mystery and Magic of Glia: A Perspective on Their Roles in Health and Disease." *Neuron* 60 (3): 430–40. doi:10.1016/j.neuron.2008.10.013.

Ben Haim, L., K. Ceyzeriat, M. A. Carrillo-de Sauvage, F. Aubry, G. Auregan, M. Guillermier, M. Ruiz, et al. 2015. "The JAK/STAT3 Pathway Is a Common Inducer of Astrocyte Reactivity in Alzheimer's and Huntington's Diseases." *Journal of Neuroscience* 35 (6): 2817–29. doi:10.1523/JNEUROSCI.3516-14.2015.

Bergemalm, Daniel, Karin Forsberg, Vaibhav Srivastava, Karin S. Graffmo, Peter M. Andersen, Thomas Brännström, Gunnar Wingsle, and Stefan L. Marklund. 2010. "Superoxide Dismutase-1 and Other Proteins in Inclusions from Transgenic Amyotrophic Lateral Sclerosis Model Mice." *Journal of Neurochemistry* 114 (2): 408–18. doi:10.1111/j.1471-4159.2010.06753.x.

Bernard-Marissal, N, and A Moumen. 2012. "Reduced Calreticulin Levels Link Endoplasmic Reticulum Stress and Fas-Triggered Cell Death in Motoneurons Vulnerable to ALS." *Journal of Neuroscience* 32 (14): 4901-12. doi:10.1523/JNEUROSCI.5431-11.2012.

Bernard-Marissal, Nathalie, Claire Sunyach, Thomas Marissal, Cédric Raoul, and Brigitte Pettmann. 2015. "Calreticulin Levels Determine Onset of Early Muscle Denervation by Fast Motoneurons of ALS Model Mice." *Neurobiology of Disease* 73: 130–36. doi:10.1016/j.nbd.2014.09.009.

Bolte, S., and F. P. Cordelières. 2006. "A Guided Tour into Subcellular Colocalization Analysis in Light Microscopy." *Journal of Microscopy* 224 (3): 213–32. doi:10.1111/j.1365-2818.2006.01706.x.

Borchelt, D R, J Davis, M Fischer, M K Lee, H H Slunt, T Ratovitsky, J Regard, et al. 1996. "A Vector for Expressing Foreign Genes in the Brains and Hearts of Transgenic Mice." *Genetic Analysis : Biomolecular Engineering* 13 (6): 159–63. http://www.ncbi.nlm.nih.gov/pubmed/9117892.

Bosco, Daryl A, Gerardo Morfini, Murat N Karabacak, Yuyu Song, Francois Gros-Louis, Piera Pasinelli, Holly Goolsby, et al. 2010. "Wild-Type and Mutant SOD1 Share an Aberrant Conformation and a Common Pathogenic Pathway in ALS." *Nature*

Neuroscience 13 (11): 1396–1403. doi:10.1038/nn.2660.

Caligari, Marco, Marco Godi, Simone Guglielmetti, Franco Franchignoni, and Antonio Nardone. 2013. "Eye Tracking Communication Devices in Amyotrophic Lateral Sclerosis: Impact on Disability and Quality of Life." *Amyotrophic Lateral Sclerosis and Frontotemporal Degeneration* 14 (7–8): 546–52. doi:10.3109/21678421.2013.803576.

Carvalho, M, M S Schwartz, and M Swash. 1995. "Involvement of the External Anal Sphincter in Amyotrophick Lateral Sclerosis." *Muscle & Nerve* 18 (8): 848–53. doi:10.1002/mus.880180808.

Cashman, Neil R., Heather D. Durham, Jan Krzysztof Blusztajn, Kenichiro Oda, Takeshi Tabira, Ivan T. Shaw, Simone Dahrouge, and Jack P. Antel. 1992. "Neuroblastoma × Spinal Cord (NSC) Hybrid Cell Lines Resemble Developing Motor Neurons." *Developmental Dynamics* 194 (3): 209–21. doi:10.1002/aja.1001940306.

Castillo, Valentina, Maritza Oñate, Ute Woehlbier, Pablo Rozas, Catherine Andreu, Danilo Medinas, Pamela Valdés, et al. 2015. "Functional Role of the Disulfide Isomerase ERp57 in Axonal Regeneration." *PLoS ONE* 10 (9). doi:10.1371/journal.pone.0136620.

Charcot, Jean-Martin, and Alix Joffroy. 1869. *Deux cas d'atrophie musculaire progressive : avec lésions de la substance grise et des faisceaux antérolatéraux de la moelle épinière*. Paris: Masson.

Charles, James P., Ornella Cappellari, Andrew J. Spence, John R. Hutchinson, Dominic J. Wells, and JR Hutchinson. 2016. "Musculoskeletal Geometry, Muscle Architecture and Functional Specialisations of the Mouse Hindlimb." Edited by William D Phillips. *PLOS ONE* 11 (4): e0147669. doi:10.1371/journal.pone.0147669.

Chen, Xueping, Huifang Shang, Xiaozhong Qiu, Noriko Fujiwara, Liying Cui, Xin-Min Li, Tian-Ming Gao, and Jiming Kong. 2012. "Oxidative Modification of Cysteine 111 Promotes Disulfide Bond-Independent Aggregation of SOD1." *Neurochemical Research* 37 (4): 835–45. doi:10.1007/s11064-011-0679-8.

Chen, Xueping, Xiaosha Zhang, Chen Li, Teng Guan, Huifang Shang, Liying Cui, Xin-Min Li, and Jiming Kong. 2013. "S-Nitrosylated Protein Disulfide Isomerase Contributes to Mutant SOD1 Aggregates in Amyotrophic Lateral Sclerosis." *Journal of Neurochemistry* 124 (1): 45–58. doi:10.1111/jnc.12046.

Chew, J., T. F. Gendron, M. Prudencio, H. Sasaguri, Y.-J. Zhang, M. Castanedes-Casey, C. W. Lee, et al. 2015. "C9ORF72 Repeat Expansions in Mice Cause TDP-43 Pathology, Neuronal Loss, and Behavioral Deficits." *Science* 348 (6239): 1151–54. doi:10.1126/science.aaa9344.

Coe, Helen, Joanna Jung, Jody Groenendyk, Daniel Prins, and Marek Michalak. 2010. "ERp57 Modulates STAT3 Signaling from the Lumen of the Endoplasmic Reticulum." *The Journal of Biological Chemistry* 285 (9): 6725–38.

doi:10.1074/jbc.M109.054015.

Dadon-Nachum, Michal, Eldad Melamed, and Daniel Offen. 2011. "The 'Dying-Back' Phenomenon of Motor Neurons in ALS." *Journal of Molecular Neuroscience* 43 (3): 470–77. doi:10.1007/s12031-010-9467-1.

Dafinca, Ruxandra, Jakub Scaber, Nida'a Ababneh, Tatjana Lalic, Gregory Weir, Helen Christian, Jane Vowles, et al. 2016. "C9orf72 Hexanucleotide Expansions Are Associated with Altered Endoplasmic Reticulum Calcium Homeostasis and Stress Granule Formation in Induced Pluripotent Stem Cell-Derived Neurons from Patients with Amyotrophic Lateral Sclerosis and Frontotemporal Demen." *STEM CELLS* 34 (8): 2063–78. doi:10.1002/stem.2388.

Das, I., A. Krzyzosiak, K. Schneider, L. Wrabetz, M. D'Antonio, N. Barry, A. Sigurdardottir, and A. Bertolotti. 2015. "Preventing Proteostasis Diseases by Selective Inhibition of a Phosphatase Regulatory Subunit." *Science* 348 (6231): 239–42. doi:10.1126/science.aaa4484.

de L'Etang, Audrey, Niran Maharjan, Marisa Braña, Céline Ruegsegger, Ruth Rehmann, Anand Goswami, Andreas Roos, et al. 2015. "Marinesco-Sjögren Syndrome Protein SIL1 Regulates Motor Neuron Subtype-Selective ER Stress in ALS." *Nature Neuroscience* 18 (2): 227–38. doi:10.1038/nn.3903.

DeJesus-Hernandez, Mariely, Ian R Mackenzie, Bradley F Boeve, Adam L Boxer, Matt Baker, Nicola J Rutherford, Alexandra M Nicholson, et al. 2011. "Expanded GGGGCC Hexanucleotide Repeat in Noncoding Region of C9ORF72 Causes Chromosome 9p-Linked FTD and ALS." *Neuron* 72 (2): 245–56. doi:10.1016/j.neuron.2011.09.011.

Deng, Han-Xiang, Yong Shi, Yoshiaki Furukawa, Hong Zhai, Ronggen Fu, Erdong Liu, George H Gorrie, et al. 2006. "Conversion to the Amyotrophic Lateral Sclerosis Phenotype Is Associated with Intermolecular Linked Insoluble Aggregates of SOD1 in Mitochondria." *Proceedings of the National Academy of Sciences of the United States of America* 103 (18): 7142–47. doi:10.1073/pnas.0602046103.

Deng, Han-Xiang X, Hong Zhai, Eileen H Bigio, Jianhua Yan, Faisal Fecto, Kaouther Ajroud, Manjari Mishra, et al. 2010. "FUS-Immunoreactive Inclusions Are a Common Feature in Sporadic and Non-SOD1 Familial Amyotrophic Lateral Sclerosis." *Annals of Neurology* 67 (6): 739–48. doi:10.1002/ana.22051.

Dirren, Elisabeth, Julianne Aebischer, Cylia Rochat, Christopher Towne, Bernard L Schneider, and Patrick Aebischer. 2015. "SOD1 Silencing in Motoneurons or Glia Rescues Neuromuscular Function in ALS Mice." *Annals of Clinical and Translational Neurology* 2 (2): 167–84. doi:10.1002/acn3.162.

Dufey, E., D. Sepulveda, D. Rojas-Rivera, and C. Hetz. 2014. "Cellular Mechanisms of Endoplasmic Reticulum Stress Signaling in Health and Disease. 1. An Overview." *AJP: Cell Physiology* 307 (7): 582–94. doi:10.1152/ajpcell.00258.2014.

Dufey, Estefanie, Hery Urra, and Claudio Hetz. 2015. "ER Proteostasis Addiction in Cancer Biology: Novel Concepts." *Seminars in Cancer Biology* 33 (August): 40–47.

doi:10.1016/j.semcancer.2015.04.003.

Ellgaard, Lars, and Eva-Maria Frickel. 2003. "Calnexin, Calreticulin, and ERp57: Teammates in Glycoprotein Folding." *Cell Biochemistry and Biophysics* 39 (3): 223–48. doi:10.1385/CBB:39:3:223.

Esmaeili, Mohammad A., Marzieh Panahi, Shilpi Yadav, Leah Hennings, and Mahmoud Kiaei. 2013. "Premature Death of TDP-43 (A315T) Transgenic Mice due to Gastrointestinal Complications prior to Development of Full Neurological Symptoms of Amyotrophic Lateral Sclerosis." *International Journal of Experimental Pathology* 94 (1): 56–64. doi:10.1111/iep.12006.

Farg, Manal A., Kai Y. Soo, Adam K. Walker, Hong Pham, Jacqueline Orian, Malcolm K. Horne, Sadaf T. Warraich, Kelly L. Williams, Ian P. Blair, and Julie D. Atkin. 2012. "Mutant FUS Induces Endoplasmic Reticulum Stress in Amyotrophic Lateral Sclerosis and Interacts with Protein Disulfide-Isomerase." *Neurobiology of Aging* 33 (12): 2855–68. doi:10.1016/j.neurobiolaging.2012.02.009.

Filareti, Melania, Silvia Luotti, Laura Pasetto, Mauro Pignataro, Katia Paolella, Paolo Messina, Elisabetta Pupillo, et al. 2017. "Decreased Levels of Foldase and Chaperone Proteins Are Associated with an Early-Onset Amyotrophic Lateral Sclerosis." *Frontiers in Molecular Neuroscience* 10 (April): 99. doi:10.3389/fnmol.2017.00099.

Flores, Brittany N, Mark E Dulchavsky, Amy Krans, Michael R Sawaya, Henry L Paulson, Peter K Todd, Sami J Barmada, and Magdalena I Ivanova. 2016. "Distinct C9orf72-Associated Dipeptide Repeat Structures Correlate with Neuronal Toxicity." *PLoS ONE* 11 (10). doi:10.1371/journal.pone.0165084.

Fritz, Elsa, Pamela Izaurieta, Alexandra Weiss, Franco R Mir, Patricio Rojas, David Gonzalez, Fabiola Rojas, Robert H Brown, Rodolfo Madrid, and Brigitte van Zundert. 2013. "Mutant SOD1-Expressing Astrocytes Release Toxic Factors That Trigger Motoneuron Death by Inducing Hyperexcitability." *Journal of Neurophysiology* 109 (11): 2803–14. doi:10.1152/jn.00500.2012.

Gonzalez-Perez, Paloma, Ute Woehlbier, Ru-Ju J Chian, Peter Sapp, Guy A Rouleau, Claire S Leblond, Hussein Daoud, et al. 2015. "Identification of Rare Protein Disulfide Isomerase Gene Variants in Amyotrophic Lateral Sclerosis Patients." *Gene* 566 (2): 158–65. doi:10.1016/j.gene.2015.04.035.

Gupta, Rahul, Matthews Lan, Jelena Mojsilovic-Petrovic, Won Choi, Nathaniel Safren, Sami Barmada, Min Lee, and Robert Kalb. 2017. "The Proline/Arginine Dipeptide from Hexanucleotide Repeat Expanded C9ORF72 Inhibits the Proteasome." *Eneuro* 4 (1): 16. doi:10.1523/ENEURO.0249-16.2017.

Gurney, M E, H Pu, A Y Chiu, Dal M C Canto, C Y Polchow, D D Alexander, J Caliendo, et al. 1994. "Motor Neuron Degeneration in Mice That Express a Human Cu,Zn Superoxide Dismutase Mutation." *Science* 264 (5166): 1772–75. doi:10.1126/science.8209258.

Hadzipasic, Muhamed, Babak Tahvildari, Maria Nagy, Minjuan Bian, Arthur L Horwich,

and David A McCormick. 2014. "Selective Degeneration of a Physiological Subtype of Spinal Motor Neuron in Mice with SOD1-Linked ALS." *Proceedings of the National Academy of Sciences* 111 (47): 16883–88. doi:10.1073/pnas.1419497111.

Harrison, Megan, Aine O'Brien, Lucy Adams, Gary Cowin, Marc J. Ruitenberg, Gulgun Sengul, and Charles Watson. 2013. "Vertebral Landmarks for the Identification of Spinal Cord Segments in the Mouse." *NeuroImage* 68 (March): 22–29. doi:10.1016/j.neuroimage.2012.11.048.

He, Jingquan, Weikang Shi, Yu Guo, and Zhen Chai. 2014. "ERp57 Modulates Mitochondrial Calcium Uptake through the MCU." *FEBS Letters* 588 (12): 2087–94. doi:10.1016/j.febslet.2014.04.041.

Heiman-Patterson, T.D., J.S. Deitch, E.P. Blankenhorn, K.L. Erwin, M.J. Perreault, B.K. Alexander, N. Byers, I. Toman, and G.M. Alexander. 2005. "Background and Gender Effects on Survival in the TgN(SOD1-G93A)1Gur Mouse Model of ALS." *Journal of the Neurological Sciences* 236 (1–2): 1–7. doi:10.1016/j.jns.2005.02.006.

Hetz, Claudio. 2012. "The Unfolded Protein Response: Controlling Cell Fate Decisions under ER Stress and beyond." *Nature Reviews Molecular Cell Biology* 13 (2): 89. doi:10.1038/nrm3270.

Hetz, Claudio, Eric Chevet, and Scott A Oakes. 2015. "Proteostasis Control by the Unfolded Protein Response." *Nature Cell Biology* 17 (7): 829–38. doi:10.1038/ncb3184.

Hetz, Claudio, and Bertrand Mollereau. 2014. "Disturbance of Endoplasmic Reticulum Proteostasis in Neurodegenerative Diseases." *Nature Reviews Neuroscience* 15 (4): 233–49. doi:10.1038/nrn3689.

Hetz, Claudio, Peter Thielen, Soledad Matus, Melissa Nassif, Felipe Court, Roberta Kiffin, Gabriela Martinez, Ana Cuervo, Robert Brown, and Laurie Glimcher. 2009. "XBP-1 Deficiency in the Nervous System Protects against Amyotrophic Lateral Sclerosis by Increasing Autophagy." *Genes & Development* 23 (19): 2294–2306. doi:10.1101/gad.1830709.

Hoffstrom, Benjamin G, Anna Kaplan, Reka Letso, Ralf S Schmid, Gregory J Turmel, Donald C Lo, and Brent R Stockwell. 2010. "Inhibitors of Protein Disulfide Isomerase Suppress Apoptosis Induced by Misfolded Proteins." *Nature Chemical Biology* 6 (12): 900–906. doi:10.1038/nchembio.467.

Honjo, Yasuyuki, Satoshi Kaneko, Hidefumi Ito, Tomohisa Horibe, Masato Nagashima, Masataka Nakamura, Kengo Fujita, Ryosuke Takahashi, Hirofumi Kusaka, and Koji Kawakami. 2011. "Protein Disulfide Isomerase-Immunopositive Inclusions in Patients with Amyotrophic Lateral Sclerosis." *Amyotrophic Lateral Sclerosis* 12 (6): 444–50. doi:10.3109/17482968.2011.594055.

Ilieva, E. V., V. Ayala, M. Jove, E. Dalfo, D. Cacabelos, M. Povedano, M. J. Bellmunt, I. Ferrer, R. Pamplona, and M. Portero-Otin. 2007. "Oxidative and Endoplasmic

Reticulum Stress Interplay in Sporadic Amyotrophic Lateral Sclerosis." *Brain* 130 (12): 3111–23. doi:10.1093/brain/awm190.

Jara, Javier H, Barış Genç, Gregory A Cox, Martha C Bohn, Raymond P Roos, Jeffrey D Macklis, Emel Ulupınar, and Hande P Özdinler. 2015. "Corticospinal Motor Neurons Are Susceptible to Increased ER Stress and Display Profound Degeneration in the Absence of UCHL1 Function." *Cerebral Cortex* 25 (11): 4259–72. doi:10.1093/cercor/bhu318.

Jeon, Gye, Tomohiro Nakamura, Jeong-Seon Lee, Won-Jun Choi, Suk-Won Ahn, Kwang-Woo Lee, Jung-Joon Sung, and Stuart A Lipton. 2014. "Potential Effect of S-Nitrosylated Protein Disulfide Isomerase on Mutant SOD1 Aggregation and Neuronal Cell Death in Amyotrophic Lateral Sclerosis." *Molecular Neurobiology* 49 (2): 796–807. doi:10.1007/s12035-013-8562-z.

Jiang, H.-Q., M. Ren, H.-Z. Jiang, J. Wang, J. Zhang, X. Yin, S.-Y. Wang, Y. Qi, X.-D. Wang, and H.-L. Feng. 2014. "Guanabenz Delays the Onset of Disease Symptoms, Extends Lifespan, Improves Motor Performance and Attenuates Motor Neuron Loss in the SOD1 G93A Mouse Model of Amyotrophic Lateral Sclerosis." *Neuroscience* 277 (September): 132–38. doi:10.1016/j.neuroscience.2014.03.047.

Jin, Hisayo, Naoya Mimura, Makiko Kashio, Haruhiko Koseki, and Tomohiko Aoe. 2014. "Late-Onset of Spinal Neurodegeneration in Knock-In Mice Expressing a Mutant BiP." *PLoS ONE* 9 (11). doi:10.1371/journal.pone.0112837.

Kaplan, Artem, Krista J Spiller, Christopher Towne, Kevin C Kanning, Ginn T Choe, Adam Geber, Turgay Akay, Patrick Aebischer, and Christopher E Henderson. 2014. "Neuronal Matrix Metalloproteinase-9 Is a Determinant of Selective Neurodegeneration." *Neuron* 81 (2): 333–48. doi:10.1016/j.neuron.2013.12.009.

Kikuchi, Hitoshi, Gabriele Almer, Satoshi Yamashita, Christelle Guégan, Makiko Nagai, Zuoshang Xu, Alexander Sosunov, Guy McKhann, and Serge Przedborski. 2006. "Spinal Cord Endoplasmic Reticulum Stress Associated with a Microsomal Accumulation of Mutant Superoxide Dismutase-1 in an ALS Model." *Proc Natl Acad Sci U S A* 103 (15): 6025–30. doi:10.1073/pnas.0509227103.

Kiskinis, Evangelos, Jackson Sandoe, Luis A Williams, Gabriella L Boulting, Rob Moccia, Brian J Wainger, Steve Han, et al. 2014. "Pathways Disrupted in Human ALS Motor Neurons Identified through Genetic Correction of Mutant SOD1." *Cell Stem Cell* 14 (6): 781–95. doi:10.1016/j.stem.2014.03.004.

Lalancette-Hebert, Melanie, Aarti Sharma, Alexander K Lyashchenko, and Neil A Shneider. 2016. "Gamma Motor Neurons Survive and Exacerbate Alpha Motor Neuron Degeneration in ALS." *Proceedings of the National Academy of Sciences of the United States of America* 113 (51): 8316–25. doi:10.1073/pnas.1605210113.

Lamanauskas, Nerijus, and Andrea Nistri. 2008. "Riluzole Blocks Persistent Na+ and Ca2+ Currents and Modulates Release of Glutamate via Presynaptic NMDA Receptors on Neonatal Rat Hypoglossal Motoneurons in Vitro." *European Journal of Neuroscience* 27 (10): 2501–14. doi:10.1111/j.1460-9568.2008.06211.x.

Li, Yun, and Patricia Camacho. 2004. "Ca $^{2+}$ -Dependent Redox Modulation of SERCA 2b by ERp57." *The Journal of Cell Biology* 164 (1): 35–46. doi:10.1083/jcb.200307010.

Ling, Shuo-Chien C, Magdalini Polymenidou, and Don W Cleveland. 2013. "Converging Mechanisms in ALS and FTD: Disrupted RNA and Protein Homeostasis." *Neuron* 79 (3): 416–38. doi:10.1016/j.neuron.2013.07.033.

Liu, Jing, Jiaxin Hu, Andrew T Ludlow, Jacqueline T Pham, Jerry W Shay, Jeffrey D Rothstein, and David R Corey. 2017. "c9orf72 Disease-Related Foci Are Each Composed of One Mutant Expanded Repeat RNA." *Cell Chemical Biology* 24 (2): 141–48. doi:10.1016/j.chembiol.2016.12.018.

Liu, Yuanjing, Amrutha Pattamatta, Tao Zu, Tammy Reid, Olgert Bardhi, David R Borchelt, Anthony T Yachnis, and Laura Ranum. 2016. "C9orf72 BAC Mouse Model with Motor Deficits and Neurodegenerative Features of ALS/FTD." *Neuron* 90 (3): 521–34. doi:10.1016/j.neuron.2016.04.005.

Mancuso, Renzo, Sara Oliván, Pilar Mancera, Andrea Pastén-Zamorano, Raquel Manzano, Caty Casas, Rosario Osta, and Xavier Navarro. 2012. "Effect of Genetic Background on Onset and Disease Progression in the SOD1-G93A Model of Amyotrophic Lateral Sclerosis." *Amyotrophic Lateral Sclerosis* 13 (3): 302–10. doi:10.3109/17482968.2012.662688.

Mancuso, Renzo, Rosario Osta, and Xavier Navarro. 2014. "Presymptomatic Electrophysiological Tests Predict Clinical Onset and Survival in SOD1 ^{G93A} ALS Mice." *Muscle & Nerve* 50 (6): 943–49. doi:10.1002/mus.24237.

Manjaly, Zita R., Kirsten M. Scott, Kumar Abhinav, Lokesh Wijesekera, Jeban Ganesalingam, Laura H. Goldstein, Anna Janssen, et al. 2010. "The Sex Ratio in Amyotrophic Lateral Sclerosis: A Population Based Study." *Amyotrophic Lateral Sclerosis* 11 (5): 439–42. doi:10.3109/17482961003610853.

Martinez, Ana, Maria del Valle Palomo Ruiz, Daniel I. Perez, and Carmen Gil. 2017. "Drugs in Clinical Development for the Treatment of Amyotrophic Lateral Sclerosis." *Expert Opinion on Investigational Drugs* 26 (4): 403–14. doi:10.1080/13543784.2017.1302426.

Martínez, Gabriela, Claudia Duran-Aniotz, Felipe Cabral-Miranda, Juan P. Vivar, and Claudio Hetz. 2017. "Endoplasmic Reticulum Proteostasis Impairment in Aging." *Aging Cell*, April. doi:10.1111/acel.12599.

Massignan, Tania, Filippo Casoni, Manuela Basso, Paola Stefanazzi, Emiliano Biasini, Massimo Tortarolo, Mario Salmona, Elisabetta Gianazza, Caterina Bendotti, and Valentina Bonetto. 2007. "Proteomic Analysis of Spinal Cord of Presymptomatic Amyotrophic Lateral Sclerosis G93A SOD1 Mouse." *Biochemical and Biophysical Research Communications* 353 (3): 719–25. doi:10.1016/j.bbrc.2006.12.075.

Matus, Soledad, Danilo B Medinas, and Claudio Hetz. 2014. "Common Ground: Stem Cell Approaches Find Shared Pathways Underlying ALS." *Cell Stem Cell* 14 (6): 697–99. doi:10.1016/j.stem.2014.05.001.

Matus, Soledad, Vicente Valenzuela, Danilo B Medinas, and Claudio Hetz. 2013. "ER Dysfunction and Protein Folding Stress in ALS." *International Journal of Cell Biology* 2013: 1–12. doi:10.1155/2013/674751.

Moore, Kristin A., and Julie Hollien. 2012. "The Unfolded Protein Response in Secretory Cell Function." *Annual Review of Genetics* 46 (1): 165–83. doi:10.1146/annurev-genet-110711-155644.

Nardo, Giovanni, Silvia Pozzi, Mauro Pignataro, Eliana Lauranzano, Giorgia Spano, Silvia Garbelli, Stefania Mantovani, et al. 2011. "Amyotrophic Lateral Sclerosis Multiprotein Biomarkers in Peripheral Blood Mononuclear Cells." *PLoS ONE* 6 (10). doi:10.1371/journal.pone.0025545.

Neff, Frauke, Diana Flores-Dominguez, Devon P. Ryan, Marion Horsch, Susanne Schröder, Thure Adler, Luciana Caminha Afonso, et al. 2013. "Rapamycin Extends Murine Lifespan but Has Limited Effects on Aging." *Journal of Clinical Investigation* 123 (8): 3272–91. doi:10.1172/JCI67674.

Neumann, Manuela, Deepak M Sampathu, Linda K Kwong, Adam C Truax, Matthew C Micsenyi, Thomas T Chou, Jennifer Bruce, et al. 2006. "Ubiquitinated TDP-43 in Frontotemporal Lobar Degeneration and Amyotrophic Lateral Sclerosis." *Science* 314 (5796): 130–33. doi:10.1126/science.1134108.

Nijssen, Jik, Laura H Comley, and Eva Hedlund. 2017. "Motor Neuron Vulnerability and Resistance in Amyotrophic Lateral Sclerosis." *Acta Neuropathologica* 133 (6): 863–85. doi:10.1007/s00401-017-1708-8.

Nishitoh, Hideki, Hisae Kadowaki, Atsushi Nagai, Takeshi Maruyama, Takanori Yokota, Hisashi Fukutomi, Takuya Noguchi, Atsushi Matsuzawa, Kohsuke Takeda, and Hidenori Ichijo. 2008. "ALS-Linked Mutant SOD1 Induces ER Stress- and ASK1-Dependent Motor Neuron Death by Targeting Derlin-1." *Genes & Development* 22 (11): 1451–64. doi:10.1101/gad.1640108.

O'Rourke, Jacqueline G., Laurent Bogdanik, A.K.M.G. Muhammad, Tania F. Gendron, Kevin J. Kim, Andrew Austin, Janet Cady, et al. 2015. "C9orf72 BAC Transgenic Mice Display Typical Pathologic Features of ALS/FTD." *Neuron* 88 (5): 892–901. doi:10.1016/j.neuron.2015.10.027.

Oka, Ojore B V, Hui Y Yeoh, and Neil J Bulleid. 2015. "Thiol-Disulfide Exchange between the PDI Family of Oxidoreductases Negates the Requirement for an Oxidase or Reductase for Each Enzyme." *Biochem. J* 469: 279–88. doi:10.1042/BJ20141423.

Paganoni, Sabrina, and Anthony Amato. 2013. "Electrodiagnostic Evaluation of Myopathies." *Physical Medicine and Rehabilitation Clinics of North America* 24 (1): 193–207. doi:10.1016/j.pmr.2012.08.017.

Peters, Owen M., Gabriela Toro Cabrera, Helene Tran, Tania F. Gendron, Jeanne E. McKeon, Jake Metterville, Alexandra Weiss, Nicholas Wightman, Johnny Salameh, Juhyun Kim, Huaming Sun, Kevin B. Boylan, Dennis Dickson, Zachary Kennedy, Ziqiang Lin, Yong Jie Zhang, Lillian Daughrity, Chris Jung, Fen Biao Gao, Peter C.

Sapp, H. Robert Horvitz, Daryl A. Bosco, Solange P. Brown, Pieter de Jong, Leonard Petrucelli, Chris Mueller, Robert H. Brown. 2015. "Human C9ORF72 Hexanucleotide Expansion Reproduces RNA Foci and Dipeptide Repeat Proteins but Not Neurodegeneration in BAC Transgenic Mice." *Neuron* 88 (5): 902–9. doi:10.1016/j.neuron.2015.11.018.

Picher-Martel, Vincent, Paul N Valdmanis, Peter V Gould, Jean-Pierre Julien, and Nicolas Dupré. 2016. "From Animal Models to Human Disease: A Genetic Approach for Personalized Medicine in ALS." *Acta Neuropathologica Communications* 4 (1): 70. doi:10.1186/s40478-016-0340-5.

Poet, Greg J, Ojore Bv Oka, Marcel van Lith, Zhenbo Cao, Philip J Robinson, Marie Anne Pringle, Elias Sj Arnér, and Neil J Bulleid. 2017. "Cytosolic Thioredoxin Reductase 1 Is Required for Correct Disulfide Formation in the ER." *The EMBO Journal* 36 (5): 693–702. doi:10.15252/embj.201695336.

Pokrishevsky, Edward, Leslie I Grad, Masoud Yousefi, Jing Wang, Ian R Mackenzie, and Neil R Cashman. 2012. "Aberrant Localization of FUS and TDP43 Is Associated with Misfolding of SOD1 in Amyotrophic Lateral Sclerosis." *PLoS ONE* 7 (4). doi:10.1371/journal.pone.0035050.

Reemst, Kitty, Stephen C. Noctor, Paul J. Lucassen, and Elly M. Hol. 2016. "The Indispensable Roles of Microglia and Astrocytes during Brain Development." *Frontiers in Human Neuroscience* 10 (November): 566. doi:10.3389/fnhum.2016.00566.

Rizzo, Federica, Giulietta Riboldi, Sabrina Salani, Monica Nizzardo, Chiara Simone, Stefania Corti, and Eva Hedlund. 2014. "Cellular Therapy to Target Neuroinflammation in Amyotrophic Lateral Sclerosis." *Cellular and Molecular Life Sciences* 71 (6): 999–1015. doi:10.1007/s00018-013-1480-4.

Rosen, Daniel R, Teepu Siddique, David Patterson, Denise A Figlewicz, Peter Sapp, Afif Hentati, Deirdre Donaldson, et al. 1993. "Mutations in Cu/Zn Superoxide Dismutase Gene Are Associated with Familial Amyotrophic Lateral Sclerosis." *Nature* 362 (6415): 59–62. doi:10.1038/362059a0.

Rotunno, Melissa S, Jared R Auclair, Stephanie Maniatis, Scott A Shaffer, Jeffrey Agar, and Daryl A Bosco. 2014. "Identification of a Misfolded Region in Superoxide Dismutase 1 That Is Exposed in Amyotrophic Lateral Sclerosis." *The Journal of Biological Chemistry* 289 (41): 28527–38. doi:10.1074/jbc.M114.581801.

Rozas, Pablo, Leslie Bargsted, Francisca Martínez, Claudio Hetz, and Danilo B Medinas. 2017. "The ER Proteostasis Network in ALS: Determining the Differential Motoneuron Vulnerability." *Neurosci Lett* 636: 9–15. doi:10.1016/j.neulet.2016.04.066.

Saxena, Smita, Erik Cabuy, and Pico Caroni. 2009. "A Role for Motoneuron Subtype–selective ER Stress in Disease Manifestations of FALS Mice." *Nature Neuroscience* 12 (5): 627–36. doi:10.1038/nn.2297.

Saxena, Smita, and Pico Caroni. 2011. "Selective Neuronal Vulnerability in

Neurodegenerative Diseases: From Stressor Thresholds to Degeneration." *Neuron* 71 (1): 35–48. doi:10.1016/j.neuron.2011.06.031.

Scott, Hilary, and Vladislav M Panin. 2014. "N-Glycosylation in Regulation of the Nervous System." *Advances in Neurobiology* 9: 367–94. doi:10.1007/978-1-4939-1154-7_17.

Sellier, Chantal, Maria-Letizia Campanari, Camille Corbier, Angeline Gaucherot, Isabelle Kolb-Cheynel, Mustapha Oulad-Abdelghani, Frank Ruffenach, et al. 2016. "Loss of C9ORF72 Impairs Autophagy and Synergizes with polyQ Ataxin-2 to Induce Motor Neuron Dysfunction and Cell Death." *The EMBO Journal* 35 (12): 1276–97. doi:10.15252/embj.201593350.

Sepúlveda, Martín. 2015. "Caracterización de Líneas de Ratones Transgénicos Que Sobreexpresan Formas Mutantes de La Foldasa ERp57 Asociadas a La Esclerosis Lateral Amiotrófica." Molecular Biotechnology Engineering undergraduate thesis. University of Chile.

Sepulveda, Martin, Pablo Rozas, Claudio Hetz, and Danilo B Medinas. 2016. "ERp57 as a Novel Cellular Factor Controlling Prion Protein Biosynthesis: Therapeutic Potential of Protein Disulfide Isomerases." *Prion* 10 (1): 50–56. doi:10.1080/19336896.2015.1129485.

Song, SungWon, Carlos J Miranda, Lyndsey Braun, Kathrin Meyer, Ashley E Frakes, Laura Ferraiuolo, Shibi Likhite, et al. 2016. "Major Histocompatibility Complex Class I Molecules Protect Motor Neurons from Astrocyte-Induced Toxicity in Amyotrophic Lateral Sclerosis." *Nature Medicine* 22 (4): 397–403. doi:10.1038/nm.4052.

Statland, Jeffrey M., Richard J. Barohn, Mazen M. Dimachkie, Mary Kay Floeter, and Hiroshi Mitsumoto. 2015. "Primary Lateral Sclerosis." *Neurologic Clinics* 33 (4): 749–60. doi:10.1016/j.ncl.2015.07.007.

Sudria-Lopez, Emma, Max Koppers, Marina de Wit, Christiaan van der Meer, Henk-Jan Westeneng, Caroline A C Zundel, Sameh A Youssef, et al. 2016. "Full Ablation of C9orf72 in Mice Causes Immune System-Related Pathology and Neoplastic Events but No Motor Neuron Defects." *Acta Neuropathologica* 132 (1): 145–47. doi:10.1007/s00401-016-1581-x.

Sun, Shuying, Ying Sun, Shuo-Chien Ling, Laura Ferraiuolo, Melissa McAlonis-Downes, Yiyang Zou, Kevin Drenner, et al. 2015. "Translational Profiling Identifies a Cascade of Damage Initiated in Motor Neurons and Spreading to Glia in Mutant SOD1-Mediated ALS." *Proceedings of the National Academy of Sciences* 112 (50). doi:10.1073/pnas.1520639112.

Swinnen, Bart, and Wim Robberecht. 2014. "The Phenotypic Variability of Amyotrophic Lateral Sclerosis." *Nature Reviews Neurology* 10 (11): 661–70. doi:10.1038/nrneurol.2014.184.

Tannous, Abla, Giorgia Pisoni, Daniel N Hebert, and Maurizio Molinari. 2015. "N-Linked Sugar-Regulated Protein Folding and Quality Control in the ER." *Seminars in Cell*

& Developmental Biology 41: 79–89. doi:10.1016/j.semcdb.2014.12.001.

Taylor, J. Paul, Robert H. Brown, and Don W. Cleveland. 2016. "Decoding ALS: From Genes to Mechanism." *Nature* 539 (7628): 197–206. doi:10.1038/nature20413.

Torres, Mauricio, Danilo B Medinas, José M M Matamala, Ute Woehlbier, Víctor H H Cornejo, Tatiana Solda, Catherine Andreu, et al. 2015. "The Protein-Disulfide Isomerase ERp57 Regulates the Steady-State Levels of the Prion Protein." *The Journal of Biological Chemistry* 290 (39): 23631–45. doi:10.1074/jbc.M114.635565.

Turner, Bradley J, and Kevin Talbot. 2008. "Transgenics, Toxicity and Therapeutics in Rodent Models of Mutant SOD1-Mediated Familial ALS." *Progress in Neurobiology* 85 (1): 94–134. doi:10.1016/j.pneurobio.2008.01.001.

Turner, Martin R, Orla Hardiman, Michael Benatar, Benjamin R Brooks, Adriano Chio, Mamede de Carvalho, Paul G Ince, et al. 2013. "Controversies and Priorities in Amyotrophic Lateral Sclerosis." *The Lancet Neurology* 12 (3): 310–22. doi:10.1016/S1474-4422(13)70036-X.

Uehara, Takashi, Tomohiro Nakamura, Dongdong Yao, Zhong-Qing Shi, Zezong Gu, Yuliang Ma, Eliezer Masliah, Yasuyuki Nomura, and Stuart A Lipton. 2006. "S-Nitrosylated Protein-Disulphide Isomerase Links Protein Misfolding to Neurodegeneration." *Nature* 441 (7092): 513–17. doi:10.1038/nature04782.

Urushitani, M., S. A. Ezzi, A. Matsuo, I. Tooyama, and J.-P. Julien. 2008. "The Endoplasmic Reticulum-Golgi Pathway Is a Target for Translocation and Aggregation of Mutant Superoxide Dismutase Linked to ALS." *The FASEB Journal* 22 (7): 2476–87. doi:10.1096/fj.07-092783.

Valenzuela, Daniel, Pedro Zitko, and Patricia Lillo. 2015. "Amyotrophic Lateral Sclerosis Mortality Rates in Chile: A Population Based Study (1994–2010)." *Amyotrophic Lateral Sclerosis and Frontotemporal Degeneration* 16 (5–6): 372–77. doi:10.3109/21678421.2015.1026827.

Valenzuela, Vicente. 2016. "Gene Therapy to Deliver the Unfolded Protein Response (UPR) Transcription Factor XBP1s into the Central Nervous System of Mutant SOD1 Models of ALS." PhD thesis. University of Chile.

Vance, Caroline, Boris Rogelj, Tibor Hortobágyi, Kurt J De Vos, Agnes L Nishimura, Jemeen Sreedharan, Xun Hu, et al. 2009. "Mutations in FUS, an RNA Processing Protein, Cause Familial Amyotrophic Lateral Sclerosis Type 6." *Science (New York, N.Y.)* 323 (5918): 1208–11. doi:10.1126/science.1165942.

Vieira, Fernando G., Qinggong Ping, Andy J. Moreno, Joshua D. Kidd, Kenneth Thompson, Bingbing Jiang, John M. Lincecum, et al. 2015. "Guanabenz Treatment Accelerates Disease in a Mutant SOD1 Mouse Model of ALS." Edited by Thomas H Gillingwater. *PLOS ONE* 10 (8): e0135570. doi:10.1371/journal.pone.0135570.

Wainger, Brian J, Evangelos Kiskinis, Cassidy Mellin, Ole Wiskow, Steve Han, Jackson Sandoe, Numa P Perez, et al. 2014. "Intrinsic Membrane Hyperexcitability of

Amyotrophic Lateral Sclerosis Patient-Derived Motor Neurons." *Cell Reports* 7 (1): 1–11. doi:10.1016/j.celrep.2014.03.019.

Walker, Adam, Manal Farg, Chris Bye, Catriona McLean, Malcolm Horne, and Julie Atkin. 2010. "Protein Disulphide Isomerase Protects against Protein Aggregation and Is S-Nitrosylated in Amyotrophic Lateral Sclerosis." *Brain: A Journal of Neurology* 133 (Pt 1): 105–16. doi:10.1093/brain/awp267.

Walker, Adam K, Manal A Farg, Chris R Bye, Catriona A McLean, Malcolm K Horne, and Julie D Atkin. 2010. "Protein Disulphide Isomerase Protects against Protein Aggregation and Is S-Nitrosylated in Amyotrophic Lateral Sclerosis." *Brain* 133 (1): 105–16. doi:10.1093/brain/awp267.

Wanamaker, Christian P, and William N Green. 2007. "Endoplasmic Reticulum Chaperones Stabilize Nicotinic Receptor Subunits and Regulate Receptor Assembly." *The Journal of Biological Chemistry* 282 (43): 31113–23. doi:10.1074/jbc.M705369200.

Wang, Jiou, Guilian Xu, and David R. Borchelt. 2002. "High Molecular Weight Complexes of Mutant Superoxide Dismutase 1: Age-Dependent and Tissue-Specific Accumulation." *Neurobiology of Disease* 9 (2): 139–48. doi:10.1006/nbdi.2001.0471.

Wang, Jiou, Guilian Xu, Hilda H. Slunt, Victoria Gonzales, Michael Coonfield, David Fromholt, Neal G. Copeland, Nancy A. Jenkins, and David R. Borchelt. 2005. "Coincident Thresholds of Mutant Protein for Paralytic Disease and Protein Aggregation Caused by Restrictively Expressed Superoxide Dismutase cDNA." *Neurobiology of Disease* 20 (3): 943–52. doi:10.1016/j.nbd.2005.06.005.

Wang, Lijun, Brian Popko, Emily Tixier, and Raymond P. Roos. 2014. "Guanabenz, Which Enhances the Unfolded Protein Response, Ameliorates Mutant SOD1-Induced Amyotrophic Lateral Sclerosis." *Neurobiology of Disease* 71 (November): 317–24. doi:10.1016/j.nbd.2014.08.010.

Wegorzewska, I., S. Bell, N. J. Cairns, T. M. Miller, and R. H. Baloh. 2009. "TDP-43 Mutant Transgenic Mice Develop Features of ALS and Frontotemporal Lobar Degeneration." *Proceedings of the National Academy of Sciences* 106 (44): 18809–14. doi:10.1073/pnas.0908767106.

Woehlbier, Ute, Alicia Colombo, Mirva J Saaranen, Viviana Pérez, Jorge Ojeda, Fernando J Bustos, Catherine I Andreu, et al. 2016. "ALS-Linked Protein Disulfide Isomerase Variants Cause Motor Dysfunction." *The EMBO Journal* 35 (8): 845–65. doi:10.15252/embj.201592224.

Zhang, Yinan, Ehtesham Baig, and David B Williams. 2006. "Functions of ERp57 in the Folding and Assembly of Major Histocompatibility Complex Class I Molecules." *The Journal of Biological Chemistry* 281 (21): 14622–31. doi:10.1074/jbc.M512073200.

and/or protein networks involved in protein folding, protein degradation, redox status and calcium homeostasis (He et al. 2014; Appenzeller-Herzog et al. 2008; Ellgaard and Frickel 2003; Wanamaker and Green 2007). Moreover, ERp57 and CNX can activate STAT3 signaling, a pathway that modulates inflammatory responses in Alzheimer's and Huntington's disease context (Ben Haim et al. 2015; Coe et al. 2010). Finally, ERp57 participates in MHC-I assembly (Zhang, Baig, and Williams 2006), which has been recently demonstrated to mediate motor neuron-astrocyte interaction preventing astrocyte toxicity towards motor neuron in ALS context (Song et al. 2016). ERp57 contribution to these molecular pathways in ALS remains to be addressed.

The fact that a reduction of SOD1G93A aggregation levels did not translate into extended lifespan challenges the idea of mutant SOD1 aggregation-driven pathology rising new questions about the causal relationship between mutant SOD1 aggregation and disease progression. Foremost, how is it possible that a significant reduction in SOD1 aggregation and oligomerization did not improve histopathological and clinical phenotypic features? This question suggests two scenarios: the first one where mutant SOD1 accumulation at end stage may be simply a consequence of ALS pathological mechanisms driven by smaller toxic forms of mutant SOD1; in the second instance, the observed reduction of mutant SOD1 aggregates is not enough to prevent ALS pathological events.

Given the time course of ALS onset and progression in double transgenic mice, it is plausible that reduction of SOD1 aggregation by ERp57 delays disease onset by impacting cell-autonomous mechanisms related to stability of motor neurons synaptic terminal while having negligible effects on disease progression marked by inflammatory